Hybrid Free Space Optical and RF Wireless Communication

A Dissertation

Presented to

the faculty of the School of Engineering and Applied Science

University of Virginia

---

in partial fulfillment

of the requirements for the degree

Doctor of Philosophy

by

Yi Tang

December

2013

APPROVAL SHEET

The dissertation

is submitted in partial fulfillment of the requirements

for the degree of

Doctor of Philosophy

AUTHOR

The dissertation has been read and approved by the examining committee:

Maite Brandt-Pearce

Advisor

Stephen G. Wilson

Toby Berger

Malathi Veeraraghavan

Peter A. Beling

Accepted for the School of Engineering and Applied Science:

Dean, School of Engineering and Applied Science

December

2013

Abstract

Hybrid free space optical/radio frequency (FSO/RF) technology has recently been proposed as a means of significantly increasing the throughput and reliability of wireless broadband communications. The motivation is to use parallel noninterfering communication channels to combat channel impairments. In order to implement and fully exploit hybrid FSO/RF technology, both point-to-point (P2P) communication system and network models need to be studied.

We develop physical-layer and network-layer models of hybrid FSO/RF networks. We address two topics: hybrid FSO/RF P2P systems and hybrid FSO/RF wireless mesh networks (WMN). Theoretical analyses are presented. In addition, we present practical implementations with performance that approaches the theoretical system performance derived. Numerical and simulation results are provided to show the advantages of hybrid FSO/RF systems.

For P2P communications, we model the hybrid FSO/RF system as an independent parallel channel system. We develop an information-theoretic analysis of the parallel channel model and implement an adaptive design resulting in a capacity-approaching and seamless joint system. Results show that this jointly optimized FSO/RF link significantly outperforms simple RF or FSO links.

In our research on hybrid FSO/RF WMN, we study both centralized and distributed routing algorithms. For centralized routing, we present network control algorithms based on both non-fading and fading communication channels using a physical interference model for the RF portion of the network. We study the throughput improvement achievable by augmenting the RF WMN with FSO links. In our distributed routing study, a hierarchical routing algorithm is developed for the hybrid FSO/RF network. The algorithm is optimized for the hybrid network so that the advantages of high-throughput FSO links and the reliability of RF links are highlighted.

FSO links are able to relieve network congestion caused by the limited capacity and interference-limited nature of pure RF networks.

Acknowledgements

I would like to sincerely thank my advisor, Professor Maïté Brandt-Pearce for her guidance, encouragement and support for my studies and research at the University of Virginia. As a mentor, her extensive knowledge, meticulous attitude and genial personality deeply infected and inspired me.

I would also like to thank Professor Stephen G. Wilson, Professor Toby Berger, Professor Malathi Veeraraghavan and Professor Peter A. Beling for serving on my advisory committee and providing valuable suggestions to improve my research. I took their courses during my Ph.D. study. Their immense knowledge and rigorous scholarship helped me to form a dedicated and creative research style which is significant for my career.

I am also lucky to have worked with many talented colleagues and friends including Houbing Song, Xu Wang, Mohammad Noshad, Anup Shrinivasan, and Tingjun Xie at the University of Virginia.

I gratefully appreciate the National Science Foundation for funding this research (under grant number ECCS-0636598).

Finally, I want to thank to my wife and parents for their support. Without their help, this dissertation would not have been possible.

Yi Tang

Chantilly, Virginia

To my family.

Contents

List of Tables

List of Figures

Chapter 1

Introduction

A communication technology that uses light to exchange information through the atmosphere is called Free Space Optical (FSO) communication. In contrast to optical fiber communication, the media is "free space", i.e., wireless instead of cabled. Thus people also call it optical wireless communications (OWC). These systems are typically stationary, foregoing the benefits of mobile access in exchange for the higher power of highly-directed laser beams. The biggest advantage of non-mobile wireless communications is the low deployment cost. Moreover, utilizing the optical spectrum for communications implies high throughput, high security and license-free operation. However, weather conditions, scintillation, and pointing issues can severely affect the FSO channel, as shown in [1, 2, 3, 4, 5, 6, 7, 8]. It is therefore wise to pair FSO with a parallel lower rate but reliable RF system, forming what is currently referred to as a hybrid FSO/RF communication system. In this dissertation we describe our comprehensive research on both physical and network layers of a hybrid FSO/RF communication system. Theoretical analyses, numerical and simulation results are provided as guidelines for the design of hybrid FSO/RF communication systems and networks.

1.1 Background

Free Space Optical (FSO) communication, an old communication technology that has existed for thousands of years, has experienced a resurgence as new devices and applications have made it especially attractive. In ancient times, soldiers used polished shields and smoke to send signals, which are forms of wireless optical communication. Nowadays, based on their implementation, we can divide FSO communication technologies into three categories: outer space, indoor and terrestrial applications.

In the outer space optical communications field, lasers are used for communication between satellites or spacecraft. The communication range currently is on the order of thousands of kilometers or more. NASA recently launched the Lunar Laser Communication Demonstration (LLCD) project [9]. The objective is to establish a two-way communication link using lasers between an earth ground station and the lunar Atmosphere and Dust Environment Explorer (LADEE) spacecraft in Lunar orbit. The proposed data rate is 622 Mbps. Success of this project can revolutionize the satellite communication industry.

Another emerging area of FSO research is indoor local area network (LAN) communications, called Li-Fi or Visible Light Communications (VLC). This technology uses visible light emitted from LEDs for communication. The interference between two Li-Fi systems is quite small, in contrast with conventional RF based indoor wireless system. Meanwhile the cost and size of transceivers are also much lower compared with those of the RF counterpart (Wi-Fi). Based on recent news, a data rate over 1.6 Gbps has been achieved in the lab. For more information about channel modeling and modulation of this technology, the reader is referred to [10, 11, 12, 13, 14]

The last category, terrestrial FSO communication, is the one of interest in this work. The communication range for such FSO links is several kilometers with throughputs on the order of Gbps. Thus it is referred to as high-speed "last-mile" connectivity. The high transmission speed and license-free bandwidth are the biggest

advantages of this technology. There has been significant recent interest in this technology, as reported in [15, 16, 17, 18, 4, 19, 20, 21, 22, 23]. The nature of hybrid FSO/RF can satisfy the current and increasing demand for wireless bandwidth. In the next section, we present the challenges associated with using this technology, as well as our solutions to these challenges.

1.2 Challenges and Motivation

Due to the considerable demand for wireless bandwidth, radio frequency resources have become cluttered and thus expensive. Communicating over the optical domain, with its nearly boundless bandwidth, has been proposed as a viable alternative for high-speed wireless connectivity. However, FSO technology cannot replace current RF communication systems. The requirement of line-of-sight limits the implementation of FSO links. Moreover, channel impairments such as visibility, atmospheric scintillation, background light interference and pointing issues can seriously affect the communication quality. An attractive solution is to build a wireless system including both FSO and RF links, forming so-called hybrid FSO/RF communication systems.

To design a hybrid FSO/RF system in practice, physical layer and network layer research is necessary. In physical layer studies, the primary problems are: to derive the theoretical throughput of such hybrid point-to-point links, and to design a system that approaches this throughput in practice. Recent research on FSO/RF point-to-point systems includes [24, 25, 2, 26, 27, 28]. In network layer research, network modeling, routing and scheduling are primary topics, as also considered by other researchers in [29, 30, 31, 32, 33]. In this dissertation, we present in-depth analyses on these topics for both architecture layers. We hope to provide insight into the implementation of hybrid FSO/RF systems for real-world application.

1.3 Overview and Literature Review

In this section we give an overview of the dissertation. As mentioned, our hybrid FSO/RF communication system study focuses on two aspects: point-to-point (P2P) communication systems and hybrid networks. The P2P work is described in Chapter 2. We divided the network layer research it into two chapters: in Chapter 3 we study the network with centralized control of scheduling and routing, and in Chapter 4 we derive a distributed routing algorithm for relatively large networks.

1.3.1 Point-to-Point Hybrid FSO/RF Communication System

In Chapter 2 we model the P2P hybrid communication system as an independent parallel channel system as shown in Figure 1.1. We solve for the parameters yielding the maximum throughput for general independent parallel channels when the channel state is known at the transmitter. The formulation is based on information theory and is independent of any particular coding scheme or statistical channel model. Then we apply this throughput optimization approach to design an adaptive transmission scheme the hybrid FSO/RF communication system. Theoretical and simulation results give insight into the relationship between the adaptive parameters and the performance of the hybrid system.

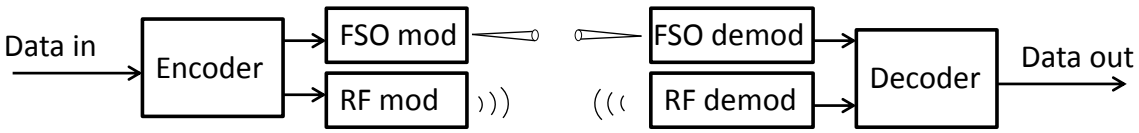

Figure 1.1: Illustration of P2P link composed of RF and FSO channels.

Literature Review

There have been several studies that consider error-control coding for FSO/RF hybrid systems and analyze the resulting performance. A parallel-channel encoder-rate adaptive scheme applied to the joint system is introduced in [24] to address the time-varying nature of the channels. The adaptivity assumes channel state information at the transmitter and is based on puncturing a low density parity check (LDPC) code, which has been shown to be capacity-achieving with increasing block length. A minimum-throughput-threshold is enforced so that the hybrid system suffers from a total outage when severe fading occurs. In [25] it is shown that the capacity of the hybrid FSO/RF channel can be improved by passing a fixed portion of the data through the RF link. A parallel system using both power and encoder rate adaptation with fixed symbol rate is introduced in [34]. These three approaches impose severe constraints on the system design, including modem rates, modulation used, and the fraction of bits sent through each channel; we are interested in maximizing the throughput of the system by allowing as much link adaptation flexibility as possible.

There has also been extensive work on general parallel channels, though not specifically the hybrid FSO/RF system. Turbo-like codes [35] and rateless codes [36] have been proposed. Achievable rates and complexity analysis of LDPC codes are presented in [37] for general parallel channels. Average error probability performance of binary parallel channels has also been evaluated in terms of reliable channel regions [38]. These studies assume fixed modulation and concern themselves with the design and performance analysis of the code itself. We consider the parallel channel from an information-theoretic perspective, to which one of these specific codes can subsequently be applied.

Contributions and Conclusions

In this section we describe our contributions as well as the major conclusions of our P2P hybrid FSO/RF communication system research.

First, we study the individual channel capacities for both RF and FSO channels in Section 2.2.2. The properties of these two capacities are discussed in detail in this section, since those properties are used to solve the throughput optimization problem. We derive four model-specific requirements on channel capacity for our optimization problem. Our optimization procedure is applicable to any parallel system, as long as those requirements are satisfied.

As shown in Figure 1.1, we model the hybrid FSO/RF communication system as a parallel channel system with a joint error control coding scheme. The encoder rate, modulations and symbol rates of each channel are parameters that are dynamically adjusted to yield maximum throughput. We derive the actual throughput, and estimate the joint channel capacity using an upper bound to the actual throughput for reliable communication.

We then present the throughput optimization problem under two different sets of constraints: an encoder-rate constraint only, and an encoder-rate constraint with additional modem bandwidth constraints. The Lagrange method is used to solve the optimization problem. With only encode-rate constraints, the conclusion is that the symbol-rate should be increased to operate as close to capacity as possible. We prove that the capacity is achievable and optimal symbol rates satisfy the constraints with equality. We also prove that the solution to the optimization problem is unique. An efficient search method to find the solution is provided.

When additional modem bandwidth constraints are imposed, the throughput optimization needs to be decoupled into four cases based on the bandwidth requirement. A flow chart for solving this optimization problem is given. The major conclusion is that when both channel conditions are good, a higher throughput is achievable

by puncturing a mother code. Otherwise, the hybrid system should operate at its minimum encoder rate and adjust symbol rates and modulations to obtain optimal throughput according to the algorithm given.

Various numerical, experimental, and simulation results for hybrid FSO/RF communication system using our adaptive technique are given. We also compare our system with nonadaptive systems to show the throughput improvement afforded by using our optimization.

1.3.2 Centralized FSO/RF Network

After our discussion of P2P hybrid FSO/RF communication systems, we present our research on hybrid FSO/RF networks, where RF links and FSO links can be used (independently or together) to connect nodes. Among various wireless mesh network architectures [39], we are interested in infrastructure WMNs (illustrated in Figure 1.2). A WMN consists of mesh routers (MRs) and mesh clients (MCs). The MRs in this infrastructure WMN form a backbone for MCs and are stationary.

In chapter 3, we assume routing and scheduling of network traffic are controlled by a centralized unit in the network. We present network control algorithms based on both non-fading and fading communication channels using the physical interference model for the RF portion of the network. We study the throughput improvement achievable by augmenting the RF WMN with FSO links. We address two questions: given a fixed number of FSO links, where should they be installed to maximize the throughput for given traffic demands, and how should the traffic be routed and scheduled in the hybrid FSO/RF network to achieve this throughput. We formulate these problems as one mixed integer linear program, and provide a computationally efficient heuristic for scheduling and routing traffic demands through the hybrid FSO/RF network. The results show that the throughput of the original RF network can be increased dramatically by properly adding FSO links.

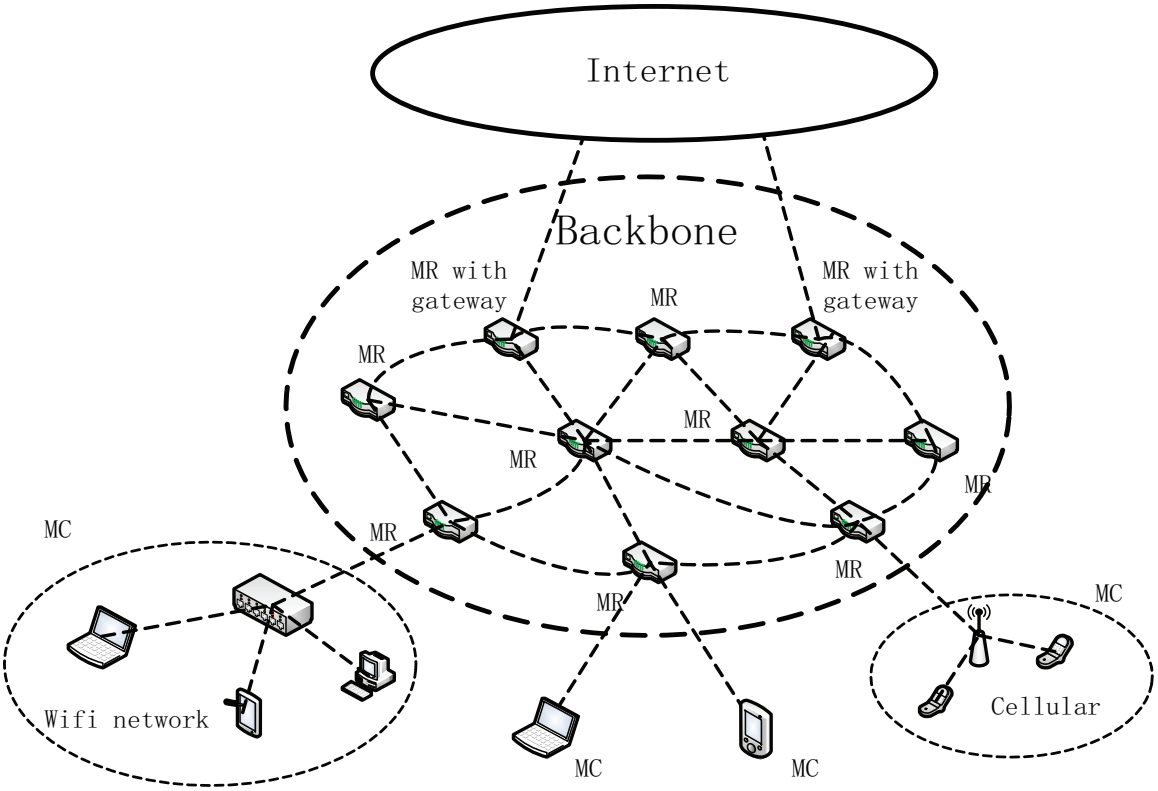

Figure 1.2: Illustration of an infrastructure wireless mesh network

Literature Review

Augmenting RF WMN with FSO links to improve the throughput has been previously explored in [29, 30, 31, 32, 33]. In [29] a mixed integer linear program (MILP) is introduced to obtain the optimal placement of FSO links. The authors assume the RF interference model is given as an input to the problem. This decoupling of the RF interference with the FSO link placement approach misses one of the fundamental advantages of using FSO technology, which is the strategic decrease in the RF interference level in the network achievable by servicing heavy traffic through the FSO subnetwork instead. There are two fundamental ways the network throughput is improved by adding FSO links: by the presence of potentially very high data rate links, and by the reduction of RF interference. Therefore, including an accurate RF interference model into the design of hybrid RF/FSO mesh networks is crucial.

There have been several studies on hybrid FSO/RF networks using different models for other research goals than those addressed here. Wang and Abouzeid [30] derived an upper bound on the per-node capacity of the hybrid FSO/RF network. In their model, some RF nodes are equipped with an additional FSO transceiver and RF and FSO transceivers are able to operate with different data rates. They prove that their capacity upper bound is asymptotically achievable using a hybrid routing scheme for a random network. However, it may not be possible to apply these asymptotic results to practical WMNs. The node reliability and availability of reconfigurable hybrid FSO/RF mesh networks are investigated in [31]. In [32], FSO links are added to WMNs when the number of RF channels is insufficient for the traffic, with a goal of maintaining a minimum network throughput using the smallest number of FSO links when unacceptable RF interference occurs. However, throughput optimization is not addressed. The authors in [33] provide a routing framework for hybrid FSO/RF networks by assigning priority to certain traffic, and establish backup routes for a fraction of the traffic. In their model, each node is equipped with both RF and FSO transceivers, which may be impractical due to the cost of FSO links and their line-of-sight requirement; however, we show that only a small number of FSO links is needed for a given throughput requirement. In [40], the authors assume an FSO network forms the upper tier backbone network. The authors propose two algorithms. The first algorithm aims minimize the number of clusters while the second one focuses on topology optimization. In [41], the authors present a topology control scheme based on RF and FSO transmitter power and optical beam-width adjustments to meet the QoS requirements, specifically end-to-end delay and throughput. The authors of [42] propose to the use FSO links in building hybrid FSO/RF gateway architecture to supplement the performance of existing wireline gateways. The goal is to minimize the number of added FSO links to satisfy the pre-defined capacity requirement.

Contributions and Conclusions

The major contributions and conclusions of the centralized hybrid FSO/RF WMN research are as follows.

We begin by describing our network model of the hybrid FSO/RF backbone model. Previous work on WMNs only considers quasi-static network models, in which all channel gains are known. In reality, fading can severely affect both FSO and RF link qualities. Thus, a modified optimization method needs to be developed for fading networks. In our work, we formulate the link allocation, routing and scheduling problem based on either the protocol interference model or the physical interference model, addressing both nonfading and fading cases.

In Section 3.3 we use a mixed integer linear program (MILP) to formulate the throughput optimization problem. Formulations for both quasi-static and fading networks are derived in this section. Since the only difference between the two formulations is the link capacity constraint, the MILPs can be solved in the same manner. By solving these MILPs, we can jointly solve the FSO link allocation, throughput optimization, routing, and scheduling problems. We address methods for finding exact solutions and upper bounds to the optimal throughput in Section 3.4. In order to solve the problem in a reasonable time for large network, two heuristic methods are also provided in this section.

The numerical results in Section 3.5 lead us to draw the following important conclusions. First, since the modeling of the physical link is more accurate by using the physical model, the routing is more robust and results in higher network throughput by using the physical model instead of the protocol model. Second, we show that our heuristic method is efficient in obtaining a near-optimal result for a mid-size network with many traffic demands. Lastly, we show numerical result for fading networks, where the influence of FSO and RF link outage probabilities are studied. An important conclusion is that higher FSO link outage probability results in lower throughput

while higher RF link outage probability does not necessary imply throughput degradation.

1.3.3 Distributed FSO/RF Network

In chapter 4, we model and study distributed routing options for FSO/RF networks. This part of the research provides a viable routing solution for relatively large hybrid FSO/RF networks in practice, where centralized algorithms become too complex to scale practically.

Literature Review

There are only a few papers on distributed FSO/RF network routing reported in current literature. In [43], the authors propose a Layer 1 restoration protocol for fast link recovery. The main purpose of that research is to maintain network availability of hybrid FSO/RF networks. In [44], the implementation of hybrid FSO/RF network for mobile ad-hoc networks is studied. The paper presents an FSO link acquisition algorithm for mobile application. The paper also proposes a hierarchical routing algorithm. The experimental results in the paper are based on a small network with only two hybrid and two RF nodes. The routing algorithm proposed in the paper is not optimized for hybrid FSO/RF applications, i.e., the algorithm does not take advantage of having both high-throughput FSO links and reliable RF links. Similarly, in [45] the protocol proposed does not consider the physical layer property of FSO links. In the simulation result, the assumption that the channel capacity of all links is set to the same value (2 Mbps) does not seem realistic for hybrid FSO/RF networks. In [46], the authors show some preliminary results characterizing hybrid FSO/RF links in WMN for routing. A Bayesian-based game-theoretic model is used to guarantee cooperativeness in hybrid FSO/RF networks in [47]. The authors use a pricing scheme in which each destination node pays a price to the source node in order to acquire a

reliable connection. The special case of FSO/RF military communication networks is modeled and discussed in [48].

There is other research focusing on pure FSO networks. Zhang proposes the architecture of broadband FSO WMNs in [49]. In [50], a mixed integer linear program is formulated to choose the optimal routes for traffic demands such that FSO network congestion is minimized. Autonomous reconfiguration, protection strategies, and fault avoidance of FSO networks are studied in [51, 52, 53, 54]. The routing problem in degree constrained FSO WMNs is addressed in [55]. Topology control of FSO networks is studied in [56].

Contributions and Conclusions

In this dissertation we present a distributed routing algorithm for hybrid FSO/RF network to improve network throughput. The algorithm is designed for hybrid FSO/RF network application such that the advantages of high throughput FSO links and reliable RF links are highlighted. Various simulation results for different size networks are also provided. As a preliminary study in this area, we provide a realistic model to guide the design of broadband FSO/RF applications. It is worth mentioning that our simulation program is customized, rather than using existing network simulation software such as NS-2. Since our model is optimized for hybrid FSO/RF applications, we need to program our own algorithm instead of using existing software that is only suitable for RF networks.

The distributed algorithms consists of two stages: a clustering part in which nodes establish local groups, and a routing part in which routing tables are formed. In Section 4.2.1 we describe our network model including the assumption of both FSO and RF links. Then the clustering algorithm based on exchanging 'hello' message is shown in Section 4.2.2. Our algorithm prioritizes the nodes with FSO links so that network clustering is suitable for hybrid FSO/RF WMNs. Our simulation results show that

even with large networks, it usually requires no more than 10 'hello' message exchanges to obtain algorithm convergence. The routing is described in Section 4.2.3. We first compare the throughput of the network with and without FSO links to show that introducing high throughput FSO links can increase the network throughput dramatically. Then we compare the throughput of the network based on our clustering algorithm with that of using other clustering algorithms that do not distinguish between FSO and RF links. The simulation results show that by using our clustering algorithm, which is designed for hybrid FSO/RF applications, the throughput of the network can be improved, depending on the number of FSO links.

1.4 Thesis Organization

This is a brief summary of the topics that are covered in each chapter.

Chapter 2 describes point-to-point hybrid FSO/RF communication systems. Theoretical throughput and methods to approach this throughput are discussed.

Chapter 3 models the centralized hybrid FSO/RF WMN. The network throughput and routing optimization problems are formulated and solved using mixed integer linear programming and heuristic methods.

Chapter 4 presents a distributed routing algorithm for hybrid FSO/RF WMNs. Detailed simulation results are provided to guide real world implementations.

Chapter 5 summarizes the dissertation and outlines possible future work.

Chapter 2

Point to Point Hybrid FSO/RF System

Broadband wireless communication has many advantages over wired systems, such as ease in deployment, mobility, and lower installation cost. Channel diversity techniques relying on multiple parallel links have been used to improve the throughput and reliability of wireless channels. We are interested in systems consisting of independent parallel channels, possibly through the use of different technologies, creating a heterogeneous system. Each channel in these systems can have a different symbol rate and modulation scheme. In this chapter we propose an adaptive transmission technique to maximize the throughput of these noninterfering parallel channel systems. We then show how this approach can be applied to hybrid FSO/RF systems to adaptively exploit the presence of both links.

2.1 Introduction

As we mentioned in Chapter 1, hybrid FSO/RF systems have been proposed to address the considerable demand for wireless bandwidth and link reliability requirement. Conventionally these systems only use the RF channel as a backup when the FSO

channel is weak, having to frequently switch between the two channels depending on variations in the channel conditions. Though simple, this non-adaptive technique results in an inefficient use of resources, especially when significant fading occurs. Instead, we propose a symbol rate and modulation adaptive jointly encoded scheme for the FSO/RF hybrid system where both the FSO and RF subsystems are simultaneously active.

In heterogeneous networks, each channel may have its own individual properties, such as different modulation types and symbol rates. The FSO system typically uses a pulse-based modulation, such as on-off-keying (OOK) or pulse position modulation (PPM), with hardware that can support multiple Gsps. The RF channel is more flexible in its modulation, including modulating the phase, such as in phase-shift-keying (PSK) and quadrature amplitude modulation (QAM), yet can typically support symbol rates no higher than a few hundred Msps. These relatively lower rates can be due to a low received SNR if operating at a high carrier frequency, such as 60 GHz, or due to a limited practical fractional bandwidth if operating with a carrier less than 5 GHz. The specific choices for modulation and symbol rates are crucial to the design of an efficient outage-free parallel channel system.

In this chapter, we adapt the modem symbol rate and modulator constellation to respond to link conditions, as opposed to power control as in most previous work [57, 58, 59, 60]. Our primary interest is in infrastructure links which are grid-connected, and thus power conservation is less important. We also note that in heterogeneous (mixed technology) applications, received power on the different channels have different 'cost', so optimizing total power consumption is not straight-forward. Instead we operate transmitters at maximum power as determined by the technology, and adjust the signaling strategy to maximize throughput. While adapting symbol rate and modulation does have its operational issues, specifically changing spectrum

occupancy and modem reconfiguration, we see these as quite manageable on slowly-varying links, particularly in unlicensed spectrum applications.

We formulate the throughput optimization problem and solve for the parameters yielding the maximum throughput for two independent parallel channels when the channel state is known at the transmitter. The formulation is based on channel capacity and is independent of any particular coding scheme or statistical channel model. We view the parallel hybrid channel as a resource for delivering a single message, encoded for the hybrid channel by a single channel encoder. We also enforce minimum encoder rate and upper-bounds on bandwidth as would be necessary for actual implementation. The maximum throughput solution for given channel conditions includes the optimal values for the fraction of the codeword to be sent through each channel, the symbol rates and modulations to be employed by the two modems, and the encoder rate. Based on our formulation, we propose a communication scheme resulting in a capacity-approaching and seamless jointly-encoded system, and show the advantage of adaptation compared to a fixed system implementation.

The remainder of the chapter is organized as follows. The system model and design variables are presented in Section 2.2. Assumptions on the channel capacity are also given. Section 2.3 formulates and solves the throughput optimization problem *without* bandwidth constraints. Sections 2.4 discusses the adaptation of design parameters under bandwidth constraints. Numerical results for a practical hybrid FSO/RF system are given in Sections 2.3 and 2.4. Section 2.5 summarizes the chapter and suggests opportunities for future work.

2.2 System Model

In this section we describe the system model and the underlying assumptions. Since the hybrid FSO/RF system we are interested in is non-mobile, the two parallel inde-

pendent channels are assumed to be quasi-static. For our models, the channel state (CS) for channel i, CS_i, refers to the received signal power P_{s_i} and receiver noise power density N_{0_i}. Due to the slowly time-varying nature of the channels, we can assume that the exact CS is known at both ends; for the transmitter to adapt to current channel conditions a feedback link is necessary from the receiver providing estimates of the CS. The code rate, modulations and symbol rates can then be adjusted dynamically at the transmitter and the signal can be optimally decoded at the receiver. We further assume that the channel is memoryless (conditioned on the input), resulting in no intersymbol interference or other memory effects.

2.2.1 Joint Error Control Coding

Figure 2.1 depicts a block diagram of the system. The channels are arbitrarily labeled with subscripts '1' and '2'; channel 1 is equated below with the FSO link and channel 2 with the RF link. k information bits enter the joint system, and are encoded to an n-bit codeword by a single encoder with a low-rate mother-code having rate $r = k/n$. A code of higher rate r/α, $r \leq \alpha \leq 1$, can be achieved by puncturing the mother-code to $k \leq n^{'} \leq n$ bits, where the puncturing ratio is defined as $\alpha = n'/n$. We fix the mother-code rate r and vary the puncturing ratio α to adjust the actual encoder rate r/α. The codeword is then partitioned into two vectors of length n_1 and n_2 such that $n' = n_1 + n_2$; n_1 and n_2 bits are transmitted through channels 1 and 2, respectively.

The modulations and modem symbol rates chosen, which depend on the channel conditions, determine the best α and the allocation of n_1 and n_2. $(\mathcal{M}_1, \mathcal{M}_2) \in \mathbf{M}_1 \times \mathbf{M}_2$ represent the modulation schemes for the two channels, where $\mathbf{M}_i$ denotes the set of candidate modulations for channel i. A modulated symbol on channel i carries $m_i = \log_2 |\mathcal{M}_i|$ coded bits. Modem equipment for channel i operates with

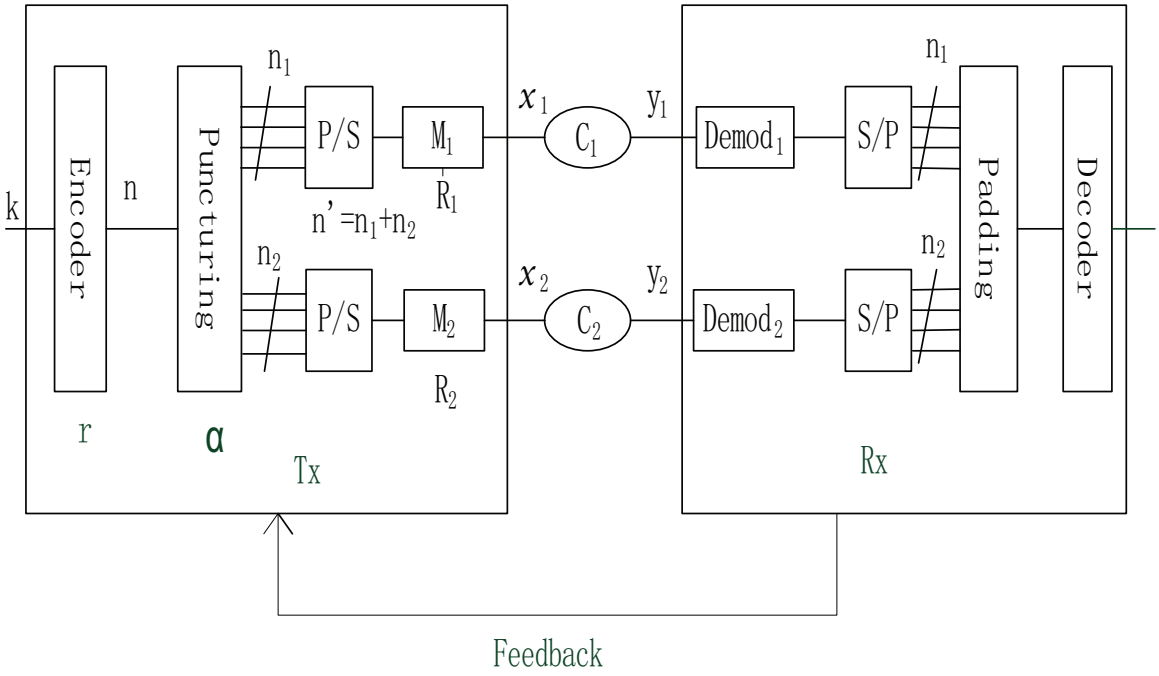

Figure 2.1: System block diagram showing two parallel channels. P/S is a parallel to serial converter.

symbol rate R_i sps, $i = 1, 2$. We assume a synchronous operation on the parallel channels, which implies

$$\frac{n_1}{n_2} = \frac{R_1 \log_2 |\mathcal{M}_1|}{R_2 \log_2 |\mathcal{M}_2|} = \frac{R_1 m_1}{R_2 m_2}. \tag{2.1}$$

This constraint ensures each portion of the codeword is received in the same time interval. We define a frame for the first channel to contain $L_1 = n_1/m_1$ symbols and a frame for the other to contain $L_2 = n_2/m_2$ symbols. The frame rate is therefore

$$F = \frac{R_1}{L_1} = \frac{R_2}{L_2} \quad \text{frames/sec.} \tag{2.2}$$

2.2.2 Channel Capacity Assumptions

Let us denote the two sub-channel instantaneous capacities as C_1 and C_2, both measured in bits/modulator symbol. For convenience, in our notation we suppress the functional dependence of the capacity of each channel on the symbol rate R_i and

modulation $\mathcal{M}_i$ for a given channel state CS_i, and write

$$C_i \doteq C_i[R_i, \mathcal{M}_i|\text{CS}_i],\ i = 1,\ 2, \quad \text{bits/modulator symbol.} \tag{2.3}$$

Thus the individual channel capacity (maximum reliable throughput) in bits/sec can be written as

$$\mathcal{T}_i = R_i C_i \text{ bits/sec.} \tag{2.4}$$

Given this notation, our optimization procedure is applicable to channels that satisfy the following four assumptions for a specific modulation and CS_i:[1]

1. $\frac{dC_i}{dR_i} \leq 0$;
2. $\frac{d\mathcal{T}_i}{dR_i} > 0$
3. $\frac{d^2\mathcal{T}_i}{dR_i^2} \leq 0$;
4. There exists a nonnegative R_i such that $\frac{d\mathcal{T}_i}{dR_i} > rm_i$.

These assumptions are required for our optimization and are generally valid for a broad class of channel models. For example, channels of interest for the hybrid FSO/RF system satisfy these conditions, as shown below.

RF Channel: For the RF channel, we use the discrete-input continuous-output memoryless (DCM) additive white Gaussian noise (AWGN) channel model as an example. In this model, the symbol SNR decreases as the symbol rate increases for a fixed power and noise level. Thus, channel capacity C_i in bits/symbol is a non-increasing function of R_i, i.e., $\frac{dC_i}{dR_i} \leq 0$. The other assumptions are shown numerically. The capacity $\mathcal{T}_i$ in bits/sec is plotted in Figure 2.2 as a function of symbol rate R_i for various modulations over an AWGN channel.[2] We denote a small change in symbol rate ΔR_i , while $\Delta\mathcal{T}_i$ represents the corresponding difference in the capacity.

[1] Note that for a given modulation and CS_i, C_i and $\mathcal{T}_i$ are only functions of R_i.

[2] The interested reader is referred to [61] for channel capacity calculations.

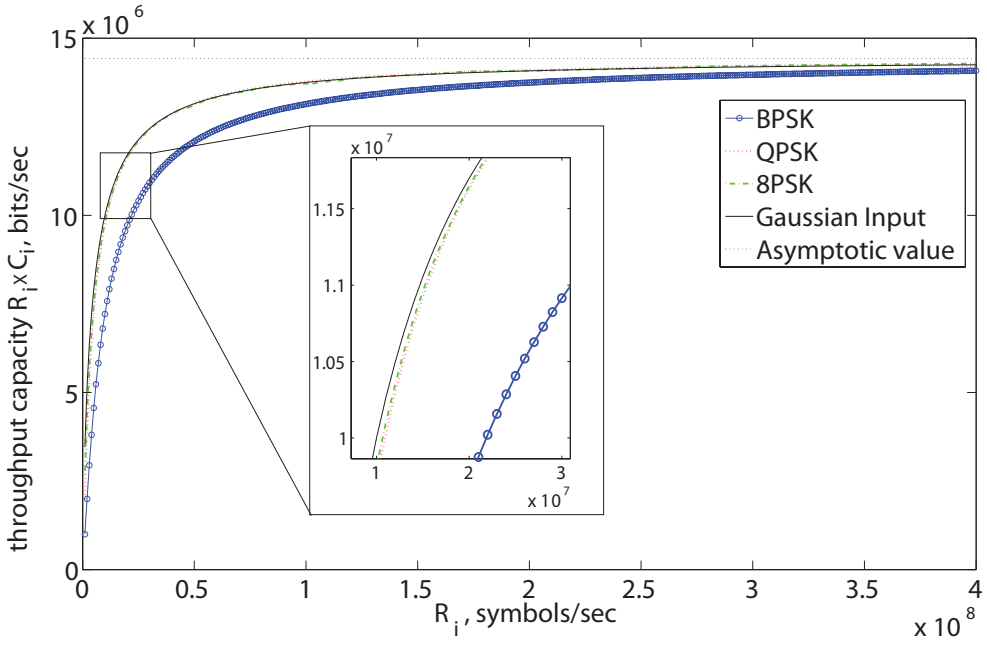

Figure 2.2: Capacity $\mathcal{T}_i$ in bits/sec as a function of R_i for various modulations over an AWGN channel with $\frac{P_s}{N_0} = 10^7$ sec^{-1}.

Numerically, we can see that $\mathcal{T}_i$ increases as R_i increases and $\Delta\mathcal{T}_i/\Delta R_i$ decreases as R_i increases. These imply assumptions 2) and 3) are valid. Note that a change in the CS would only result in scaling of the x-axis, with no change in the shape of the function.

Since for a fixed CS$_i$ and finite alphabet modulation, C_i approaches a constant m_i as R_i decreases, we find that $d\mathcal{T}_i/dR_i$ converges to m_i for small R_i. Thus for any $r < 1$, assumption 4) holds.

Note that assumptions 1) to 3) are simple to validate for the AWGN channel with Gaussian channel inputs, since the capacity has a simple closed form expression of $C_i = \log_2(1+X)$ bits/symbol, where $X = \frac{P_{s_i}}{N_{0_i} R_i}$. The capacity in bits/sec, $\mathcal{T}_i$, satisfies assumptions 2), 3), since

$$\frac{d\mathcal{T}_i}{dR_i} = \frac{1}{\ln(2)} \left[\ln(1+X) - \frac{X}{1+X} \right] > 0, \; X > 0, \tag{2.5}$$

and $\frac{d^2\mathcal{T}_i}{dR_i^2} < 0$. Assumption 4) does not apply to the Gaussian input case, since the alphabet is not finite.

FSO Channel: The FSO channel can either be modeled as Gaussian, as above, or as Poisson, depending on the dominant noise mechanism. For the Poisson case, we consider 2^{m_i}-ary PPM as in [3], where an optical pulse is sent in one of 2^{m_i} slots. If we assume negligible background radiation and photon-counting reception, the capacity of the FSO channel can be expressed as

$$C_i = m_i(1 - e^{-\frac{\eta P_{s_i}}{hfR_i 2^{m_i}}}) \text{ bits/symbol.} \tag{2.6}$$

Here η represents the detector's quantum efficiency, h is Planck's constant and f denotes the optical carrier frequency. It is clear that the capacity is a non-increasing function of R_i. We can also easily verify that $\frac{d\mathcal{T}_i}{dR_i} > 0$ and $\frac{d^2\mathcal{T}_i}{dR_i^2} < 0$. Also $\frac{d\mathcal{T}_i}{dR_i}$ again approaches m_i for small symbol rate.

2.3 Throughput Optimization Without Bandwidth Constraint

Our objective is to maximize the parallel channel throughput for reliable communication for given channel conditions by setting system parameters, namely α, R_i, and $\mathcal{M}_i$, to optimal values. The optimization procedure derived in this work is suitable for channels which satisfy the conditions described in Section 2.2.2. For simplicity, we first optimize the throughput for channels not subject to bandwidth (or symbol rate) constraints in this section. The method developed here is extended in Section 2.4 to a more practical model that includes bandwidth constraints.

2.3.1 Formulation

The noisy channel coding theorem of information theory asserts that reliable communication is possible as block length becomes large if the information rate in bits/second is less than the available capacity (also in bits/second) for the channel. The sum capacity of the parallel channel can be written as[3]

$$C_{\text{sum}} = L_1 C_1 + L_2 C_2 \quad \text{bits/frame.} \tag{2.7}$$

The conditional sum capacity in bits/second associated with a choice of symbol rates (R_1, R_2) and modulations $(\mathcal{M}_1, \mathcal{M}_2)$, for given channel conditions, is denoted $\mathcal{T}$ and given by

$$\begin{aligned} \mathcal{T}(R_1, R_2, \mathcal{M}_1, \mathcal{M}_2 | \text{CS}_1, \text{CS}_2) &= C_{\text{sum}} F = R_1 C_1 + R_2 C_2 \\ &= \mathcal{T}_1 + \mathcal{T}_2 \text{ bits/sec.} \end{aligned} \tag{2.8}$$

(Recall that C_i depends on R_i for a given channel condition and choice of modulation.) Given this available conditional capacity, the goal is to maximize the actual *achieved* throughput of the parallel channel system, T, which can be written as

$$T(r, \alpha, R_1, R_2, \mathcal{M}_1, \mathcal{M}_2) = \frac{r}{\alpha}(R_1 m_1 + R_2 m_2) \text{ bits/sec.} \tag{2.9}$$

Our design for reliable communication, in light of the channel coding theorem, requires that

$$T(r, \alpha, R_1, R_2, \mathcal{M}_1, \mathcal{M}_2) \leq \mathcal{T}(R_1, R_2, \mathcal{M}_1, \mathcal{M}_2 | \text{CS}_1, \text{CS}_2). \tag{2.10}$$

Since we propose to use a joint encoder supplying bits to both subsystems, each subsystem need not satisfy its individual capacity – only the joint parallel system throughput must be bounded.

[3]Note the two channels are non-coupled and statistically independent.

Now, the problem can be formalized as

$$\max_{\alpha, R_1, R_2, \mathcal{M}_1, \mathcal{M}_2} T \quad \text{for given CS}_i \text{ and a fixed } r \tag{2.11}$$

subject to

$$\frac{r}{\alpha}(R_1 m_1 + R_2 m_2) \leq \mathcal{T}_1 + \mathcal{T}_2 \tag{2.12}$$

$$r \leq \alpha \leq 1 \tag{2.13}$$

Note that the constraint $\alpha \geq r$ in (2.13) can be removed; since $C_i \leq m_i$, (2.12) already guarantees $r/\alpha \leq 1$. We provide a geometric interpretation of the constraints in Section 2.4.

2.3.2 Solution

Since the above optimization problem is mixed discrete and continuous, the optimal solution is obtained as follows:

1. We temporarily fix the modulation schemes for both channels and find the optimal operating symbol rates and puncturing ratio. We then evaluate various candidate modulation pairs to choose a combination that results in the highest throughput. This exhaustive method over all candidate modulations ($\mathcal{M}_1$, $\mathcal{M}_2$) $\in \mathbf{M}_1 \times \mathbf{M}_2$ is practical, since the number of candidates is small in general. Thus the objective function becomes

$$\max_{\alpha, R_1, R_2} T \quad \text{for given CS}_i \text{ and modulations.} \tag{2.14}$$

2. Function (2.14) is also non-convex. We first prove that the optimal symbol rates are always located on the boundary $\frac{r}{\alpha}(R_1 m_1 + R_2 m_2) = \mathcal{T}_1 + \mathcal{T}_2$ for any fixed α. Then, we prove $\alpha = 1$ is optimal. By doing this, the optimization problem

for given modulations can be converted to an equivalent convex problem. The conclusion implies that no puncturing is needed in this case. Note that, although we operate at the lowest encoder rate ($r/\alpha = r$), the throughput of the joint system is maximum. This is because both channels can operate at higher symbol rates in this situation (no bandwidth constraint).

For given α and modulation schemes (i.e. α and m_i are constant), the optimization problem with constraint (2.12) is convex, since $\mathcal{T}_i$ is $\cap$-convex by assumption 3) in Section 2.2.2, and since $R_i m_i$ is linear. We can use the Lagrange method [62] to find the optimal symbol rates. Define the Lagrangian

$$L(R_1, R_2) = \frac{r}{\alpha}(R_1 m_1 + R_2 m_2) - \lambda \left[\frac{r}{\alpha}(R_1 m_1 + R_2 m_2) - (\mathcal{T}_1 + \mathcal{T}_2)\right], \tag{2.15}$$

where λ is the Lagrange multiplier. The optimal symbol rates and encoder rate can be found by solving

$$\begin{aligned} \frac{\partial L}{\partial R_1} = \frac{r}{\alpha} m_1 - \lambda \frac{r}{\alpha} m_1 + \lambda \frac{d\mathcal{T}_1}{dR_1} &= 0 & (2.16)\\ \frac{\partial L}{\partial R_2} = \frac{r}{\alpha} m_2 - \lambda \frac{r}{\alpha} m_2 + \lambda \frac{d\mathcal{T}_2}{dR_2} &= 0 & (2.17)\\ \lambda \left[\frac{r}{\alpha}(R_1 m_1 + R_2 m_2) - (\mathcal{T}_1 + \mathcal{T}_2)\right] &= 0 & (2.18) \end{aligned}$$

where (2.18) is a complementary slackness condition. $\lambda \neq 0$ by contradiction. Thus the optimal symbol rates are located on the boundary $\frac{r}{\alpha}(R_1 m_1 + R_2 m_2) = \mathcal{T}_1 + \mathcal{T}_2$ for a given α and modulation.

The conclusion claims that we should operate at capacity $\mathcal{T}_1 + \mathcal{T}_2$, which seems trivial. However, it leads to an important fact. Suppose for given $\tilde{\alpha}$ and $\tilde{\tilde{\alpha}}$, the optimal symbol rates are $(\tilde{R}_1, \tilde{R}_2)$ and $(\tilde{\tilde{R}}_1, \tilde{\tilde{R}}_2)$, respectively. If $\tilde{R}_i \leq \tilde{\tilde{R}}_i$ for $i = 1, 2$, then $\tilde{T} \leq \tilde{\tilde{T}}$, where $\tilde{T}$ and $\tilde{\tilde{T}}$ denote the maximum throughput for $\tilde{\alpha}$ and $\tilde{\tilde{\alpha}}$,

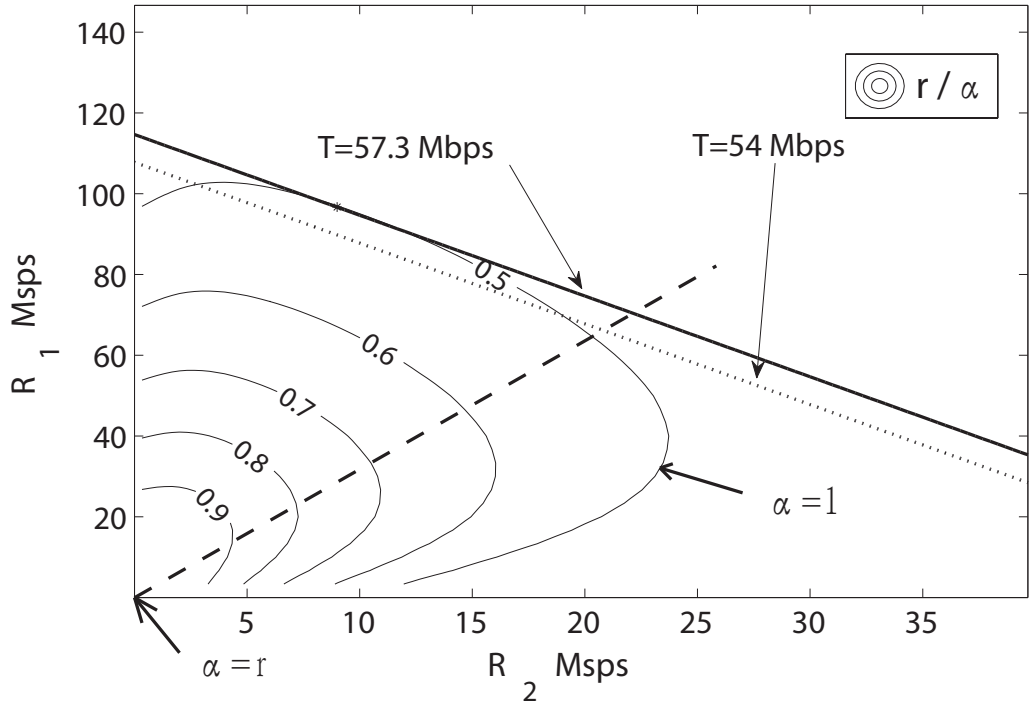

Figure 2.3: Contour plot of encoder rate $\frac{r}{\alpha}$ satisfying the equality of (2.12) for $r = 0.5$. The solid straight line is tangent to the $r = 0.5$ contour with $T = 57.3$ Mbps; FSO uses BPPM with $\frac{P_{s_1}}{N_{0_1}} = 10^8$ sec^{-1}; RF uses QPSK with $\frac{P_{s_2}}{N_{0_2}} = 10^7$ sec^{-1}. The dotted line corresponds to $T = 0.94 \times 57.3$ Mbps. The thick dashed line denotes an arbitrary line $R_2 = bR_1$ for some slope b.

respectively. This is because for a given α, the maximum $T = \mathcal{T}_1 + \mathcal{T}_2$, and $\mathcal{T}_i$ is a non-decreasing function of R_i.

Based on the above fact, if the following proposition is valid, we can claim that the optimal symbol rates, the solution to problem (2.11)-(2.13), are located on the curve $r(R_1 m_1 + R_2 m_2) = \mathcal{T}_1 + \mathcal{T}_2$, i.e., the optimal $\alpha = 1$.

Proposition: For every $(\tilde{R}_1, \tilde{R}_2)$ satisfying $\frac{r}{\alpha}(\tilde{R}_1 m_1 + \tilde{R}_2 m_2) = \mathcal{T}_1[\tilde{R}_1] + \mathcal{T}_2[\tilde{R}_2]$, for a given α, $r \leq \alpha < 1$, there exists a pair $(\tilde{\tilde{R}}_1, \tilde{\tilde{R}}_2)$ satisfying $r(\tilde{\tilde{R}}_1 m_1 + \tilde{\tilde{R}}_2 m_2) = \mathcal{T}_1[\tilde{\tilde{R}}_1] + \mathcal{T}_2[\tilde{\tilde{R}}_2]$ (i.e. $\alpha = 1$) such that $\tilde{R}_i \leq \tilde{\tilde{R}}_i$ for $i = 1, 2$.

Proof: Suppose $(\tilde{R}_1, \tilde{R}_2)$ is an arbitrary point on the curve defined by $\frac{r}{\alpha}(R_1 m_1 + R_2 m_2) = \mathcal{T}_1 + \mathcal{T}_2$ on the plane $((R_1, R_2) \in \mathbf{R}_+^2)$, for a given $r \leq \alpha < 1$. As shown in Figure 2.3, define a straight line that crosses both the origin and $(\tilde{R}_1, \tilde{R}_2)$ as $R_2 = bR_1$,

where $b = \tilde{R}_2/\tilde{R}_1$. Thus,

$$\frac{r}{\alpha}(m_1 + bm_2) = C_1[\tilde{R}_1] + bC_2[b\tilde{R}_1], \tag{2.19}$$

where we explicitly show the capacity C_i as a function of the rate R_i. Let $(\tilde{\tilde{R}}_1, \tilde{\tilde{R}}_2)$ be the intersection of line $R_2 = bR_1$ and the curve $r(R_1m_1 + R_2m_2) = \mathcal{T}_1 + \mathcal{T}_2$, i.e., for $\alpha = 1$. Thus $\tilde{\tilde{R}}_1$ satisfies

$$r(m_1 + bm_2) = C_1[\tilde{\tilde{R}}_1] + bC_2[b\tilde{\tilde{R}}_1]. \tag{2.20}$$

From (2.19) and (2.20), we obtain:

$$\alpha = \frac{C_1[\tilde{\tilde{R}}_1] + bC_2[b\tilde{\tilde{R}}_1]}{C_1[\tilde{R}_1] + bC_2[b\tilde{R}_1]}. \tag{2.21}$$

Since $\alpha \leq 1$ and C_i is a non-increasing function of R_i, $\tilde{R}_1 \leq \tilde{\tilde{R}}_1$. Similarly, $\tilde{R}_2 \leq \tilde{\tilde{R}}_2$. Thus, $\alpha = 1$ results in the largest (R_1, R_2) pair, and the largest throughput T by assumption 2). □

Thus, for specific modulation choices, maximizing T with a mother-code rate constraint is equivalent to solving

$$\max_{R_1,R_2} \; r(R_1m_1 + R_2m_2) \tag{2.22}$$

with equality constraint

$$(\mathcal{T}_1 + \mathcal{T}_2) - r(R_1m_1 + R_2m_2) = 0, \tag{2.23}$$

where the optimal encoder rate is $r/\alpha = r$ without puncturing. The problem can again be solved using the Lagrange method, yielding optimal symbol rates that satisfy

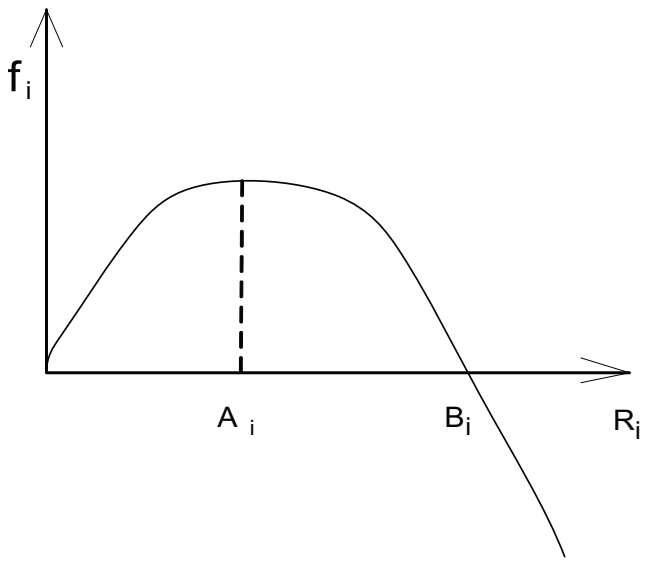

Figure 2.4: $f_i(R_i)$ defined in (2.25) as a function of R_i.

.

(2.23) and

$$\frac{1}{m_1}\frac{d\mathcal{T}_1}{dR_1} = \frac{1}{m_2}\frac{d\mathcal{T}_2}{dR_2}. \tag{2.24}$$

Next we prove that there exists a unique optimal symbol rate pair, denoted as (R_1^*, R_2^*), satisfying (2.23) and (2.24). A search method is embedded in the proof.

Let us define

$$f_i(R_i) = R_i C_i - rR_i m_i = \mathcal{T}_i - rR_i m_i. \tag{2.25}$$

Based on the channel capacity assumptions in Section 2.2.2, $f_i(R_i)$ has the form illustrated in Figure 2.4. From (2.25),

$$\frac{df_i}{dR_i} = \frac{d\mathcal{T}_i}{dR_i} - rm_i. \tag{2.26}$$

Let A_i and B_i denote the symbol rates such that $\frac{d\mathcal{T}_i}{dR_i}|_{R_i=A_i} = rm_i$ and $C_i[R_i]|_{R_i=B_i} = rm_i$, respectively. $f_i(R_i)$ is maximized when $R_i = A_i$ and $f_i(R_i) = 0$ when $R_i = B_i$ and $R_i = 0$, as shown in Figure 2.4. For every $R_i \in [0, A_i)$, there exists a $R_i \in (A_i, B_i]$ yielding the same $f_i(R_i)$, due to the continuity of $f_i(R_i)$. Since the objective function

in (2.22) is monotone-increasing in R_i, the optimal R_i lies in the range $[A_i, \infty)$, which implies

$$\frac{d\mathcal{T}_i}{dR_i} \leq r m_i, \tag{2.27}$$

based on (2.26).

In our search algorithm, we initially set $R_1 = B_1$ and $R_2 = B_2$ (an obvious solution of (2.23)). Without loss of generality, assume $\frac{1}{m_i}\frac{d\mathcal{T}_1}{dR_1}|_{R_1=B_1} < \frac{1}{m_2}\frac{d\mathcal{T}_2}{dR_2}|_{R_2=B_2}$. Since both $f_i(R_i)$ and $\frac{d\mathcal{T}_i}{dR_i}$ are monotone functions of R_i, we have to decrease R_1 and increase R_2 to achieve equality in both (2.23) and (2.24). Based on the inequality (2.27), when $R_1 = A_1$,

$$\frac{1}{m_1}\frac{d\mathcal{T}_1}{dR_1} = r \geq \frac{1}{m_2}\frac{d\mathcal{T}_2}{dR_2}. \tag{2.28}$$

Thus the optimal symbol rate pair (R_1^*, R_2^*) exists and is unique. The search algorithm terminates before R_1 reaches A_1.

The optimization of symbol rates as a function of the known instantaneous channel states is performed as described above for each pair of modulation schemes $(\mathcal{M}_1, \mathcal{M}_2)$. The optimal throughput for each pair of candidate modulation schemes can be computed and the best pair chosen.

2.3.3 Application to FSO/RF System

The optimization of symbol rates and puncturing ratio is illustrated by applying it to a hybrid FSO/RF system with fixed modulation schemes. Modulation adaptation is shown in the next section for the more practical case where the symbol-rate is constrained. For simplicity, an AWGN model is used for both channels, assuming the FSO system to be thermal-noise-limited. We assume the FSO channel adopts binary PPM (BPPM) with $\frac{P_{s_1}}{N_{0_1}} = 10^8$ sec^{-1}, while quadrature PSK (QPSK) is used for the RF channel with $\frac{P_{s_2}}{N_{0_2}} = 10^7$ sec^{-1}. We adopt a mother-code rate $r = 1/2$ with no puncturing as was shown above to be optimal. Figure 2.3 shows how the throughput

contours of (2.22) meet the constraint contour of (2.23) as tangents at the optimum rates. The optimal symbol rates are located on the constraint boundary (2.23). In this case, the optimal throughput $T = 57.3$ Mbps with $R_1 = 96.7$ Msps and $R_2 = 9$ Msps. The algorithm makes the best of these limited channel conditions.

The optimization procedure outlined here does not reveal how sensitive the performance is to choosing the correct rate pairs. To illustrate the sensitivity of the design to these parameter choices, a simulation of the bit error rate (BER) is shown in Figure 2.5 for a hybrid system using a fixed rate 6% below capacity, as the rates of the two channels vary. The total throughput is held constant at $T = 0.94 \times 57.3$ Mbps, i.e., the values of (R_1, R_2) fall on a line parallel to and below the tangent contour at the optimum point, as drawn in Figure 2.3. A regular (64800, 32400) low density parity check (LDPC) code is used, making the results code-dependent but representative of a realistic implementation. The error performance degrades rapidly as the symbol rates deviate from their optimal values because the attempted throughput eventually exceeds capacity. This can be seen in Figure 2.3 where the straight line of constant throughput comes close to and eventually violates the below-capacity rate-region defined for encoder rate $r = 1/2$.

In [25], the authors present a density evolution design strategy for LDPC codes to be used on the hybrid FSO/RF channel. For a particular LDPC code, they conclude that for medium quality optical links, allocating a small fraction of code bits to the RF channel can reduce the optical link's density evolution threshold significantly. According to our method, the optimal allocation of n_1 and n_2 can be calculated [through (2.1)] and this can be used in the algorithm in [25] to find the optimal system parameters for the hybrid system.

In practice, channel properties, hardware limitations and standard regulations impose symbol rate or bandwidth constraints that affect the choice of system param-

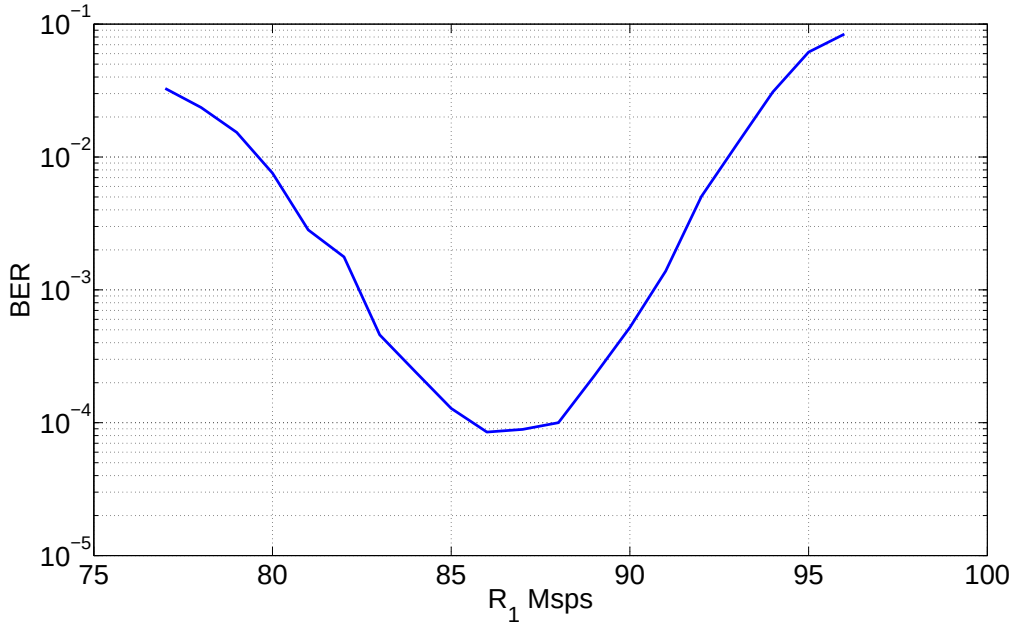

Figure 2.5: Simulation showing the bit error probability (BER) of the hybrid system using a (64800, 32400) LDPC code as the symbol rate R_1 varies for a constant total throughput $T = 0.94 \times 57.3 = 54$ Mbps. The FSO signal is BPPM modulated and the RF signal is QPSK modulated, with $\frac{P_{s_1}}{N_{0_1}} = 10^8$ sec^{-1}, $\frac{P_{s_2}}{N_{0_2}} = 10^7$ sec^{-1}.

eters. In cases where the optimal rate R_1^* or R_2^* above is not practically achievable, finding the optimal throughput becomes more difficult, as shown in the next section.

2.4 Throughput Optimization with Modem Bandwidth Constraints

In this section we develop a technique to optimize the throughput for independent parallel channels whose modems have constrained bandwidth. The parameters that can be adapted are the encoder puncturing ratio α, the symbol rates for both channels, and their modulations.

2.4.1 Formulation and solution

Restricting the bandwidth for a given modulation implies a corresponding maximum symbol rate constraint, denoted as $R_{\max_i}$ for channel i. Thus we add two more constraints $R_1 \leq R_{\max_1}$ and $R_2 \leq R_{\max_2}$ to the optimization problem in (2.11). This optimization problem is still not convex. However, we can obtain a solution by discussing various situations. The procedure is similar to that of the previous section: modulations and α are fixed initially, while optimal symbol rates are obtained. Second, we discuss which α leads to the highest throughput. Lastly, we compare all modulation candidates to choose the best schemes.

We define the allowable region A of the parallel system as consisting of symbol rate pairs (R_1, R_2) that satisfy all system constraints, for given modulations and CSs. To do so, we define the allowable region $A_{r|\alpha}$ satisfying only the encoder rate constraint for a given α as

$$A_{r|\alpha} = \left\{ (R_1, R_2)|\alpha,\ \left[\frac{r}{\alpha}(R_1 m_1 + R_2 m_2) - (\mathcal{T}_1 + \mathcal{T}_2) \right] \leq 0 \right\}. \tag{2.29}$$

For a given channel state, a smaller r/α implies a larger allowable rate region. Conversely, the size of the allowable region increases as the channel conditions improve for a fixed encoder rate constraint. Note that when $\alpha = r$, i.e, $r/\alpha = 1$, only one point $(R_1 = 0, R_2 = 0)$ satisfies (2.12), since, $C_i \leq m_i$ and $C_i = m_i$ only when $R_i = 0$ (i.e. infinite $P_{s_i}/(N_0 R_i)$. This observation is consistent with our claim that the constraint $\alpha \geq r$ is not necessary as long as symbol rates are positive.

The set of rate pairs satisfying only the symbol rate constraints forms another allowable rate region, named $A_{R_{\max}}$, which is simply the rectangular region

$$A_{R_{\max}} = \{ (R_1, R_2)|\ R_i \leq R_{\max_i},\ i = 1,\ 2 \}. \tag{2.30}$$

The allowable region satisfying both the encoder rate and symbol rate constraints for a given α and modulations pair becomes

$$A = A_{r|\alpha} \cap A_{R_{\max}}. \tag{2.31}$$

The shape of the set A is crucial to finding the optimal rate pair. Given α, $R_{\max_i}$, and the modulations, without loss of generality there are four possible situations depending on the channel conditions, as shown in Figure 2.6. For notational convenience we define a reference encoder rate as

$$r_{\text{ref}} = \frac{R_{\max_1} C_1[R_{\max_1}] + R_{\max_2} C_2[R_{\max_2}]}{R_{\max_1} m_1 + R_{\max_2} m_2}, \tag{2.32}$$

which is the encoder rate that would result if both modems operate at their maximum symbol rate and there is no puncturing. Note that $r_{\text{ref}} \leq 1$. We use r_{ref} to decide which case the system is operating under because it reveals the position of $(R_{\max_1}, R_{\max_2})$ relative to $A_{r|\alpha=1}$.

In each of the four cases identified by the four sub-figures in Figure 2.6, the optimal operational symbol rate pair, denoted by $(R_{\text{opt}_1}, R_{\text{opt}_2})$ and marked with a '$\star$' in the figure, and the optimal puncturing ratio α_{opt}, are derived as follows:

(a) $r_{\text{ref}} > r$.

This corresponds to the situation that both channels are strong enough, or R_{max_i} is low enough that the symbol rate constraints become the dominant limit:

$$A = A_{R_{\max}} \subset A_{r|\alpha=1}. \tag{2.33}$$

In this situation, the encoder rate constraint (2.12) is always satisfied. Setting $R_{\text{opt}_i} = R_{\max_i}$ results in a maximum $\mathcal{T} = R_{\max_1} C_1[R_{\max_1}] + R_{\max_2} C_2[R_{\max_2}]$. To achieve equality in (2.12), we should operate at the largest possible encoder

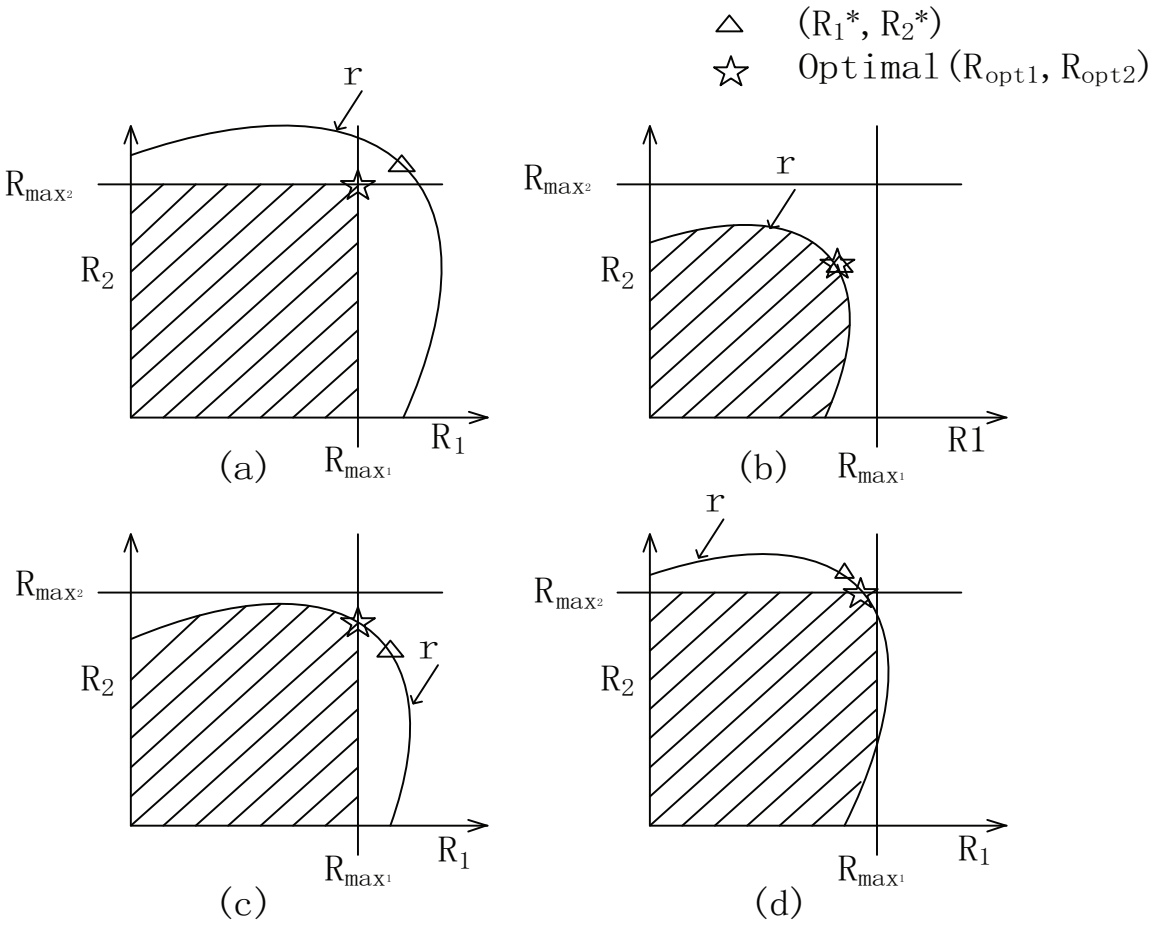

Figure 2.6: Illustration of the four possible cases that the constraints can impose on symbol rates for different channel conditions. In each case, the allowable rate region is shaded. The solution (R_1^*, R_2^*) for the unconstrained bandwidth case is marked with a '$\triangle$' for comparison.

rate, which is $r/\alpha = r_{\text{ref}}$. This implies that we can puncture the mother code to a higher rate r_{ref} with puncturing ratio $\alpha_{\text{opt}} = r/r_{\text{ref}}$. This increases the achieved throughput so that $T = \mathcal{T}$.

(b) $R_{\max_i} > R_i^*$ for $i = 1, 2$.

This is equivalent to the situation described in Section 2.3 where the encoder rate is the only constraint because the symbol rate limits are above the optimal unconstrained rates,

$$A = A_{r|\alpha=1} \subset A_{R_{\max}} \tag{2.34}$$

The throughput is optimized by using $R_{\text{opt}_i} = R_i^*$, the solution to (2.22), for channels $i = 1$ and 2, and letting $\alpha_{\text{opt}} = 1$. The relatively small allowable region $A_{r|\alpha=1}$ compared with $A_{R_{\max}}$, as evident in Figure 2.6(b), occurs when either both channel conditions are poor (making their capacities small) or r is too constraining, i.e., too large for those conditions.

(c) $r_{\text{ref}} < r$, $R_{\max_1} < R_1^*$ and $R_{\max_2} > R_2^*$.

We can use a similar method as in Section 2.3 to prove that the optimal $\alpha = 1$. If equality in (2.12) is achievable, the right side of (2.12), which is only a function of R_i given the modulations, determines the maximum throughput. Thus, we always want to pick the largest possible symbol rates, even if it means that we operate at the lowest encoder rate $r/\alpha = r$.

The problem can again be converted to a convex problem. The only difference between this case and the one addressed in Section 2.3 is that we have two additional linear symbol-rate constraints. Using the Lagrange method again, the optimal parameters must satisfy the following equations, including the last four complementary slackness conditions:

$$\frac{\partial L}{\partial R_1} = rm_1 - \lambda_1 rm_1 + \lambda_1 \frac{d\mathcal{T}_1}{dR_1} - \lambda_2 = 0 \tag{2.35}$$

$$\frac{\partial L}{\partial R_2} = rm_2 - \lambda_1 rm_2 + \lambda_1 \frac{d\mathcal{T}_2}{dR_2} - \lambda_3 = 0 \tag{2.36}$$

$$\lambda_1 \left[r(R_1 m_1 + R_2 m_2) - (\mathcal{T}_1 + \mathcal{T}_2) \right] = 0 \tag{2.37}$$

$$\lambda_2 (R_1 - R_{\max_1}) = 0 \tag{2.38}$$

$$\lambda_3 (R_2 - R_{\max_2}) = 0, \tag{2.39}$$

where λ_i, $i = 1, 2, 3$, are Lagrange multipliers. In this situation, both the encoder rate and symbol rate constraints play important roles in the optimization

procedure because neither $A_{r|\alpha}$ nor $A_{R_{\max}}$ is completely a subset of the other. As seen in Figure 2.6-(c), constraint (2.38) is binding while (2.39) is not. Thus, the maximum capacity $\mathcal{T}$ is achieved by setting $R_{\text{opt}_1} = R_{\max_1}$, $\alpha_{\text{opt}} = 1$, and solving

$$\frac{R_{\max_1} C_1[R_{\max_1}] + R_{\text{opt}_2} C_2[R_{\text{opt}_2}]}{R_{\max_1} m_1 + R_{\text{opt}_2} m_2} = r \tag{2.40}$$

for R_{opt_2}. The optimal solution tells us that we must operate channel 1 at its maximum symbol rate while operating channel 2 at a lower rate, since channel 1 has a relatively strong channel, as evidenced by the large R_1^*. The fact that the optimal R_{opt_2} is solved from (2.40) demonstrates the interdependence of the optimal symbol rate parameters for the two channels.

(d) $r_{\text{ref}} < r$, $R_{\max_1} > R_1^*$ and $R_{\max_2} < R_2^*$.

This situation is similar to case (c) above. Here constraint (2.39) is binding while (2.38) is not. The solution is to set $R_{\text{opt}_2} = R_{\max_2}$, $\alpha_{\text{opt}} = 1$, and solving

$$\frac{R_{\max_2} C_2[R_{\max_2}] + R_{\text{opt}_1} C_1[R_{\text{opt}_1}]}{R_{\max_2} m_2 + R_{\text{opt}_1} m_1} = r \tag{2.41}$$

for R_{opt_1}.

The flowchart in Figure 2.7 clarifies the adaptation procedure for each pair of candidate modulations. The optimization algorithm can be summarized as follows. First a mother-code with encoder rate r is chosen. When the signals of both channels are strong, reliable communication is possible with a higher information rate by puncturing the mother-code with ratio $\alpha = r/r_{\text{ref}}$. Otherwise, the parallel channel must work at its minimum encoder rate for maximum throughput, which means puncturing is not optimal.

In practice the two individual modems may not be able to adjust their symbol rates arbitrarily due to the increased complexity and cost in designing more flexible circuits;

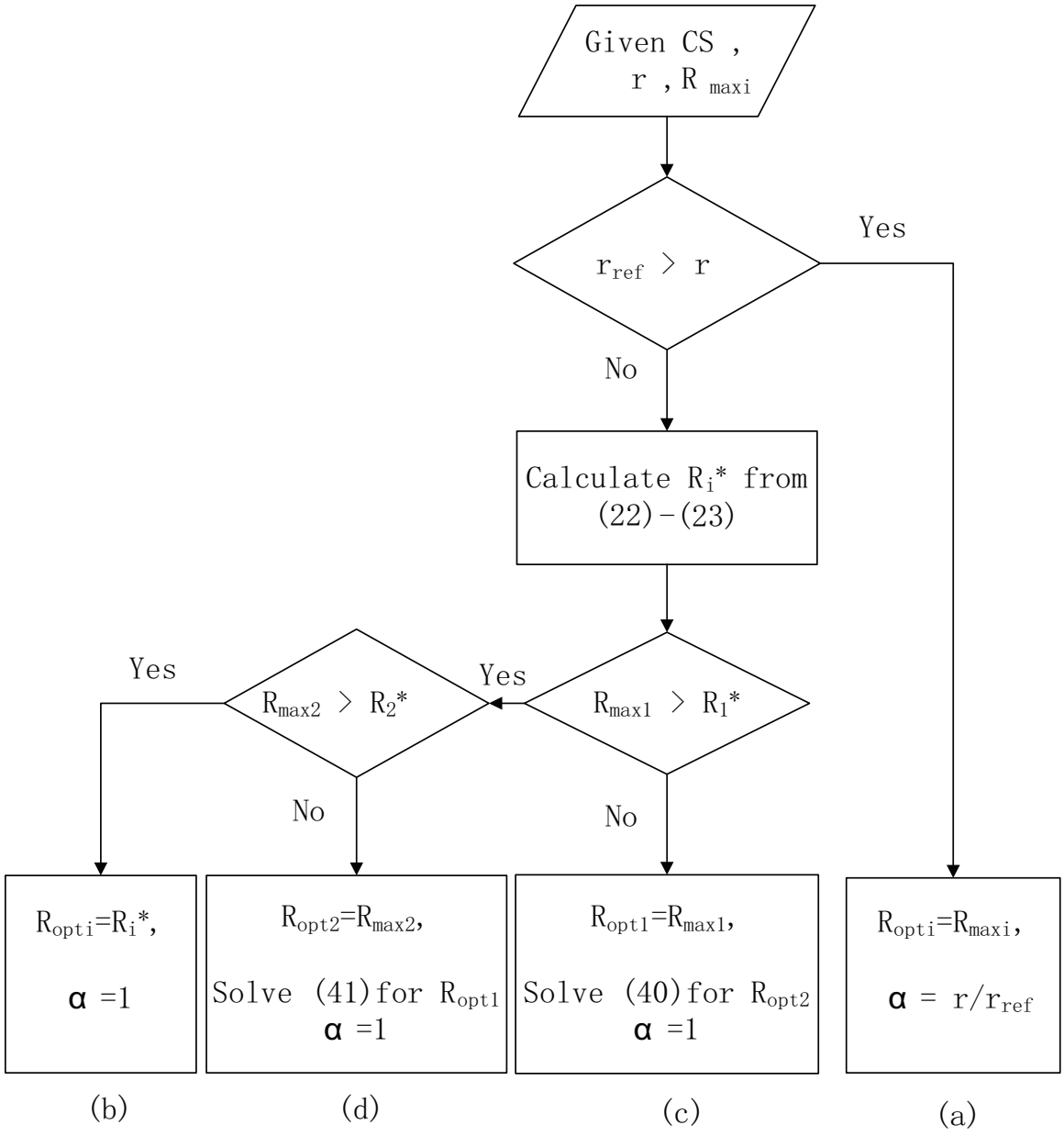

Figure 2.7: Flowchart of symbol rate and puncturing ratio optimization.

instead they must choose from a discrete set of implementable rate pairs, say $A_{\text{realizable}}$. Most common in rate-adaptive systems is to halve or quarter the maximum symbol rate when the channel conditions require it. For example, in Figure 2.3 this may mean that only rate pairs $(R_1, R_2) \in A_{\text{realizable}} = (\{2, 4, 8\}$ Msps $\times \{0.5, 1, 2\}$ Msps$)$ are possible. The procedure depicted in Figure 2.7 would be replaced by a search over the discrete set $A_{\text{realizable}} \cap A$ for the pair resulting in the largest throughput. Modulation selection would then follow to determine which pair of modulations yields the largest total throughput.

2.4.2 Results for a Hybrid FSO/RF System

In this section, we evaluate the achieved throughput for the adaptive technique derived above applied to a FSO/RF hybrid system and compare it to a static (nonadaptive) implementation. We show that a high average throughput hybrid system *with no outage* is possible by adapting the encoder rate, symbol rate and modulation. We assume the system is subject to encoder rate and bandwidth constraints, but not limited to specific implementable modem rates.

Symbol Rate Adaptation

Assume the FSO channel adopts 4PPM with a maximum symbol rate of $R_{\max_1} = 100$ Msps and QPSK is used for the RF channel with $R_{\max_2} = 10$ Msps. The mother-code has a rate of $r = 1/2$. Each channel can experience either good or poor channel conditions, as given in Table 2.1. The table also shows the results of the optimization procedure described above for the four cases.

From the above examples, we see that when the channel conditions are both good, operating both channels at their symbol rate limits and the minimum encoder rate is suboptimal. A higher throughput is possible by puncturing the mother-code to a higher rate as shown in case (a) above and in Table 2.1. Since the FSO channel has

Table 2.1: Optimal System Parameters for Various Channel Conditions, $r = 1/2$, $R_{\max_1} = 100$ Msps, and $R_{\max_2} = 10$ Msps

Case	(a)	(b)	(c)	(d)
FSO channel $\frac{P_{s_1}}{N_{0_1}}$, $\sec^{-1}$	Good 3.16×10^8	Poor 10^8	Good 3.16×10^8	Poor 10^8
RF channel $\frac{P_{s_2}}{N_{0_2}}$, $\sec^{-1}$	Good 3.16×10^7	Poor 9×10^3	Poor 9×10^3	Good 3.16×10^7
R_{opt_1}, Msps	100	76.67	100	88.93
R_{opt_2}, Msps	10	0.036	3.57	10
α_{opt}	0.6073	1	1	1
T, Mbps	181.13	76.70	103.57	99.93

larger throughput, more coded bits are sent through the FSO link in general, based on (2.1). On the other hand, under severe degradation of the FSO channel, case (d), transmitting a large portion of the codeword through a reliable RF channel is preferable. As shown in cases (c) and (d), if one channel is better than the other, the maximum symbol rate is chosen for the stronger channel, while operating the other channel at a lower symbol rate to satisfy the encoder rate constraint. Note that when both channels are poor, the RF system's optimal symbol rate is so low that it may be more practical to idle the RF subsystem.

Modulation Adaptation

Various modulation techniques may be applied to the hybrid FSO/RF system. The throughput can be improved by choosing the appropriate modulation scheme for each different channel condition.

To examine the effects of choosing various modulation pairs, we first fix the modulation and channel conditions for the FSO channel and choose among the four possible modulation schemes for the RF channel: BPSK, QPSK, 8PSK and 16QAM. We again assume $R_{\max_1} = 100$ Msps for the FSO modem and $R_{\max_2} = 10$ Msps for the RF modem. For each possible modulation pair, the symbol rates are optimized according

to the flowchart in Figure 2.7. As shown in Figure 2.8(a), a different modulation scheme may be superior to the others under different RF channel conditions. When the RF channel is poor, the hybrid system operates under case (b) above, and QPSK (or BPSK) is best [63]. As channel conditions improve, 8PSK becomes the optimal choice due to the symbol rate constraint. When the RF channel is very strong, we operate at $R_{\max_2}$ and use 16QAM since it has the largest alphabet.

We then fix the modulation and channel conditions for the RF channel and choose either OOK, BPPM or 4PPM for the FSO channel. This situation is a little different from the case above since, for a fixed bandwidth, varying the modulation changes the maximum symbol rate. For instance, the same symbol rate using BPPM uses twice the bandwidth as OOK. Thus for fair comparison, with a same bandwidth constraint for different modulations, symbol rate constraints vary accordingly. For our numerical example we constrain the pulse width to 5 ns, which gives $R_{\max_1} = 200$ Msps for OOK, 100 Msps for BPPM, and 50 Msps for 4PPM. $R_{\max_2}$ remains the same as above. As shown in Figure 2.8(b), 4PPM is superior to the others when the FSO channel conditions are poor. But as the channel improves, all three modulations operate at their maximum symbol rates and OOK (with the highest $R_{\max}$) becomes the optimal choice.

Application to Slowly Fading Channels

In this section, we compare simulation results of our model to nonadaptive hybrid FSO/RF systems to show that the throughput of a reliable communication system can be improved by symbol rate and modulation adaptation when the channels are subject to various fading mechanisms. We consider two cases. In the first case, the two sub-systems are subject to mild fading, as may occur with atmospheric turbulence or shadowing. In the second case both channels are affected by strong losses due to severe weather conditions.

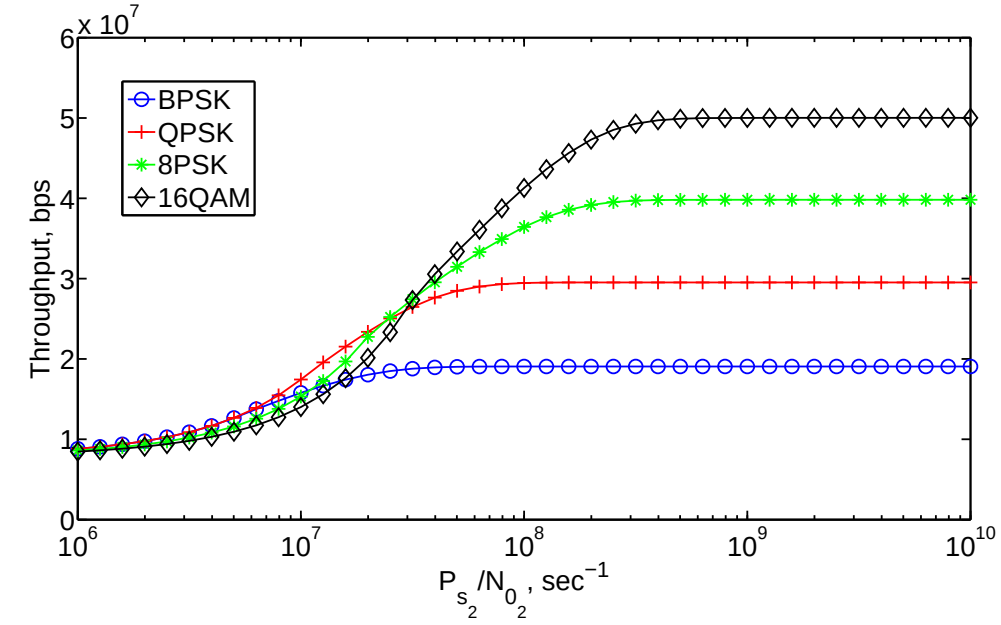

(a)

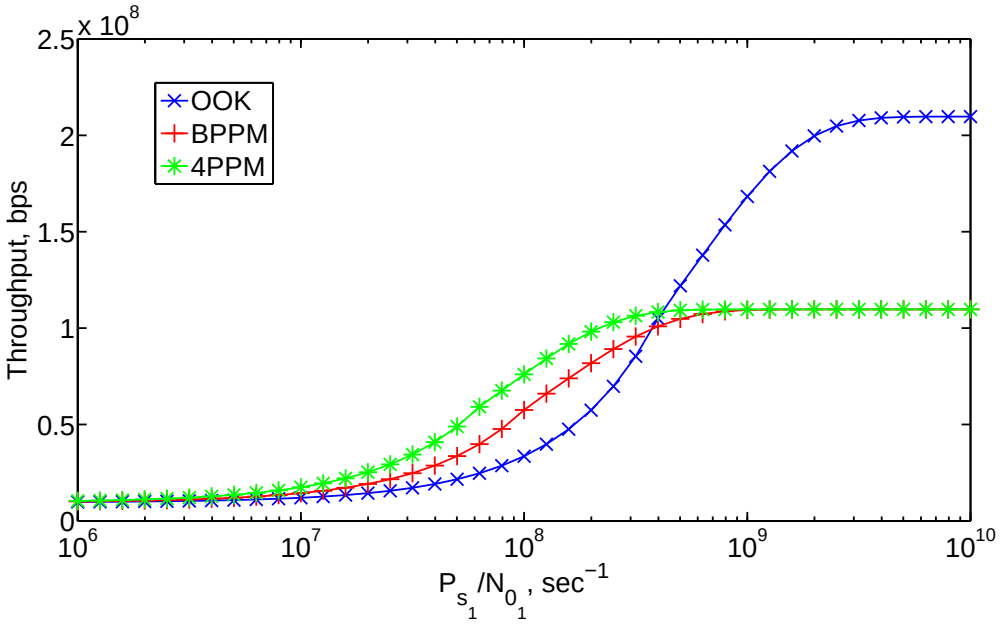

(b)

Figure 2.8: Optimal throughput as channel conditions vary: (a) four RF modulations when the FSO channel adopts 4PPM and $\frac{P_{s_1}}{N_{0_1}} = 10^7$ sec^{-1}, (b) three FSO modulations when the RF channel adopts QPSK and $\frac{P_{s_2}}{N_{0_2}} = 10^7$ sec^{-1}.

Let us explore the first case. The system model we use for comparison is similar to the one described in [24] and [25]. Although for strong turbulence conditions the gamma-gamma model for FSO is more accurate, for simplicity we assume a log-normal fading model for both channels. The conclusions can be easy extended to other models. Since the signal power is proportional to the intensity and we assume thermal-noise-limited operation for both channels, $\frac{P_{s_i}}{N_{0_i}}$, also log-normal distributed, is a valid measure of the state of channel i. In our simulation, we assume the mean channel state for the FSO channel is given by $\frac{P_{s_1}}{N_{0_1}} = 10^8$ sec^{-1} with a normalized variance of 0.4; the mean channel state for the RF channel is $\frac{P_{s_2}}{N_{0_2}} = 10^7$ sec^{-1} with a smaller normalized variance of 0.2. The candidate modulations and bandwidth constraints are the same as that of Section 2.4.2. For all 12 possible modulation pairs $(\mathcal{M}_1, \mathcal{M}_2)$, we perform the optimization procedure described in Figure 2.7. To see the effect that the choice of modulation has on system throughput, we highlight the results for two interesting modulation pairs: (4PPM, 16QAM) resulting in an average rate-optimized throughput of 60 Mbps, and (OOK, BPSK) resulting in 27.2 Mbps. This implies that by choosing appropriate modulation schemes, the average throughput can be improved by over a factor of 2. The maximum average throughput for the hybrid system can be obtained by picking the optimal modulation pairs for each channel realization. Our simulation indicates that the average throughput does not improve noticeably beyond that achievable with (4PPM, 16QAM) by dynamically adapting the modulation for these channel state means and variances; the variations in channel conditions are not strong enough to warrant modulation adaptation. Note that symbol-rate adaptation is still essential to avoid outages; a non-adaptive fixed symbol-rate FSO/RF hybrid scheme with data-rate fixed at the average throughput of our adaptive system would experience an outage nearly 50% of the time.

From Figure 2.9, a non-adaptive fixed symbol-rate FSO/RF hybrid scheme with throughput fixed at the level of our adaptive system average throughput of 60 Mbps

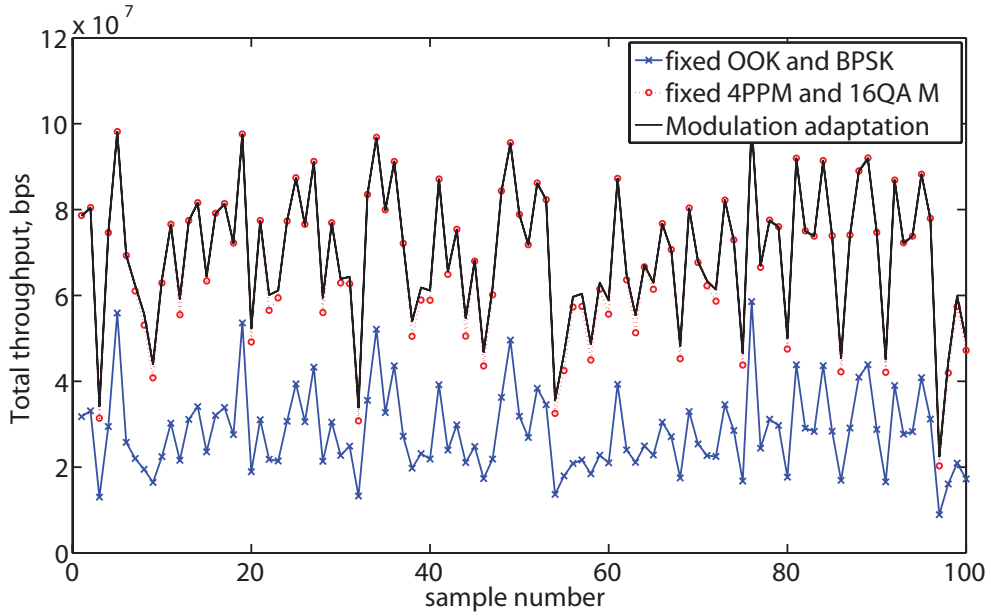

Figure 2.9: Throughput for two different fixed modulation pairs and the optimal adaptive solution. Both FSO and RF channels are lognormal with average $\frac{P_{s1}}{N_{0_1}} = 10^8$ sec^{-1} and $\frac{P_{s2}}{N_{0_2}} = 10^7$ sec^{-1}, respectively.

would be in outage almost half the time. The system could operate at a fixed throughput of about 40 Mbps with no appreciable outage. Rate adaptation has therefore increased the achievable outage-free throughput in this case by about 50%.

Modulation adaptation is needed to respond to gross changes in channel conditions. Let us now consider the case where the links are severely faded due to adverse weather. We use data from a 300 m hybrid FSO/RF experimental system at the University of Virginia collecting received power measurements for a 870 nm unmodulated optical link and simultaneously a 60 GHz RF link. The received power collected during a strong rainstorm varied by over an order of magnitude, perhaps surprising for such a short link. The throughput achieved is shown in Figure 2.10 for all pairs of modulations listed above. The fixed modulation that gives the highest average throughput of 141 Mbps is (OOK, 16QAM). With modulation adaptation, the average throughput can be increased to 155 Mbps, about 10% higher. Another interesting fixed modulation choice is (4PPM, 16QAM), which yields a modest average through-

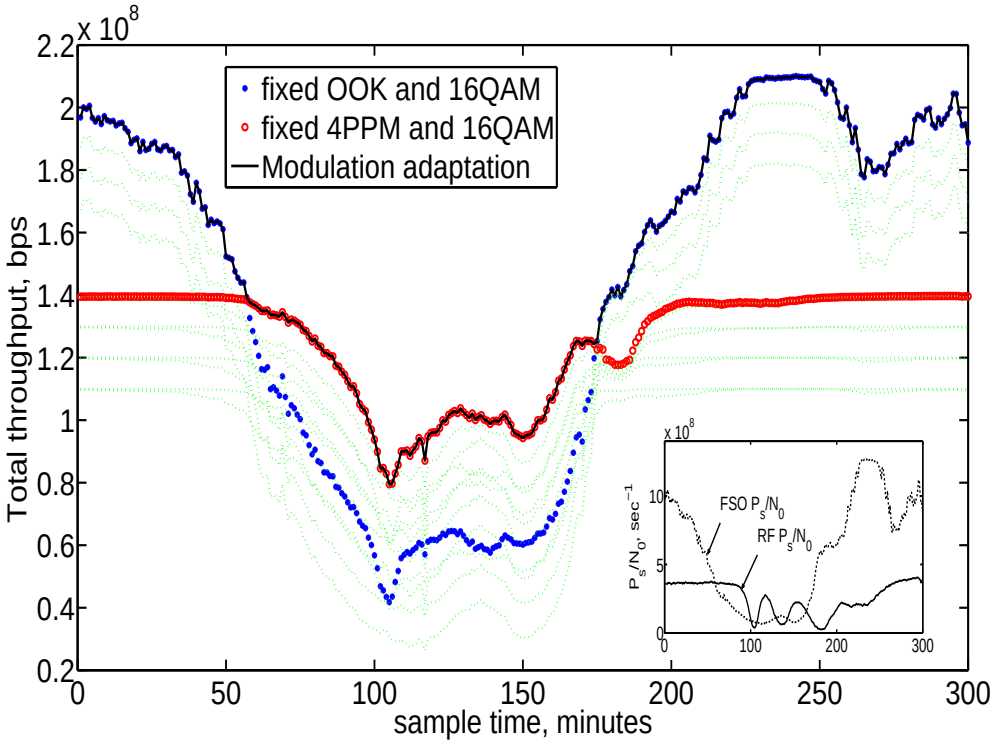

Figure 2.10: Throughput for five hours of channel conditions collected through a severe storm using an experimental FSO/RF system (channel states are shown in the inset). The throughput resulting from the 10 remaining pairs of modulations tested are shown as green dotted lines.

put of 126 Mbps, yet results in the highest minimum throughput of 80 Mbps (same as in the adaptive case). The benefits of modulation adaptation seen here would be even stronger in longer, more severely faded links.

2.5 Chapter Summary and Future Work

Hybrid FSO/RF systems have emerged as a promising solution to satisfy broadband wireless access needs. The channel conditions of both the FSO and RF subsystems can vary widely, suggesting the need for some link adaptation. The major contribution of this work is an algorithm for determining the values for system parameters that maximize the total parallel channel throughput in a seamless manner. Our proposed approach uses adaptive bit allocations, modem symbol rates and encoder rate. The

general formulation presented in this Chapter can serve as a guide for the design of any parallel system satisfying our capacity assumptions.

Results are given for the link adaptation algorithm applied to a typical hybrid FSO/RF system. The average throughput achieved is found to be comparable to adaptive schemes that suffer from outage conditions, and significantly higher than fixed nonadaptive designs.

Before implementation can proceed, further research on code design for hybrid systems is needed. Since the encoder rate and allocation of messages carried in each channel vary with CS, an error control code designed for the hybrid system must be capable of being punctured to a potentially large range of rates, and must be able to handle a nonuniform channel. The design of codes particularly suited to these channels and operating near capacity is an opportunity for future work. In addition, the practical issue of how to achieve reliable communication when exact channel state information is not available at the transmitter needs to be studied. A possible solution is to combine our method with the rateless code described in [36]. Once a single FSO/RF parallel system is fully understood, an extension of the link adaptation technique to a multiple-input multiple-output (MIMO) system is another fruitful area of future research.

The approach presented in this chapter optimizes the joint use of the FSO and RF links for point to point transmission. Using the two technologies jointly in a network environment adds an additional dimension of flexibility, and is subject of the next two chapters.

Chapter 3

Centralized Hybrid FSO/RF Network

An attractive solution for implementing flexible wireless broadband networks uses so-called wireless mesh networks (WMNs). Currently proposed WMNs are based on RF technology, for which RF bandwidth scarcity and co-channel interference fundamentally limit network throughput. One alternative is to design an advanced WMN using multiple wireless technologies with fewer bandwidth and interference problems. Since the optical spectrum remains unlicensed and under-utilized, hybrid free space optics (FSO)/RF technology has been introduced in [29, 64, 30, 31, 32, 33] to improve the network throughput. FSO links do not interfere with each other due to their narrow beams, nor with RF links, and typically have a higher capacity; thus, already deployed networks can be upgraded by installing FSO links without compromising the existing systems. In this chapter, we derive the theoretical maximum throughput of WMNs achievable by adding a fixed number of FSO links. In addition, we develop centralized control algorithms that achieve this throughput by properly allocating the FSO links and determining the appropriate routing and scheduling scheme for the resulting topology.

3.1 Introduction

As stated, among various wireless mesh network architectures [39], we are interested in infrastructure WMNs (illustrated in Figure 1.2), comprising mesh routers (MRs) and mesh clients (MCs). The MRs in this infrastructure WMN form a backbone for MCs and are stationary. Thus, FSO technology, difficult to use in mobile environments but well adapted to stationary systems, can be added to this network to improve the network throughput. Several MRs in this network operate as gateways that connect to terminals, other networks, or the Internet. Given a network topology, traffic demands on the backbone network are fixed, and occur only between gateways. We define the throughput of our FSO-augmented RF WMN as the sum rate achievable to serve all traffic demands. The major contributions of this chapter are:

1. We maximize the total throughput of the system assuming a "physical model" of the RF network based in the signal to interference plus noise of each link, which is more realistic than the previously-used "protocol model" based on valid-transmission and interference-free radii. The optimization problem using the physical model is more complex due to the large number of variables involved. To the best of our knowledge, this is the first work that discusses the problem of hybrid FSO/RF optimization using the RF physical model. We provide various numerical results for different network topologies using the physical model to give insight into the benefits of using a hybrid FSO/RF solution.

2. We propose a method to incorporate the fading nature of communication links, more realistic for certain applications, into the hybrid FSO/RF model. This is the first work that introduces the concept of a *reliable set* of links, and applies this notion to optimizing hybrid FSO/RF fading networks. We compare the optimization results based on quasi-static and fading network models to demonstrate the importance of appropriate modeling.

3. Our formulation results in a routing and scheduling scheme that achieves a maximum throughput using the hybrid FSO/RF network. The exact results can be obtained by solving a mixed integer linear program. An efficient bound on throughput is given, which can be a valuable tool for network administrators to rapidly evaluate the tradeoff between the cost of adding FSO links and the throughput improvement, especially for large networks. A computationally efficient heuristic routing and scheduling algorithm is also presented.

The rest of the chapter is organized as follows. In Section 3.2, we describe our network by listing our assumptions and presenting various network interference and scheduling models. The problem of joint link allocation, routing and scheduling is formulated in Section 3.3. In Section 3.4, the exact solution to the problem based on solving a MILP (suitable for small networks) is described, a bound on the optimal throughput is derived, and a heuristic link allocation approach is given. Numerical results are presented in Section 3.5 for three interference models, and a summary is provided in Section 3.6.

3.2 Network Model

The entire hybrid network is modeled as a directed graph $G = (N, L)$, where N represents the set of mesh routers/nodes and L denotes the set of feasible links in the network. Let $l_{ij} \in L$ denote the directed link from node $i \in N$ to node $j \in N$. The hybrid network is divided into FSO and RF subnetworks. We define L^{RF} and L^{FSO} as the set of *feasible* RF and FSO links, respectively, where $L = L^{RF} \bigcup L^{FSO}$. A link $l_{ij}^{RF} \in L^{RF}$ (or $l_{ij}^{FSO} \in L^{FSO}$), i.e., a link is feasible, if node i can reach node j with one hop, which is determined by how the interference is modeled, as discussed below. In general, L^{RF} and L^{FSO} are different, since a link being feasible using RF

technology does not necessarily imply that it is feasible using FSO technology, and vice versa.

A common assumption in research on wireless networks is to let channel gains for all links be known and fixed (nonfading). This is a practical model when channel fading can be considered quasi-static, i.e., slowly varying compared with the network adaptability. However, this assumption is not always realistic. For example, FSO links may experience an outage due to scintillation, or under heavy snow or fog, and time-varying multipath fading can affect RF communication systems. To develop a hybrid FSO/RF network for these applications, a time-varying fading network model must be considered. Current research on hybrid FSO/RF networks uses the protocol RF interference model exclusively, to the best of our knowledge. This is because the joint optimization problem using the physical RF interference model becomes complicated when FSO links are introduced. However, one major advantage of using FSO links is that they can effectively reduce RF link interference in the network. Thus it is crucial to consider the physical model if we want to take full advantage of the hybrid FSO/RF technology. Below we discuss three different network models: the quasi-static protocol network model, the quasi-static physical network model, and the fading physical network model.

3.2.1 Protocol and Physical Models for Quasi-Static Networks

To define interference and scheduling models used in quasi-static networks, we first define the notion of an *independent set* (IS), from [65, 66], as a set of links that can transmit successfully and simultaneously under a given network model. Our scheduling scheme is based on time-division conflict free scheduling presented in [65]. Since FSO links do not interfere with RF links, all ISs include all feasible FSO links. Since here there is no link interference or fading in the FSO subnetwork, the definition

of link feasibility is the same for both the protocol model and the physical model. The ISs are scheduled by breaking up one unit of time into fractions represented by λ_k, $k = 1, 2, ...K$, where in each time fractions we schedule one IS. The λ_k's determine the network route and schedule. The independent sets are denoted as $\mathcal{I} = \{I_1, I_2, ..., I_k\}$, where I_k is associated with time fraction λ_k.

Once $\mathcal{I}$ has been found, the joint optimization problem for quasi-static networks based on either the protocol or physical model can be solved, as shown below in Section 3.3. Note that the network routing problem formulation can be separated from the RF interference model. This means that once the ISs are constructed, whether using the protocol or physical model, our optimization formulations are identical.

In stationary WMNs, power usage is not a major concern, thus each FSO transmitter is operated at its maximum power. Given a fixed channel gain and receiver noise, links in the FSO subnetwork are fully characterized by their link capacity C_{ij}^{FSO}, with $C_{ij}^{FSO} = 0$ if link l_{ij}^{FSO} is not feasible, i.e., non-line-of-sight or out of transmission range r^{FSO}. For the RF subnetwork, each link has a fixed known capacity C_{ij}^{RF} depending on its transmit power.

Protocol Model

In the protocol model, each RF node i has a communication range and an interference range, denoted as r_i and r_i', respectively. Normally, $r_i < r_i'$. Define d_{ij} as the distance between node i and node j. Transmission between nodes i and j using RF technology is *feasible* if they are within the communication range, i.e., $r_i \geq d_{ij}$; it is successful only if in addition both the transmitter and receiver are free of interference, i.e., $r_k' \leq d_{ki}$ and $r_k' \leq d_{kj}$ for all nodes k that transmit at the same time. We further assume that an RF node cannot transmit and receive data at the same time.

The transmit power P_i of node i determines r_i, r_i' and the capacity C_{ij}^{RF} of the link. Thus, in the protocol model, each RF link $l_{ij}^{RF} \in L^{RF}$ is identified by its transmitter

i, receiver j and transmit power P_i. Note that each element of L^{RF} defines a logical link rather than a physical link, as links with same transmitter and receiver but different P_i are considered distinct links. Based on the definition of an IS, if links l_{ij}^{RF} and l_{pq}^{RF} are in the same independent set, the following conditions are satisfied: $r_i^{'} \leq d_{ip}, r_i^{'} \leq d_{iq}, r_p^{'} \leq d_{pi}$, and $r_p^{'} \leq d_{pj}$.

Physical Model

In the physical model, an RF logical link is represented by four parameters: the transmitter i, receiver j, transmit power P_i and the link rate R_{ij}^{RF}. A link l_{ij}^{RF} is considered *feasible* if the signal to noise ratio (SNR) at the receiver satisfies:

$$\frac{G_{ij}P_i}{N_0 R_{ij}^{RF}} \geq \phi(R_{ij}^{RF}) \tag{3.1}$$

where G_{ij} is the channel gain from node i to node j and N_0 is the receiver noise power spectral density, assumed to be fixed and the same for all nodes. $\phi(R_{ij}^{RF})$ is a function that identifies the minimum SNR corresponding to the transmission rate R_{ij}^{RF}. We can write the channel gain as:

$$G_{ij} = \left(\frac{d_{ij}}{d_0}\right)^{-\eta}, \tag{3.2}$$

where $d_0 < d_{ij}$ is a reference distance and η is the path loss exponent.

In the presence of interference, a link l_{ij}^{RF} can transmit successfully only if the receiver signal to interference plus noise ratio (SINR) satisfies:[1]

$$SINR_{ij}^{\text{nonfading}} \doteq \frac{G_{ij}P_i}{N_0 R_{ij}^{RF} + \sum\limits_{k:k\neq i} G_{kj}P_k} \geq \phi(R_{ij}^{RF}). \tag{3.3}$$

[1]Several published papers, such as [66] ignore the rate dependence of the noise term in the SINR expression, which is only correct if all transmission rates are equal, or if N_0 depends explicitly on the transmission rate.

We define an IS as a set of links that each satisfy (3.3) assuming the other transmitters needed for all the links in the IS are also transmitting. In this model, we assume links that share a node cannot operate at the same time, i.e., no two links share a source or destination, and no node can transmit and receive simultaneously.

3.2.2 Physical Model for Fading Networks

In this section, we define the network model for a fading communication channel case. The approach we take is to perform a fixed link allocation for the FSO subnetwork such that, under time-varying RF and FSO channel conditions, the data can be buffered and transmitted as links recover, given a constraint on the maximum outage probability. The goal is to optimize the throughput under these conditions.

FSO links are characterized by two parameters: link capacity C_{ij}^{FSO} and link availability π_{ij}^{FSO}, where π_{ij}^{FSO} denotes the probability that an FSO link transmits successfully at a data-rate of C_{ij}^{FSO}, and thus $1 - \pi_{ij}^{FSO}$ represents the outage probability of this link. We assume link outages are statistically independent, i.e, the availability of an FSO link does not depend on that of other FSO links. We make no assumptions about the temporal behavior of the link outages, as we expect the data buffers to cope with this issue.

The fading model for the RF subnetwork is developed based on [67]. We assume each link experiences fading independently from other links, and that RF links fade independently from FSO links. Thus the SINR in (3.3) is modified to be

$$SINR_{ij}^{\text{fading}} = \frac{G_{ij}F_{ij}P_i}{N_0R_{ij}^{RF} + \sum_{k:k\neq i} G_{kj}F_{kj}P_k}, \tag{3.4}$$

where, at any point in time, F_{ij} is a random variables corresponding to the channel fade between nodes i and j. With this SINR expression, the probability that an RF

link successfully transmits in the presence of interference is defined as

$$\pi_{ij}^{RF} = \Pr\left\{SINR_{ij}^{\text{fading}} \geq \phi(R_{ij}^{RF})\right\}. \tag{3.5}$$

According to [67], for a Rayleigh fading model, we can derive the expression of π_{ij}^{RF} as follows. To simplify the notation, we define the power received for link $l_{ij}^{(RF)}$ as:

$$X_{ij} = G_{ij}F_{ij}P_i, \tag{3.6}$$

which is an exponentially distributed random variable. Thus, the PDF of X_{ij} is:

$$f_{X_{ij}}(x_{ij}) = \frac{1}{\overline{X}_{ij}} \exp(-\frac{x_{ij}}{\overline{X}_{ij}}), \tag{3.7}$$

where $\mathbf{E}[X_{ij}] = \overline{X}_{ij} = P_i G_{ij}$ denotes the average received power of $l_{ij}^{(RF)}$. With this notation,

$$\begin{aligned}
\pi_{ij}^{(RF)} &= \text{Prob}\left\{X_{ij} \geq \phi(R_{ij}^{RF}(\sum_{k\neq i} X_{kj} + N_0 R_{ij}^{(RF)})\right\} \\
&= \int_0^\infty ... \int_0^\infty \exp(-\frac{1}{\overline{X}_{ij}}\phi(R_{ij}^{RF}(\sum_{k\neq i} x_{kj} + N_0 R_{ij}^{(RF)})) \prod_{k\neq i} \frac{1}{\overline{X}_{kj}} \exp(-\frac{x_{kj}}{\overline{X}_{kj}}) \underbrace{dx_{kj}...}_{k\neq i} \\
&= \exp(-\frac{\phi N_0 R_{ij}^{(RF)}}{\overline{X}_{ij}}) \prod_{k\neq i} \int_0^\infty \frac{1}{\overline{X}_{kj}} e^{(-\frac{\phi(R_{ij}^{RF}}{\overline{X}_{ij}} - \frac{1}{\overline{X}_{kj}})x_{kj}} dx_{kj} \\
&= \exp(-\frac{\phi(R_{ij}^{RF} N_0 R_{ij}^{(RF)}}{\overline{X}_{ij}}) \prod_{k\neq i} \frac{1}{1 + \phi(R_{ij}^{RF} \frac{P_k}{P_i}(\frac{d_{kj}}{d_{ij}})^{-\eta}}.
\end{aligned} \tag{3.8}$$

The probability of successful transmission is the product of two terms. The first term is the probability of successful transmission without link interference, while the second term represents the probability of successful transmission without noise. Under other fading models, π_{ij}^{RF} can be calculated numerically.

The novelty in our approach is the introduction of what we call a *reliable set* (RS), as a counterpart to the IS in a nonfading network. An RS is a set of links that activate simultaneously in a time fraction and all have a successful transmission probability greater than a given requirement ρ. Thus we define an RS as a set of links that each satisfy $\pi_{ij}^{RF} \geq \rho$ assuming the other transmitters needed for all the links in the RS are also transmitting. We can then use any heuristic method suitable for finding ISs to construct the RSs of the fading network. The only modification required is to use the criterion $\pi_{ij}^{RF} \geq \rho$ instead of (3.3).

3.3 Problem Formulation

In this section, we formulate our problem as a mixed integer linear program (MILP). The formulations for the quasi-static protocol and physical models are the same, while the formulation for the fading network requires a minor modification. Thus, once the ISs or RSs are constructed based on the network model of interest, the optimization procedures are similar. We assume all ISs or RSs have been constructed prior to optimization.

3.3.1 Quasi-Static Networks

In a backbone WMN, illustrated in Figure 1.2, traffic demands are generally fixed to be between gateway MRs. Other MRs in the network act only as routers. We denote traffic demands by $b = 1, 2, \ldots, B$, and each is identified by its source and destination nodes (s, d). Let $f_{ij}^{(b)}$ represent the flow of traffic for demand b on link l_{ij}. Thus the throughput for demand b is equal to $\sum_{l_{si} \in L} f_{si}^{(b)}$. The network throughput is defined as the sum flow for all demands served by the jointly defined network composed of the RF and FSO subsystems. Supposing M FSO links are to be installed, we aim to maximize the total throughput by choosing the optimal FSO link allocations, flow

routing and scheduling scheme. D_{ij}^{FSO} is an indicator of an FSO link from node i to node j. The total capacity for a hybrid link is the sum of the capacity provided by the RF and FSO subsystems. Using these definitions and notation, the problem is formalized as a MILP as follows:

$$\max_{f_{ij}^{(b)},\lambda_k,D_{ij}^{FSO}} \sum_{b=1}^{B} \sum_{l_{si}\in L} f_{si}^{(b)} \tag{3.9}$$

Subject to

$$\sum_{l_{ij}\in L} f_{ij}^{(b)} = \sum_{l_{jh}\in L} f_{jh}^{(b)}, \quad \text{all } j \neq s \text{ or } d, \forall b \tag{3.10}$$

$$\sum_{l_{is}\in L} f_{is}^{(b)} = 0, \forall b \tag{3.11}$$

$$\sum_{l_{di}\in L} f_{di}^{(b)} = 0, \forall b \tag{3.12}$$

$$f_{ij}^{(b)} \geq 0 \text{ and } \ 0 \leq \lambda_k \leq 1, \forall b, k, i, j \tag{3.13}$$

$$\sum_{k=1}^{K} \lambda_k = 1 \tag{3.14}$$

$$\sum_{b=1}^{B} f_{ij}^{(b)} \leq \Big(\sum_{\substack{k=1 \\ l_{ij}^{RF}\in I_k}}^{K} \lambda_k R_{ij}^{RF} \Big) + \left(D_{ij}^{FSO} C_{ij}^{FSO} \right), \forall i, j \tag{3.15}$$

$$D_{ij}^{FSO} = \begin{cases} 1 & \text{a directed FSO link from } i \text{ to } j \\ 0 & \text{otherwise} \end{cases} \tag{3.16}$$

$$\sum_{i,j} D_{ij}^{FSO} = M \tag{3.17}$$

Constraint (3.10) follows from the flow conservation law: flows cannot be generated and terminated on any node except for the source and destination. Constraints (3.11) and (3.12) indicate that there is no flow into the source or out of the sink. Bounds on variables are given by constraint (3.13). Since an RF link can only be

active for a fraction of the time, the sum flow on each link is limited by capacity constraint (3.15). Constraints (3.16) and (3.17) define and limit the number of FSO links.

By solving the above MILP, we answer both questions posed in Section 3.1. The optimal value of the objective function is the maximum achievable throughput when augmenting the RF WMN with M FSO links. The optimal values of D_{ij}^{FSO}, $f_{ij}^{(b)}$ and λ_k answer the question of how to achieve the optimal throughput by allocating FSO links and properly choosing a routing and scheduling scheme.

3.3.2 Fading Networks

For fading networks, instead of having links in the same IS transmit simultaneously with no severe degradation, we let links in the same RS transmit simultaneously with limited outage probability. Since the RS is analogous to the IS, the formulation of the fading problem is the same as the formulation for the nonfading problem, except that we must modify the capacity constraint (3.15). The new capacity constraint limits the link transmission to what can be handled by the link on average, i.e.,

$$\sum_{b=1}^{B} f_{ij}^{(b)} \leq \Big(\sum_{\substack{k=1 \\ l_{ij}^{RF} \in I_k}}^{K} \lambda_k R_{ij}^{RF} \rho \Big) + \left(D_{ij}^{FSO} C_{ij}^{FSO} \pi_{ij}^{FSO} \right), \tag{3.18}$$

where I_k now represents an RS rather than an IS. In this formulation, the network can support the traffic at the optimal rate if the fading is changing sufficiently rapidly by buffering the data when a link is not available and transmitting when it recovers. (If the fading is not "fast", then the quasi-static nonfading model can be used.) The MILPs that results when (3.15) or (3.18) are used can be solved in the same manner.

3.4 Exact and Heuristic Solutions

Standard methods to solve MILP exist; we use the branch and bound method described in [68]. Solving this MILP can be broken down into two parts: (i) finding the set of ISs or RSs for the RF network, which is known to be an NP-hard problem [65], and (ii) given this set, solving the optimization problem, which is itself complex since the number of variables increases rapidly as the traffic demands, network size, and number of FSO links increase.

Since the presence of FSO links does not affect the structure of the RF ISs or RSs, these only need to be calculated once for a given topology using any existing algorithm, such as the method described in [66]. The choice of which technique to use to determine the ISs or RSs models does not affect the formulation in Section 3.3. Our method of adding FSO links is thus general and could be used for various RF network models. As research on RF WMN matures, the technique presented in this work could potentially still be applied.

Because of the high computational complexity required to solve an MILP exactly, it is infeasible to solve the problem described in (3.9) for large networks with many traffic demands and a large number of FSO links. Even using the branch and bound method, which tries to find the solution by solving a linear program (LP) recursively, as the number of variables increases it takes an unreasonable time to find the optimal solution. Thus it is important to provide an efficient algorithm to estimate the improvement of the RF network throughput achievable by installing M FSO links. In this work we propose an upper bound on the throughput to quickly estimate the potential benefits of adding M FSO links. We then define a heuristic algorithm to allocate the FSO links and determine the best traffic route and schedule for the resulting hybrid network.

3.4.1 Upper Bound on Throughput

An upper bound on the optimal throughput can be obtained by solving an LP relaxation of the MILP in Section 3.3. In an LP relaxation, the integer constraints are changed to real values, so that the MILP can be solved using the computationally much more efficient real LP. For our problem, constraint (3.16) is replaced by:

$$0 \leq D_{ij}^{FSO} \leq 1 \quad \forall i, j. \tag{3.19}$$

Unfortunately, the routing and scheduling scheme obtained by solving the LP relaxation problem is not useful, since the D_{ij}^{FSO}'s are no longer indicator functions. The upper bound is only useful in dimensioning the network and approximating the throughput.

3.4.2 Heuristic Solution

A simple heuristic algorithm based on a greedy method to assign the M FSO links is described in Algorithm 1. The resulting throughout is a lower bound on the throughput achievable using the MILP since a network consisting of M given FSO links can perform no better than the optimal one obtained using MILP.

Algorithm 1 Simple Heuristic

Step 1. Solve the LP relaxation of the MILP in Section 3.3 by replacing constraint (3.16) with (3.19);
Step 2. Assign the largest M D_{ij}^{FSO} equal to 1 and set the rest equal to zero;
Step 3. Convert the MILP in Section 3.3 into a LP by using the D_{ij}^{FSO} obtained in **Step 2**;
Step 4. Solve the LP of **Step 3** and return a solution;

Obtaining the simple suboptimal FSO link allocation requires solving the LP problem twice. The algorithm is greedy since we use D_{ij}^{FSO} (obtained in the LP relaxation) to determine how important installing an FSO link on l_{ij} is, adding FSO channels on links with high D_{ij}^{FSO}. (If two links have same the D_{ij}^{FSO}, we randomly

select one to install first). It takes into account bottlenecks of the network. Links with high D_{ij}^{FSO} have large sum flows, thus we need to increase the capacity of those links by adding FSO links.

Since the greedy algorithm assigns M FSO links simultaneously, it is possible that a smaller number of FSO links occasionally outperforms a larger number. We can improve the algorithm by using a recursive method, i.e., adding one FSO link at a time. The improved heuristic for m FSO links is based on the solution for $m-1$ FSO links, assuming the $m-1$ link locations are fixed and placing the last FSO link using the LP relaxation technique on just one link, as described in Algorithm 2. This modified algorithm guarantees that the throughput achieved increases as more FSO links are installed. The tradeoff for obtaining this better solution is that we must run the LP algorithm M times, instead of twice for Algorithm 1.

Algorithm 2 Improved Heuristic

Step 1. Let $m = 1$.
Step 2. Assuming $m-1$ FSO links have been assigned and are fixed, solve the LP relaxation of the MILP in Section 3.3 by replacing constraint (3.16) with (3.19) setting the parameter $M = 1$. Assign the largest D_{ij}^{FSO} equal to 1.
Step 3. Let $m := m + 1$. If $m \leq M$, go to Step 2.
Step 4. Convert the MILP in Section 3.3 into a LP by using the D_{ij}^{FSO} obtained in **Step 2**;
Step 5. Solve the LP of **Step 4** and return a solution;

Both algorithms provide a fast FSO link allocation solution that can be used for larger networks and/or more traffic demands than possible with the optimal algorithm based on the full MILP. In all the results presented in this chapter we use Algorithm 2.

3.5 Numerical Results

In this section, numerical results based on our optimization are given to demonstrate the advantages achievable by upgrading purely RF mesh networks to hybrid FSO/RF networks.

3.5.1 Quasi-Static Networks

We first consider the throughput improvement possible by adding FSO links to RF mesh networks when the communication channels can be modeled as quasi-static. The ISs are constructed based on either the protocol or the physical model. Although it is difficult to make a fair comparison between the two models, we wish to determine if using the physical model provides an important enough advantage in our optimization to warrant the increased complexity.

Construction of ISs

For a fair comparison, we define the communication range in the protocol model so that the set of feasible links is the same as for the physical model. In the physical model, feasible links are determined based on (3.1). Substituting (3.2) into (3.1) and enforcing equality, d_{ij} can be calculated given other system parameters. If we pick $r_i = d_{ij}$ in the protocol model, we produce the same set of feasible links for both models. The search algorithm described in [66] is used to generate the ISs in this section as well as the RSs in the next section.

The protocol model introduces a "hard" limit on the interfering links while the physical model imposes a "soft" limit. Let us consider a rectangular 4×4 node grid network with horizontal and vertical neighbor nodes 2 km apart as shown in Figure 3.1, with other parameters defined in Table 3.1.[2] Assume $N_0 = kT$ where k is Boltzmann's constant and T is the noise temperature. For this discussion, let us

[2]These parameters are used for all simulation results unless otherwise stated.

Table 3.1: 4×4 Grid Network Parameters

Parameter	Symbol	Value
Number of nodes	$\|N\|$	16
Reference distance	d_0	10 m
Path-loss exponent	η	4
Transmit power	P_i	20 dBm
RF data rate	R_{ij}^{RF}	100 Mbps
SINR threshold	$\phi(R_{ij}^{RF})$	20
Noise temperature	T	298 K
FSO commun. range	r^{FSO}	3 km
FSO capacity	C_{ij}^{FSO}	0.2 or 1 Gbps

Table 3.2: Number of ISs for Various Quasi-Static RF Channel Models

RF Model	Interference range r_i'	# of ISs
Protocol	$r_i' = 1.5r_i$	4704
Protocol	$r_i' = 1.7r_i$	293
Protocol	$r_i' = 2r_i$	100
Protocol	$r_i' = 4r_i$	92
Physical	–	572

assume only one power level and one RF transmission rate are available. Table 3.2 compares the number of ISs generated in the protocol model for various interference distances with that in the physical model. The number of ISs decreases sharply as the interference range increases. In practice, the choice of r' is tricky: on one hand, choosing a small r' can underestimate the interlink interference; on the other hand, picking a large r' can cause network throughput degradation, since a large r' implies fewer ISs, i.e, less scheduling flexibility. r' is usually chosen to be $2r$ to $4r$ in realistic networks. In contrast, the physical model provides an accurate interference model for RF subnetworks without the need for this parameter. Note that the set of ISs constructed in the protocol model is not necessary a subset of the set constructed in the physical model, and thus for some protocol model ISs the SINR requirement in (3.3) is violated.

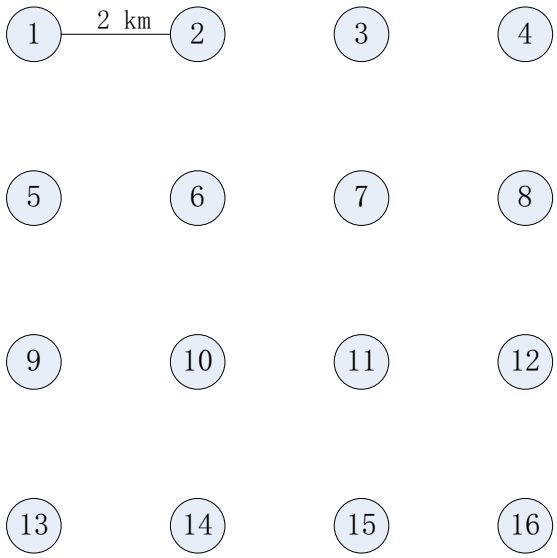

Figure 3.1: Illustration of symmetric 16 node network topology.

Exact Solutions

In this section the results shown are obtained by solving the MILP described in Section 3.4. First the total throughput (using both subsystems) from (3.9) for the protocol and the physical models are compared. Then we show how to choose the RF network model based on the network topology and parameters.

In the first example, let us consider the 16 node rectangular grid network topology described above and in Table 3.1. In Figure 3.2, the optimal throughput obtained by solving the MILP is shown for various RF interference models. We assume gateway nodes are placed at the outer corners, and there is one traffic demand diagonally across the network. The FSO link capacity of $C_{ij}^{FSO} = 200$ Mbps is notably larger than $R_{ij}^{RF} = 100$ Mbps, but not orders of magnitude larger. First note that increasing the number of FSO links in the network significantly increases the total throughput for all network models. When using the protocol model, different r' lead to different optimal throughput values. For example, at $M = 5$ the difference is about 10%, or 50 Mbps (still substantial).

In another example also shown in Figure 3.2, we assume $B = 12$ (12 traffic demands) among four corner gateways, from each gateway to the other three, while keeping all other assumptions the same. The simple protocol model does lead to obvious throughput improvement for small r's. However, this throughput is not achievable in reality: the protocol model with $r' < 2r$ leads to many ISs that do not exist in the physical model, and thus using these would violate the true SINR threshold constraints (used in the physical model). Thus, using the protocol model can result in unrealistic network throughput estimation.

In both examples above, FSO channel capacities are comparable with RF channel capacities, and the protocol model could then give inaccurate optimal throughput of the hybrid network, either underestimation or overestimation. For this case, the physical model is recommended. In contrast, when $C_{ij}^{FSO} = 1$ Gbps, much larger than the RF link rate, different models result in similar results, as can be seen in Figure 3.2. It is reasonable to use the simple protocol model when the FSO subnetwork has much higher capacity, since non-interfering FSO links dominate the network throughput.

To show the full advantage of using the physical model, we demonstrate the benefits of allowing multiple power levels and/or RF link rates on network throughput for a more general 15-node asymmetric network topology. We assume that four gateways are located in the corners of a 5 km $\times$ 5 km area with again 12 traffic demands. The other 11 MRs are arbitrarily placed in the area. In Figure 3.3 we compare the optimal throughput for 4 cases for the RF subnetwork: (1) one power level, 20 dB, and one link rate, 100 Mbps (with corresponding SINR threshold of $\phi = 20$), (2) two possible RF transmit power levels, 20 and 40 dBm, and one RF link rate, 100 Mbps; (3) one power level, 20 dBm, and two RF link rates, 100 and 200 Mbps (with SINR thresholds 20 and 40, respectively); and (4) two power levels and two link rates as in cases (2) and (3). As we can see, since in case (4) the network has more ISs and robust routing and scheduling schemes, it results in the highest throughput, as expected.

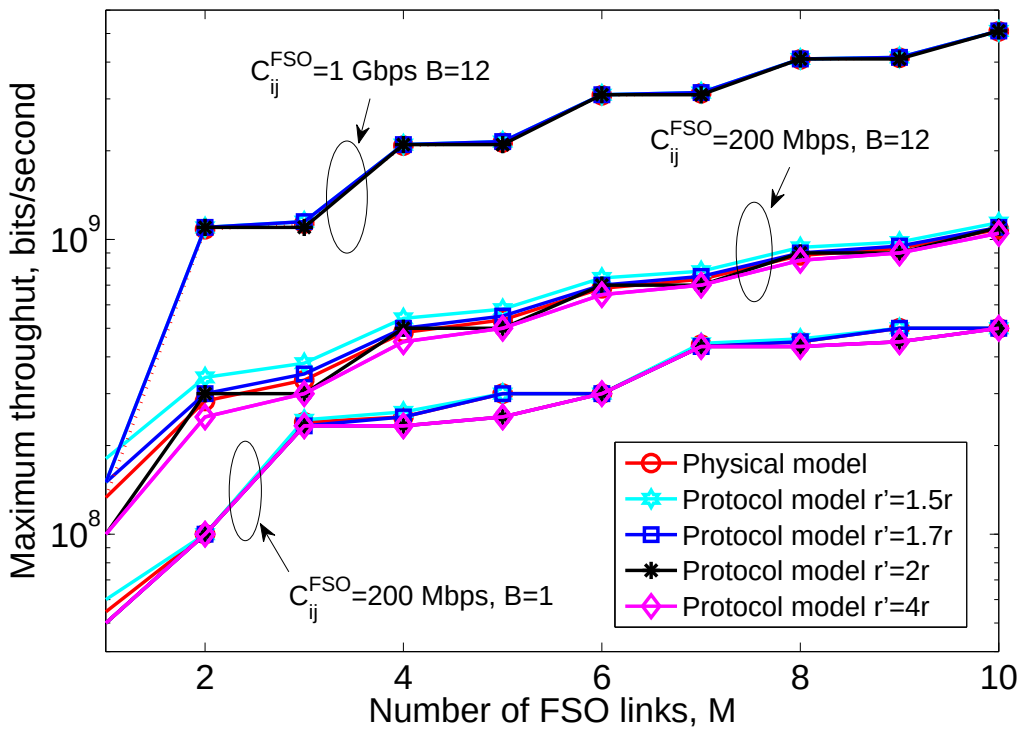

Figure 3.2: Optimal sum throughput for a 16 node grid network under different traffic demands, RF interference models, number of FSO links, and FSO link capacities

The relative effect of the RF network flexibility, especially in assigning various power levels, diminishes as the number of FSO links increases.

Throughput Upper Bound and Heuristic Solution

In this section, numerical results are shown for the upper bound to the optimal throughput and the heuristic FSO allocation algorithm derived in Sections 3.4.1 and 3.4.2. Two topologies are again used, one regular and one random.

Consider the 16 node grid network as above using the physical model for the RF network. Again, we assume there are 12 traffic demands among 4 corner gateways. Figure 3.4 shows the relationship between the upper bound, the heuristic, and the exact solution for C_{ij}^{FSO} = 200 Mbps and 1 Gbps. The heuristic solution in this

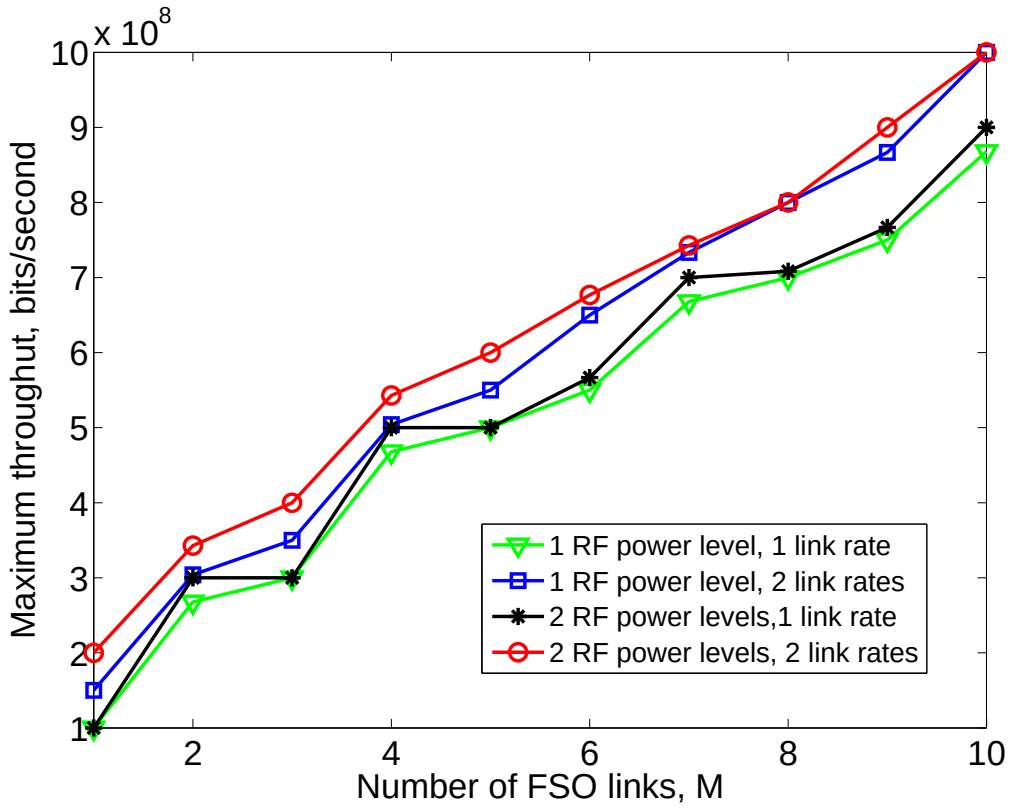

Figure 3.3: Optimal sum throughput for a 15-node asymmetric network topology with different RF link power and rate assumptions. $B = 12$, $C_{ij}^{FSO} = 200$ Mbps.

case is tight. The calculation time to find the heuristic solution is dramatically lower compared with the time needed to obtain the exact solution; we only show results for the exact solution for $M \leq 10$, as for a larger value of M the computation time becomes excessive.

Another important observation we draw from the results presented is that there is an M for which installing more FSO links cannot improve the network throughput. Thus the assumption made by some researchers that all nodes should be equipped with FSO transceivers is excessive for the given traffic demand.

Next, we consider a relatively larger asymmetric network topology with 28 nodes. The four gateways are located in the corners of a 5 km $\times$ 5 km area with 12 traffic demands among them. The other MRs are uniformly distributed in the area. With the

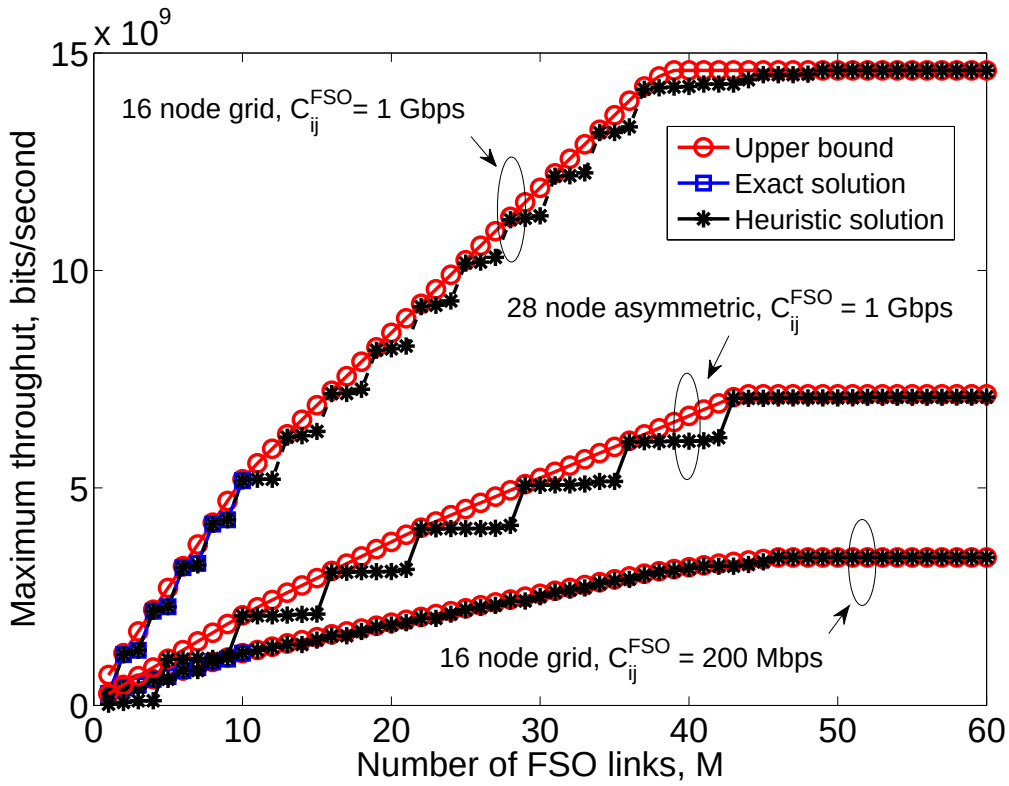

Figure 3.4: Sum throughput computed vs number of FSO links using the MILP, the upper bound, and the heuristic algorithm for two networks, a 16-node grid network [two RF power levels (20 and 30 dBm) and two RF link rates (100 and 200 Mbps)] and a 28 node asymmetric topology [one RF power level (20 dBm) and data rate (100 Mbps)].

physical model, we obtain 66,248 ISs with 178 feasible links for the RF subnetwork. Due to the increase in the number of ISs, the computation time for the MILP becomes excessive.[3] Thus we only show upper bound and heuristic results for this network in Figure 3.4. Our greedy algorithm provides a near-optimal heuristic solution with low computation time (about 120 seconds for each M), which is important in practice.

[3]With an Intel i7 CPU and 8GB RAM computer, it takes about 4 hours to obtain the exact solution for just $M = 1$.

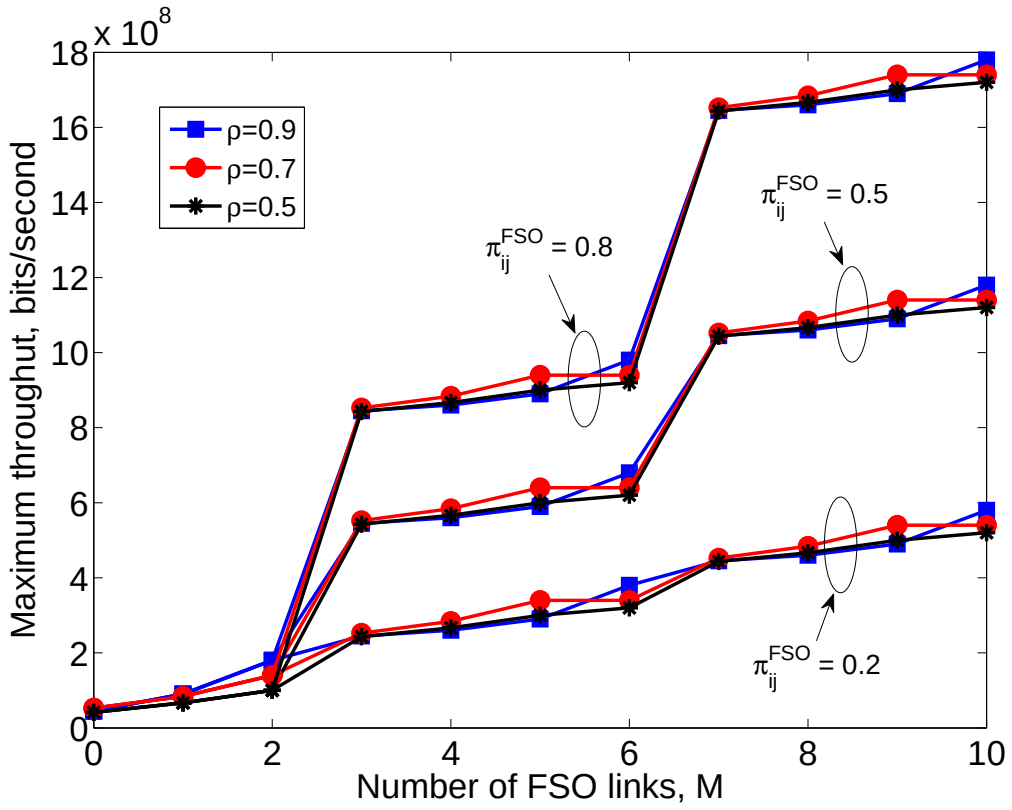

Figure 3.5: Maximum throughput for a 16-node grid network as a function of the number of FSO links for different π_{ij}^{FSO}'s and ρ's, for $C_{ij}^{FSO} = 1$ Gbps

3.5.2 Random Fading Networks

In this section, we illustrate the joint optimization problem for random fading FSO/RF networks. The RSs are constructed based on the physical model assuming independent Rayleigh fading RF links.

Effect of Outage Parameters

In Figure 3.5 we illustrate the optimal throughput for different values of π_{ij}^{FSO} and ρ. The same regular 16-node network topology used in Section 3.5.1 is used in this example. The assumptions are also the same as those in Section 3.5.1, except that there are only two traffic demands, diagonally across the network (top-left to bottom-right and top-right to bottom-left). If we fix ρ, we see that varying π_{ij}^{FSO} has a large

impact of the throughput, because the effective capacity of a hybrid link, i.e, the right hand side of (3.18), depends strongly on the outage probability of FSO links, and the π_{ij}^{FSO}'s affect no other constraint. Note that the throughput depends on the product $C_{ij}^{FSO} \times \pi_{ij}^{FSO}$; for the same value of $C_{ij}^{FSO} \times \pi_{ij}^{FSO}$, decreasing π_{ij}^{FSO} requires the system to have larger buffers to temporarily store data during a fade.

On the other hand, it is surprising that if we fix the FSO link availability π_{ij}^{FSO}, increasing ρ does not necessarily increase the throughput. This is because ρ affects both the number of RSs and the effective RF link capacities. As ρ decreases, the effective link capacity for the RF subnetwork decreases proportionally. Yet the number of RSs increases as ρ decreases; we find 329, 1104, 3359 RSs for $\rho = 0.9$, 0.7 and 0.5, respectively, for this network topology. This result also suggests that we may sometimes benefit from poor link conditions, since link interference is also decreased.

Routing and Scheduling

We now show that the network throughput improvement resulting from our routing and scheduling schemes can originate from two effects: interference mitigation and forming direct FSO routes. To illustrate this, we present results on randomly generated network topologies, each with 15 nodes. In order to clearly visualize our optimal routing, we assume there is one traffic demand from the top-left corner to the bottom-right corner of a square area of 10 km $\times$ 10 km. The other 13 nodes are uniformly distributed within the square.

We demonstrate the two benefits obtained by adding FSO links by examining the solution to our MILP for the two topologies shown in Figure 3.6. For Figure 3.6(a), we show the routing and link allocation for $M = 1$. Due to the communication range limit of FSO links, it is impossible to form a direct (even multihop) FSO route from the source to the destination, irrespective of the number of FSO links available. The throughput improvement in this topology is solely due to the interference mitigation

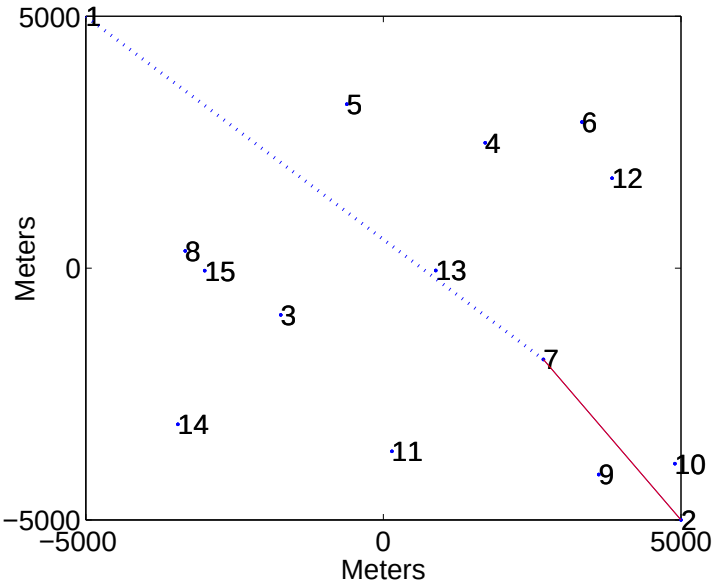

(a)

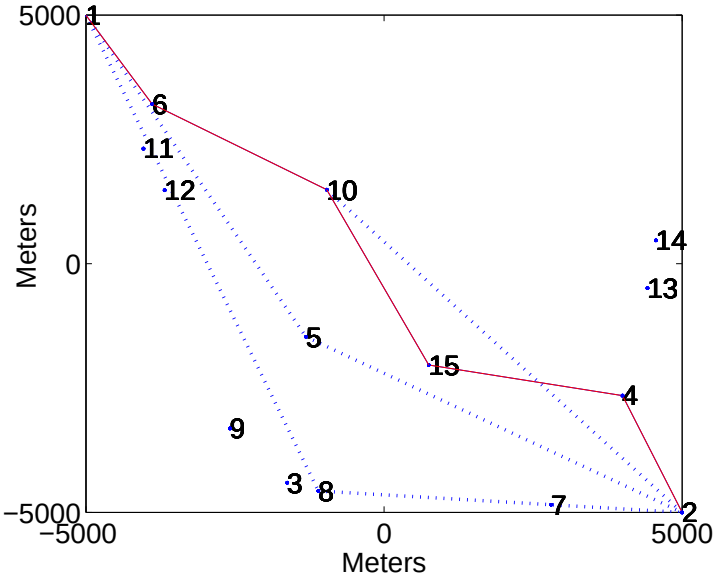

(b)

Figure 3.6: Example network topologies, with dotted lines representing RF links and solid lines representing FSO links: (a) 1 FSO link, and (b) 5 FSO links. For the FSO subnetwork, $r^{FSO} = 4$ km, $C_{ij}^{FSO} = 1$ Gbps, and $\pi_{ij}^{FSO} = 0.9$. For the RF subnetwork, $R_{ij}^{RF} = 20$ Mbps, $\phi(20) = 10$, $P_i = 30$ dBm, and $\rho = 0.5$.

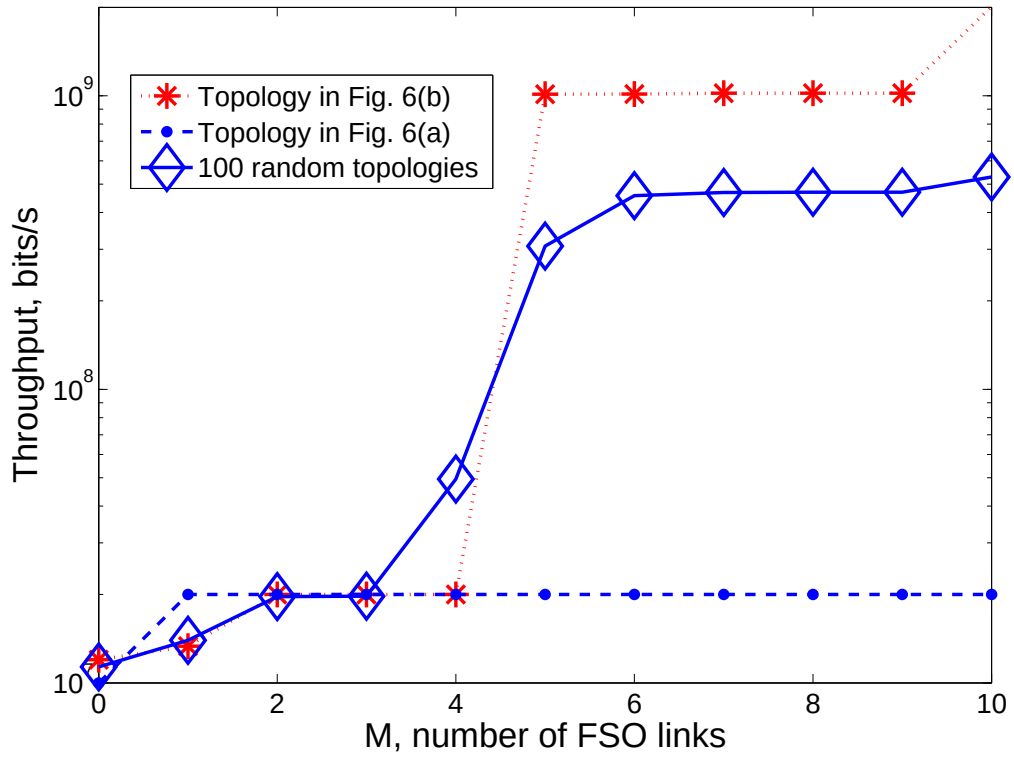

Figure 3.7: Throughput as a function of the number of FSO links for the network topologies shown in Figure 3.6 and average throughput for 100 randomly generated networks with fixed source and destination and a single demand

achieved by adding FSO links. For Figure 3.6(b), we show the routing and link allocation for $M = 5$ FSO links, where a direct multihop FSO route is formed from the source to the destination.

Figure 3.7 shows the optimal throughput as a function of the number of FSO links for the two cases, plus results corresponding to an average maximum throughput over 100 randomly generated topologies all satisfying the same conditions listed above. For Figure 3.6(a), the throughput is doubled by adding only one FSO link. Further increase in the number of FSO links does not boost the network throughput. For Figure 3.6(b), the improvement in the network throughput is approximately a factor of 100 over an RF-only network after $M = 10$ FSO links have been installed. The average throughput for a random network is between these two extremes. Since the

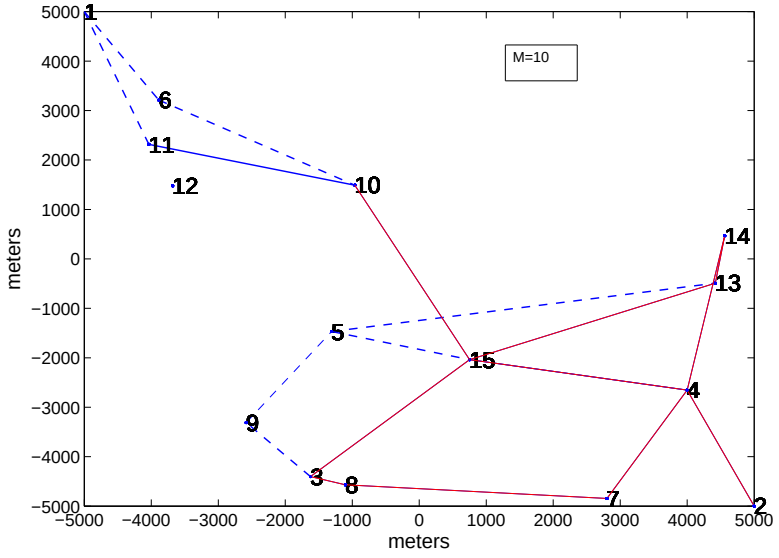

Figure 3.8: Optimal FSO and RF link placement solution for two traffic demands with $M = 10$.

shortest distance from the source to the destination is $10\sqrt{2}$ km and $r^{FSO} = 4$ km, at least four FSO links are needed to form a direct multihop FSO route from the source to the destination. As we can see in Figure 3.7, some network topologies can have a direct FSO with four FSO links, while others require five or six FSO links. For the same reason, the throughput of some networks can be further improved for $M = 10$, when it is possible to have two direct FSO routes.

Two Traffic Demands

In this section we add one more traffic demand from node 3 to node 14, while keeping other assumptions the same. As shown in Figures 3.8 and 3.9 for the example topology of Figure 3.6(b), the total throughput of the network can be improved dramatically by adding more FSO links. However, our current objective function that maximizes the total throughput may cause fairness problems, as shown in Figure 3.10. With 7 FSO links and two traffic demands, all flows are allocated to one traffic demand.

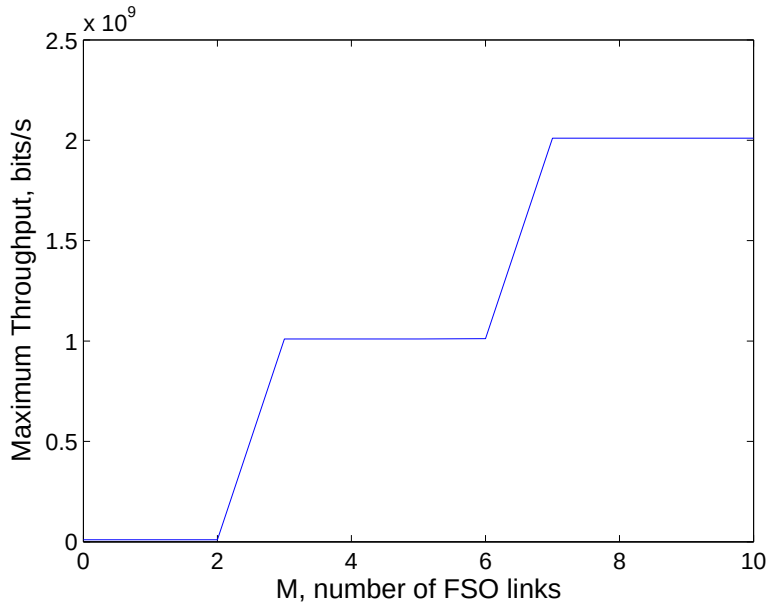

Figure 3.9: Maximum total throughput for two traffic demands as a function of the number of FSO links. Topology from Figure 3.6(b).

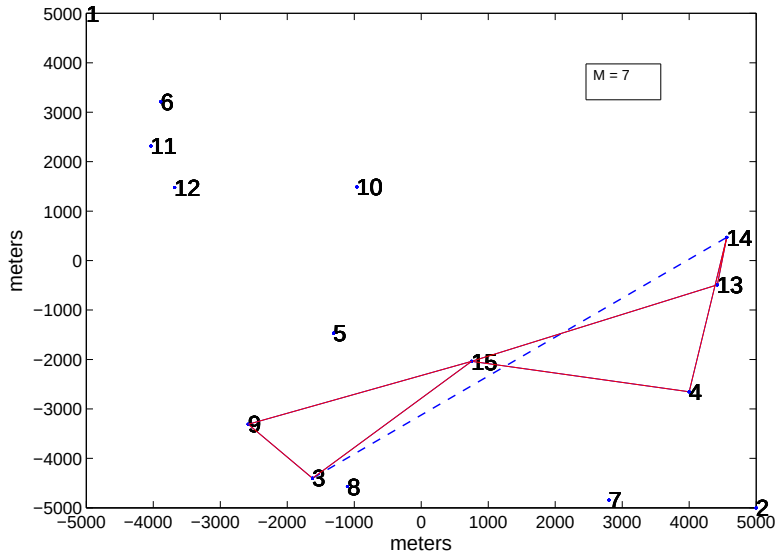

Figure 3.10: Optimal FSO and RF link placement solution for two traffic demands with $M = 7$.

In our future work, we will improve our objective function formulation to consider fairness.

3.6 Chapter Summary

In this chapter, we present a joint FSO link allocation, routing and scheduling algorithm for hybrid FSO/RF WMNs. We describe network models appropriate for either quasi-static or fading link models. For quasi-static models, we compare the widely used protocol model with the accurate but complex physical model. We introduce the concept of reliable sets (RSs) for fading networks, to replace the interference sets (ISs) typically used for quasi-static networks. We present a general MILP formulation to solve for the optimal throughput. Moreover, we provide a heuristic algorithm to find a near-optimal FSO allocation when the network is large. Various numerical results are provided to show the advantage of combining the two wireless technologies in implementing WMNs.

The methods presented in this chapter require centralized control. In the next chapter, a distributed routing algorithm is presented.

Chapter 4

Distributed Hybrid FSO/RF Network

In the previous chapter, network throughput optimization and routing are assumed to be regulated by a centralized node in the network. For small size networks, the algorithm is computationally efficient. However, as the size of the network grows, it may take a long time or even become impossible to obtain the optimal solution. Moreover, it may be impractical to have a single control center in every network to handle the routing. The scalability of centralized routing and scheduling networks is also limited. As shown in [69, 70], for large networks, routing algorithms that have small overhead need to be designed to achieve routing scalability. In order to solve this problem, in this chapter we design a distributed routing algorithm for the hybrid FSO/RF network.

4.1 Introduction

It is crucial to develop routing algorithms that are distributed for hybrid FSO/RF networks, especially for networks that are large in size. Unlike centralized routing algorithms, distributed algorithms rely on information exchanges between adjacent

nodes. Each node in the network periodically updates the network information such as: link state, neighbor nodes, and routing tables. An algorithm designed for hybrid FSO/RF networks requires both FSO and RF subnetwork information to be updated efficiently. Moreover, routing also depends on both FSO and RF link states. In RF mobile wireless networks, as presented in [69, 70], the transmission of routing-related information consumes most of the bandwidth as the network population increases. Thus reducing routing control overhead is a primary issue in achieving network scalability. The authors propose a hierarchical routing algorithm to solve the problem. In hierarchical routing, we first group nodes in a network. Then different nodes are defined with different functionalities inside and outside of the group. The hierarchical routing method is also suitable for stationary networks.

In this chapter, we present a hierarchical distributed routing algorithm that is tailored for realistic hybrid FSO/RF network implementations. The algorithm contains two parts: first node clustering and then call routing. The clustering algorithm handles node grouping while the routing algorithm generates the routing table and controls the traffic flow. The algorithm is optimized for hybrid FSO/RF application so that the advantage of using multiple technologies is highlighted.

The rest of the chapter is organized as follows. In Section 4.2, we describe the network model for the distributed hybrid FSO/RF network. The clustering algorithm that partitions the hybrid network is presented in Section 4.2.2. Then we discuss the routing algorithm that is suitable for the hybrid network in Section 4.2.3. In Section 4.3, simulation results of clustering and routing for various network topologies are demonstrated.

4.2 Architecture of Distributed Hybrid FSO/RF WMN

In this section, we describe the architecture of the hybrid FSO/RF WMN. Distributed clustering and routing protocols suitable for the hybrid network are presented. The clustering algorithm is designed so that network nodes with FSO technology hold important roles in the clusters (such as cluster heads and gateways, defined below). FSO technology enables high throughput transmission through the network, but FSO links are also vulnerable. Thus the routing algorithm presented tries to take advantage of the high throughput afforded by FSO links as well as the reliability of RF links.

4.2.1 Network Model

As stated, the WMN that we are interested in (shown in Fig. 1.2) is a stationary backbone network. Hierarchical routing is suitable for such a network. It is clear that the throughput achieved by using a distributed routing algorithm is lower than that obtained by using a centralized control method that relies on global network state information. However, when the network scale is large, distributed routing is the only feasible routing algorithm. In the distributed routing model, we focus on the routing algorithm and assume the network topology, including the allocation of FSO links, is predetermined. In practice, when deploying such a network, an administrator will first determine where to install FSO links based on network traffic demands and the environment (such as line-of-sight requirements), using, for instance, the method presented in Chapter 3. Then the network uses the distributed routing algorithm described in this chapter for routing.

In our hybrid FSO/RF network model, we assume that all nodes are equipped with an RF transceiver while only some nodes have FSO technology due to line-of-sight and cost limitations. We assume the RF subnetwork uses an orthogonal multiple

access method (such as frequency division multiple access, FDMA), and each node can only process one channel at a time. We assume a node can only process incoming RF messages when it is idle, i.e., not sending or receiving other RF data. Otherwise, the message is ignored. Moreover, we assume that RF and FSO links are independent so that a node equipped with both RF and FSO transceivers can use both links at the same time.

In our model, the network is first divided into partitions based on our clustering algorithm. The clustering algorithm described in Section 4.2.2 identifies each node as having one of following roles: cluster head (CH), gateway (GW), distributed gateway (DG), normal node (NN) or solo node (SL). We assign a unique numerical identifier (ID) to each node in the network. First we define the notion of priority among node pairs. When determining the priority between two nodes, we first compare the number of FSO links connected to each node. The node with the most FSO links is labeled as having higher priority. If they have the same number of FSO links, the one with the smaller ID has higher priority. This is a modified version of the lowest-ID cluster algorithm proposed in [71, 72] by taking into account FSO links. The definitions and functionalities of each kind of node are summarized as follows:

- Cluster Head (CH): the node in a cluster that has the highest priority. Each cluster has a unique CH. The cluster is defined such that its CH can communication with all nodes in the same cluster with just one hop, using either an RF or FSO link. The CH is responsible for updating and storing network topology information of the whole network. It also updates and stores link state information between CHs, GWs, and DGs. Routing tables are calculated by the CH, and this information is shared by the CH with other CHs. The CH also serves as the central node for the cluster, i.e., to/from which aggregated data is transmited/received from other CHs, and also from other nodes within the cluster.

- Gateway (GW): a node that belongs to multiple clusters. GW nodes can pass data from one CH to another CH. They must be connected to at least two CHs.

- Normal Node (NN): a node that is only connected to one CH. NNs only transmit/receive data to/from its own CH.

- Distribute Gateway (DG): a node designated to act as a GW when there is no GW to handle the data transfer between two clusters. DGs are connected to only one CH. They only exist when there is no GW available. Each DG is paired with another DG in a different cluster acting as a GW, i.e, passing data from one CH to another CH. They have to be within hearing range of each other and reside in different clusters.

- Solo Node (SL): a node that cannot be reached by any other nodes in the network. A SL is a special node that is disconnected from the rest of the network. Thus, if a network can be modeled as a complete graph, there is no SL. In this case, SLs are only used to initialize the simulation and each is eventually assigned to one or more CH.

Fig. 4.1 shows an example of different node types. In each cluster there is a unique CH acting as the hub of that cluster. All traffic demands that are not initiated from a CH must be sent to the CH first. The CH calculates the routing table and forwards the aggregated data along with the routing table through GW/DG if the destination is located in another cluster. Otherwise, the CH directly sends the data to the destination. A GW is a node that can see more than one CHs. DGs are special gateways used to connect two clusters as shown in Fig. 4.1. We can treat a pair of DGs as one GW. In the figure, if DGs are not defined, the right-most cluster would be isolated from the rest of the network since no node satisfies the definition of a GW. Note that the introduction of DGs is a double-edged sword: they enable more

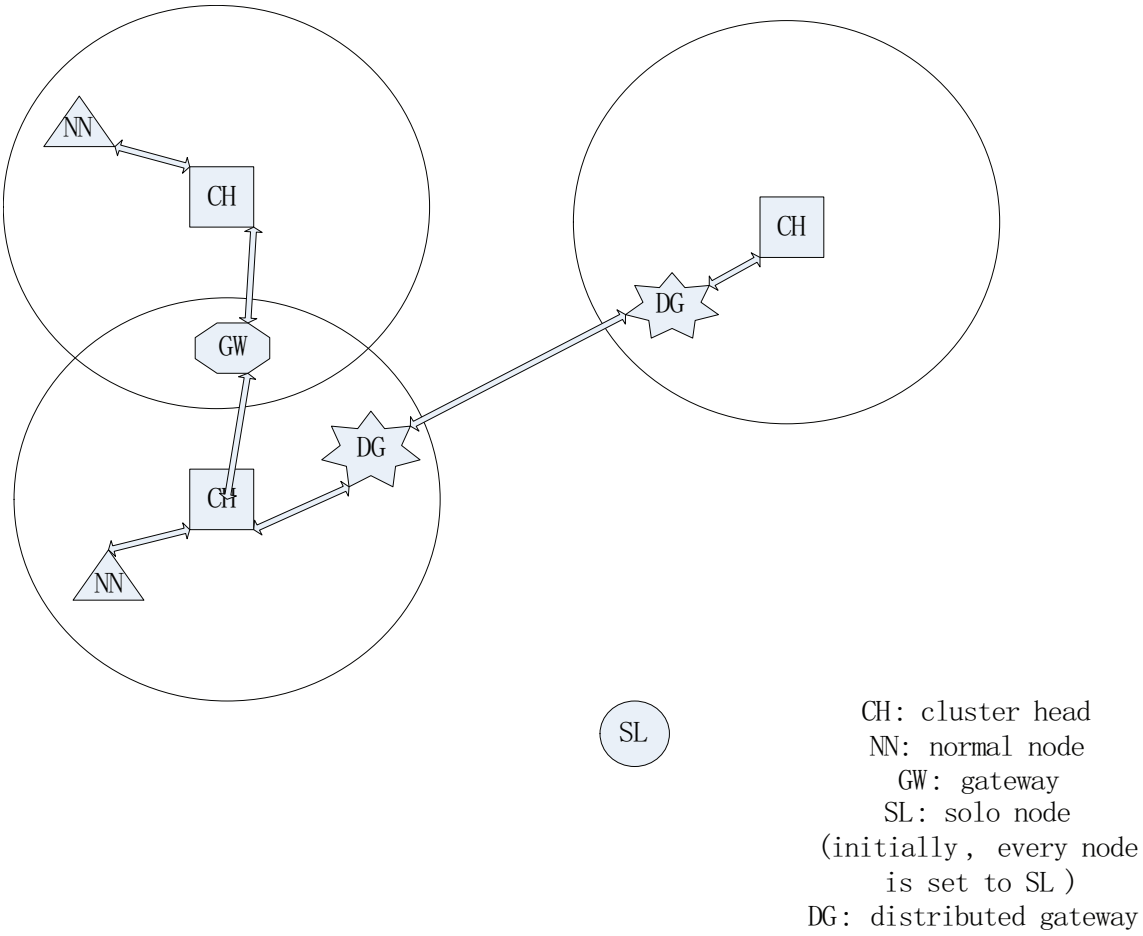

Figure 4.1: Illustration of different node types: CHs, GWs, NNs, DGs and SLs.

potential routes while creating more header information. Thus in our model, we only enable this option if there are no GWs in the cluster.

In hierarchical clustering, additional layers can be defined where multiple CHs can be grouped together into superclusters, and supercluster GWs must be defined. In our algorithm, we only have two layers, i.e., no superclusters.

In non-hierarchical algorithms, all nodes are treated equally. But in hierarchical algorithms, we treat different nodes differently. This is very suitable for our application since we need some nodes (with FSO links) to handle more traffic. Moveover, in non-hierarchical algorithms if one node fails, the whole network may be affected since all nodes are 'equal'. The network is more robust using a hierarchical algorithm. Of cause, another benefit is that, since only some nodes (CHs, GWs, DGs) handle

the routing, the routing table as well as overhead needed are much smaller compared with non-hierarchical methods. Consequently, the higher layers only contain few nodes that handle the routing. As discussed below, for our 100 nodes example we only have 11 - 12 cluster CHs.

4.2.2 Clustering Algorithm

To divide the network, especially large networks, into clusters has many advantages. After forming the clusters, only the CH in each cluster keeps the network clustering and link state information, and calculates the routes for traffic demands. This can reduce the overhead information in the packets and thus improve the network throughput. For backbone hybrid FSO/RF WMNs, network topology is relatively stable compared with ad-hoc networks. Thus the network does not need to recalculate the clusters very often, which further reduces the network bandwidth consumption. Moreover, from the cost point of few, we only need to equip the CHs with more powerful computers that handle routing calculations and store network information data.

The existing RF based clustering algorithms [71, 72] are not suitable for our application since they assume that all nodes in the network are equivalent. If we use these algorithms, nodes equipped with FSO transceiver will be treated the same as other RF nodes. The algorithm we designed is customized for hybrid FSO/RF networks. Nodes with FSO technology are prioritized and if possible elected as CHs, since FSO links can provide more bandwidth. Meanwhile, the algorithm ensures the connectivity in case some links, especially FSO links, are down.

The clustering algorithm determines the role of nodes as well as the partitions. At the start of the algorithm all nodes are initialized as SLs, which indicates that they do not belong to any cluster yet. Then each node begins to send out two types of 'hello' message periodically: RF broadcasting messages and FSO dedicated messages

(if equipped with FSO transceivers). The RF 'hello' message contains the following information:

1. The current node-type of the transmitter;
2. Clustering information indicating which cluster the node belongs to. CHs always keep clustering information of the whole network. GWs and DGs only temporarily hold whole clustering tables, which are deleted after they are broadcasted. NNs only know their own CH.
3. Link state information. Again, CHs permanently keep the network-wide link state information while GWs and DGs only pass the information. NNs only know the local link state.

The FSO 'hello' message does not contain clustering information. The FSO 'hello' message is used to update the FSO subnetwork topology and FSO link state information. We use the RF subnetwork to exchange clustering information since RF messages are broadcasted and RF communication is more reliable.

The algorithm used by a node upon receiving an RF 'hello' message is summarized as follows. The action is based on the role of the receiver and transmitter.

- The receiver (Rx) of the 'hello' message is a SL:
  - If the transmitter (Tx) is a SL or CH: The Rx compares the Tx and Rx priorities and assigns the one with higher priority as CH, while assigning the other as NN.
  - If the transmitter is a NN, GW or DG: The Rx changes itself into a CH.
- The receiver of the 'hello' message is a CH:
  - If the transmitter is a SL or CH: The Rx compares the Tx and Rx priorities and assigns the one with higher priority as CH, while assigning the other as a NN.

- If the transmitter is a NN:

    1. The Rx checks if it is the CH of the Tx, and if not, performs step 2, otherwise it performs step 3;
    2. The Rx changes the Tx to a GW and updates link state and clustering information. It stops executing;
    3. The Rx compares the Tx and Rx priorities and assign the one with higher priority as CH, while assigning the other as a NN.

- If the transmitter is a GW or DG: The Rx only updates link state and clustering information from the Tx.

- The receiver of the 'hello' message is a NN:

    - If the transmitter is a SL: The Rx compares the Tx and Rx's CH priority. If the Tx has a higher priority, it changes the Tx to be the CH of the Rx.
    - If the transmitter is a CH:

        1. The Rx checks if Tx is the CH of the Rx, and if not, performs step 2; otherwise it performs step 3;
        2. The Rx changes itself to a GW and updates link state and clustering information. It then stop executing;
        3. The Rx compares the Tx and Rx priorities and assign the one with higher priority as CH, while assigning the other as a NN.

    - If the transmitter is a NN:

        1. If the Tx is the CH of the Rx, the Rx performs 2. Otherwise it performs step 3;
        2. The Rx changes itself to be CH and updates link state and clustering information. It then stops executing;

3. The Rx checks if its CH is the CH of the Tx. If so it stop executing the following steps. Otherwise it proceeds to step 4;
4. The Rx checks if there is a GW in its own cluster. If so, it stops executing. Otherwise it proceeds to step 5;
5. The Rx changes itself and the Tx to DGs. It then updates link state and clustering information.

- If the transmitter is a GW or DG: The Rx checks if there is a GW in its own cluster. If so, it stops executing. Otherwise, it changes itself and the Tx to DGs. The Rx then updates link state and clustering information.

- The receiver of the 'hello' message is a GW:
  - If the transmitter is a SL: The Rx changes the Tx to become its CH;
  - If the transmitter is a CH, GW or DG: The Rx only updates link state and clustering information.
  - If the transmitter is a NN: The Rx node does nothing.

- The receiver of the 'hello' message is a DG:
  - The Rx checks if there exists a GW in its cluster that can communicate with at least one of the CHs of the Tx. If so, it changes itself to a NN and stop executing the following steps. Otherwise it continues as described below.
  - If the transmitter is a SL: The Rx changes the Tx to become its CH.
  - If the transmitter is a CH: The Rx checks if the Tx is its CH, and if so the Rx updates link state and clustering information and stops executing. Otherwise it changes itself to a GW and updates link state and clustering information.

- If the transmitter is a NN: The Rx checks if the Tx's CH is also its own CH, and if so it does nothing and stop executing. Otherwise it changes the Tx to a DG and updates link state and clustering information.
- If the transmitter is a GW or DG: The Rx only updates link state and clustering information.

The receiver updates link state and clustering information at the end of each action. Note that in the algorithm the Rx performs this task differently based on its own role. For CHs, GWs and DGs, global information are exchanged, while for NN and SL, only local information is updated. We introduce a time-stamp to avoid confusion when a node receives multiple copies of link state and clustering information from different nodes. Once an entry of information is updated, a time-stamp of the current time is added to that entry. For example, at time T_1, node i updates the clustering information from node j. At time T_2, node i receives an RF 'hello' message from another node k and starts to update the clustering information again. However, the clustering information from node k is different from that of node j. Then node i needs to compare the time-stamps of all entries in the clustering information and keeps only the latest version. When a node receives an FSO 'hello' message, it only updates the FSO link state information.

We claim the algorithm has converged when all CHs share identical network information, assuming network conditions have not changed. Based on the time-stamp, for a quasi-static network, only the latest clustering and link state information are kept and propagated though the network. Thus all CHs will eventually share the same link state and clustering information.

4.2.3 Distributed Routing

In general, there are two major classes of routing protocols: distance-vector routing and link-state routing protocols [73, 74, 75, 76]. In the distance-vector routing algorithm, a node keeps updating its own routing table based on routing tables from neighboring nodes. The Bellman-Ford algorithm is one of the algorithms used for distance-vector routing. Routing Information Protocol (RIPv1), RIPv2 and Interior Gateway Routing Protocol (IGRP) [77, 78] are examples of distance-vector routing protocols. In contrast, for link-state routing, each node calculates routing tables independently based on the knowledge of the whole network topology and link state information. Examples include open shortest path first (OSPF) and intermediate system to intermediate system (IS-IS) [79, 80]. Compared with distance-vector routing, the routing table in the link-state routing algorithm converges faster. However, link-state routing also requires more overhead.

For our hybrid FSO/RF network model, we choose the link-state routing algorithm. The FSO links may not be stable in serious weather conditions, and the nodes need to recalculate routes when such link states are changed. The link-state routing algorithm is more suitable for this purpose. Moreover, since we use a hierarchical routing method, the routing table only contains CHs, GWs and DGs, which can decrease the overhead information.

After the clustering algorithm has converged, all CHs have the latest network information: topology and link states. The information we use for routing includes: (1) clustering information that indicates the location and CH of every node, (2) link rate in bits/second for both RF and FSO subnetworks, and (3) link availabilities (with unavailable links equivalently represented as having a link rate of 0 bits/sec).

Compared with the conventional link-state routing algorithm for pure RF networks, in our case the link state metric includes both RF and FSO link states. Moreover, our routing protocol also gives FSO links higher priority when they are

available for routing traffic. Our routing algorithm is based on the shortest path algorithm (using Dijkstra's algorithm in our simulation) as described in Algorithm 3.

Algorithm 3 Distributed Routing Algorithm

Step 1. When receiving an initial traffic demand, check the role of the source. If the source is not a CH, go to **Step 2**, otherwise jump to **Step 3**.
Step 2. Send data to its CH. For GW nodes, it arbitrarily chooses a CH to send the data.
Step 3. This CH calculates the route using the shortest path algorithm. The nodes in the graph include CHs, GWs and DGs. The weight of each link is $1/(\text{RF link rate} + \text{FSO link rate})$.
Step 4. If the destination is not a CH, the destination is set to the CH of the original destination.
Step 5. Transmit data according to the route.
Step 6. If a link is down in the route, the transmitter keeps trying until timeout. If it hits the timeout, go back to **Step 2**.
Step 7. Finish transmission if the traffic reaches the destination.

When a traffic demand is initiated, the source node first checks its own role as a node in the network. Unless it is a CH, the traffic needs to be sent to the CH. Since the CH knows the topology and link state of the network, it calculates the route to the destination. The link desirability metric is the sum throughput of RF and FSO links, and thus the cost of using the link is simply the reciprocal of this value. During transmission, data are partitioned and send through RF and FSO links simultaneously if both links are available. If a link in the route is not available for a pre-defined time, the traffic will be sent to the current CH for recalculating a new route. Note that in the current design if the source is a GW node, the first hop CH is arbitrarily picked. If we can sacrifice some overhead and let GWs store network information and calculate routes, the routing can be more efficient. However, due to the increase in overhead, the throughput of the network is not necessarily improved.

We keep our point to point transmission protocol simple since this is not the primary objective of this chapter. Before sending data from a transmitter to a receiver, the Tx node sends an acquisition (ACQ) message to the Rx to ask for transmit bandwidth. If the Rx has resources available, i.e., RF and/or FSO links, it sends back an

acknowledgment (ACK) message and holds the link for the data transmission. The link is released after transmission has finished. If the Tx node does not hear back, it will resend an ACQ message after an arbitrary time. Timeout is claimed after a predefined number of tries. In the current model, we dedicate all available bandwidth to one traffic demand. In the future, more complicated duplexing models can be used to improve the throughput.

4.3 Simulation Results

In this section, we present some preliminary simulation results to show the advantages of the hybrid FSO/RF network. Current simulation software does not cover the hybrid technology environment we are interested in, and thus we build our own simulation model using Matlab. The simulator model is inspired by [81]. The model and protocols are programmed based on the description in Section 4.2.

4.3.1 Clustering

In this section, we demonstrate the simulation of our clustering algorithm on two example topologies, a small sparse network and a large dense network. For both topologies our clustering algorithm results in fast convergence, which is important for real-time applications.

In the first example, 10 nodes in the network are sparse and located in a 10 km $\times$ 10 km area. The communication range for both RF and FSO links is assumed to be 2750 m. In Fig. 4.2(a), we assume there are no FSO links. For simplicity we use the CH ID number to represent the cluster. Each node broadcasts RF 'hello' messages periodically. Based on the simulation, after 6 'hello' message exchanges, the clustering algorithm has converged, i.e., all CHs contain the same network information, assuming network topology and link states have not changed. Note that in this example there

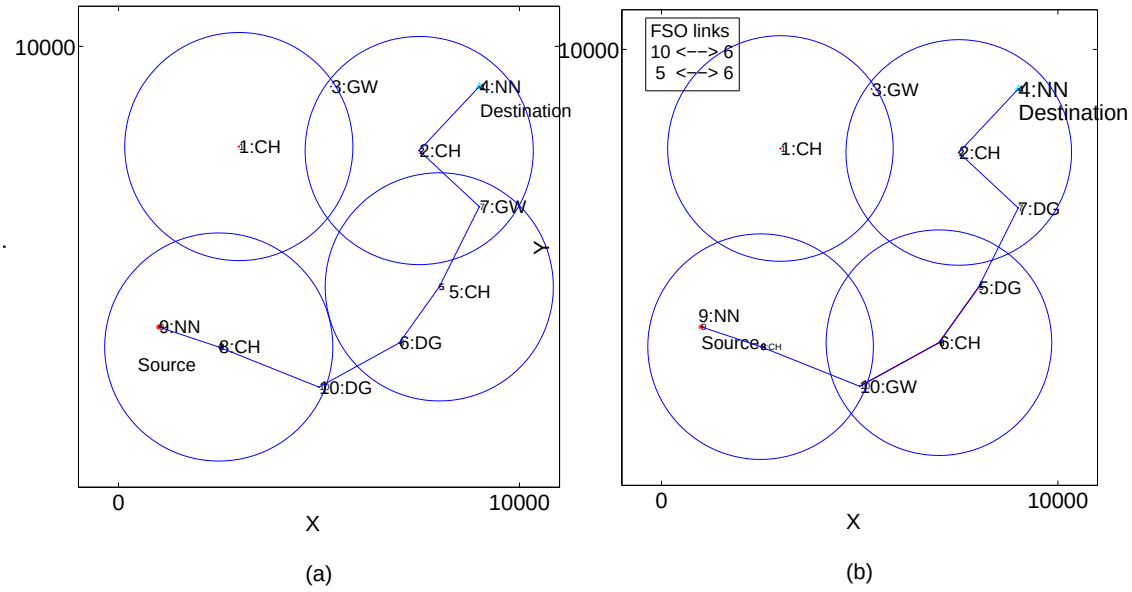

Figure 4.2: Clusters of a sparse network: (a) without FSO links (b) with FSO links $10 \leftrightarrow 6$ and $5 \leftrightarrow 6$.

is no GW node in cluster 8, thus a DG pair using nodes 10 and 6 is formed. Without these DGs, cluster 8 would be separated from the rest of the network. DG 10 and DG 6 form the gateway between cluster 8 and cluster 5 for data exchange.

In Fig. 4.2(b), we assume links $10 \leftrightarrow 6$ and $5 \leftrightarrow 6$ are the only two line-of-sight links and equipped with FSO transceivers. For this example, the simulation results in a different clustering topology. Since node 6 has a higher priority than other nodes now based on our algorithm, it becomes the new CH. As we know, CHs handle aggregated data either from or to GWs, DGs and NNs. Allocating nodes with higher bandwidth as CHs can relieve network congestion. Note that in this example, since node 10 is a GW node, there is no DG in cluster 8 anymore, and thus another DG pair using nodes 5 and 7 is formed for handling data transmission between clusters 6 and 2.

In the second example, we randomly place 100 nodes in a 10 km $\times$ 10 km area. In this demonstration, we also show the different clustering results without FSO links (Fig 4.3(a)) and with FSO links (Fig 4.3(b)). In Fig 4.3(b), we randomly place 50

FSO links in the network as shown. Since FSO link allocation is not the main topic of this chapter, we just assume FSO links are predetermined either by cost and line-of-sight constraints or using the allocation algorithm in Chapter 3. The communication for both RF and FSO links is 2480 meters, which guarantees the network graph is complete. Based on the simulation, even for this large network, it takes no more than 7 'hello' message exchanges to achieve converged clustering for both topologies. As we mentioned above, our current algorithm tries to minimize the number of DGs to decrease the routing overhead. However, the throughput of the network may be increased by having more DGs, since we have more routes to choose from in this case. In future research, how to choose the optimal number of DGs in a cluster needs to be studied.

4.3.2 Routing

In this section, we use the topology generated above in Section 4.3.1 to show the results of our routing algorithm. In our simulation, we use the average throughput for all traffic demands as a performance metric. In the model, the overhead is assumed to be proportional to the total number of CHs, GWs and DGs. For every 1% of the total number of nodes that become a CH, GW, or DG, the overhead as a percentage of the data transmitted increases by 0.5%. For example in a 100 node network, if there are 20 CHs, GWs and DGs, the overhead occupies 10% of the data. We assume the time taken to transmit a traffic demand consists of three major parts: the ACQ time, the actual transmission time on each hop, and the waiting time if a link is not available. Here we assume the data processing time at each node is negligible. In future research, we can develop a more sophisticate model to take into account this delay. In our simulation, we assume all RF links have a rate of 100 Mbps while the transmission rate for FSO links is 1 Gbps. In our transmission model, we also assume a relay node needs to receive all the data before forwarding it to the next node. Based

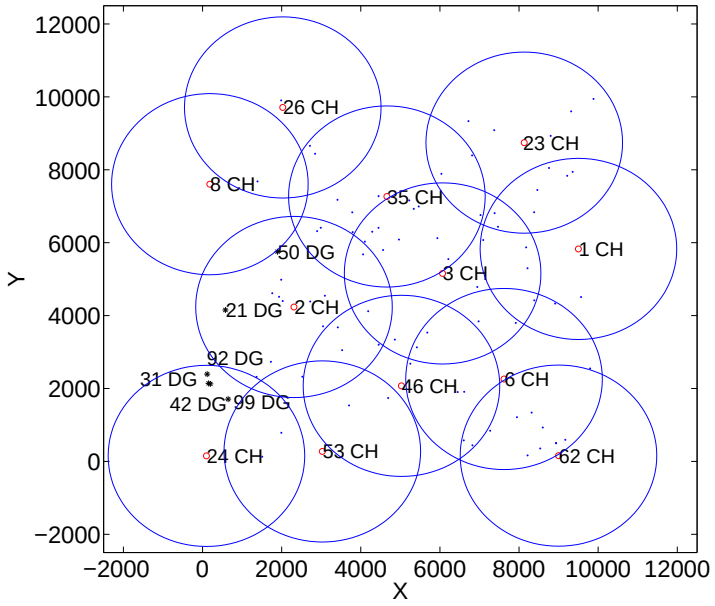

(a)

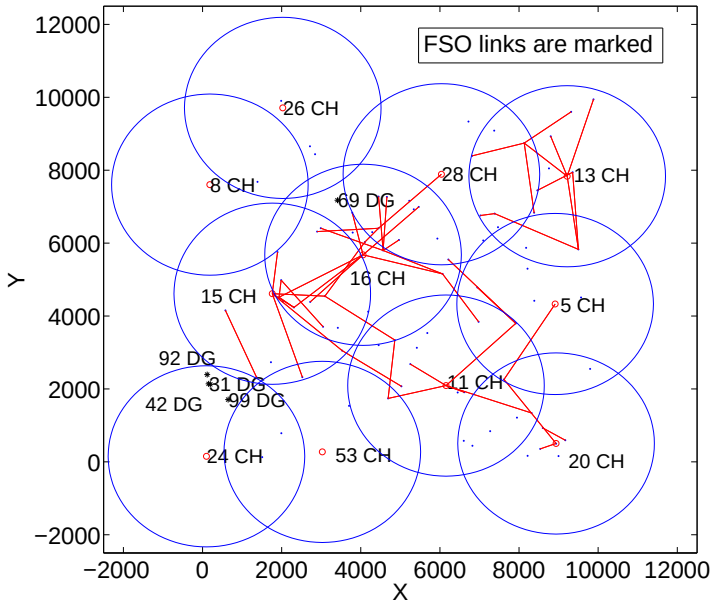

(b)

Figure 4.3: 100 node network clustering example. (a) without FSO links (b) with FSO links marked with red lines

on these assumptions, the throughput of a traffic demand can be calculated as:

$$\text{Throughput} = \frac{\text{data size(bytes)} \times (1 - \text{overhead ratio})}{\text{total transmission time from source to destination}} \tag{4.1}$$

In the small network example, we only create one traffic demand so that we can clearly see the advantage of having hybrid links. In the large network example, multiple traffic demands are present so that we can show the throughput improvement by allocating high throughput FSO links.

Throughput improvement due to added FSO links

In the sparse network shown in Fig 4.2, we assume there is a traffic demand from NN 9 to NN 6. Since there is only one viable route for this traffic, the routes for the network without and with FSO links are the same. However, since for the network with FSO links the transmission speed of link $10 \rightarrow 6$ and $6 \rightarrow 5$ is much faster, the throughput is 7.7 Mbps compared with 5.7 Mbps for the network without FSO links (35% improvement).

In the large network example in Fig 4.3, we assume there are two traffic demands: from node 26 to node 58 and from node 99 to node 84 as shown in Fig 4.4 for both networks without and with FSO links. We mark the sources with 'S' and the destinations with 'D'. As we can see, since there are multiple choices for routes in each topology, the shortest distance algorithm results in different routes for Fig 4.4(a) and Fig 4.4(b). The routes calculated in Fig 4.4(b) take full advantages of the high throughput FSO links. The thicker lines in Fig 4.4(b) highlight the links using FSO technology. With FSO technology, the throughput for the two traffic demands are 7.5 Mbps and 7.7 Mbps respectively, resulting in an average throughput of 7.6 Mbps. Without FSO technology, the throughputs are 4.9 Mbps and 6.5 Mbps individually,

resulting in an average throughput of 5.7 Mbps. The average throughput improvement is 33.3%.

Throughput improvement due to our clustering algorithm

In the previous section, we show the throughput improvement due to the added FSO links, which is expected since more resources are added to the network. In this part, we compare the throughput of the same network topology using the RF-only network clustering algorithm in [71, 72] and our clustering algorithm. Without using our clustering algorithm that is optimized for hybrid FSO/RF networks, the clustering result will be the same as that in Fig 4.4(a). Then we use our routing algorithm on this topology but with FSO links. The average throughput is 6.9 Mbps, compared with the 7.6 Mbps obtained using our clustering algorithm (10% improvement). This is because our clustering algorithm allocates nodes with more FSO links to roles and places where the congestion is likely to happen. As we can see in Fig 4.4(b), CH 15, which has the highest number of FSO links among all nodes, handles the most congested point in the network. Moreover, we find an interesting behavior of our algorithm, which can be further studied in the future: using our clustering algorithm, the throughputs obtained for the two traffic demands are closer in value when we use our algorithm compared with the other clustering algorithm. This implies that our algorithm may result in better traffic fairness. In the example given, by using our algorithm the throughputs are 7.5 Mbps and 7.7 respectively. However, the throughputs are 5.2 Mbps and 7.2 Mbps using the clustering algorithm designed for pure RF networks.

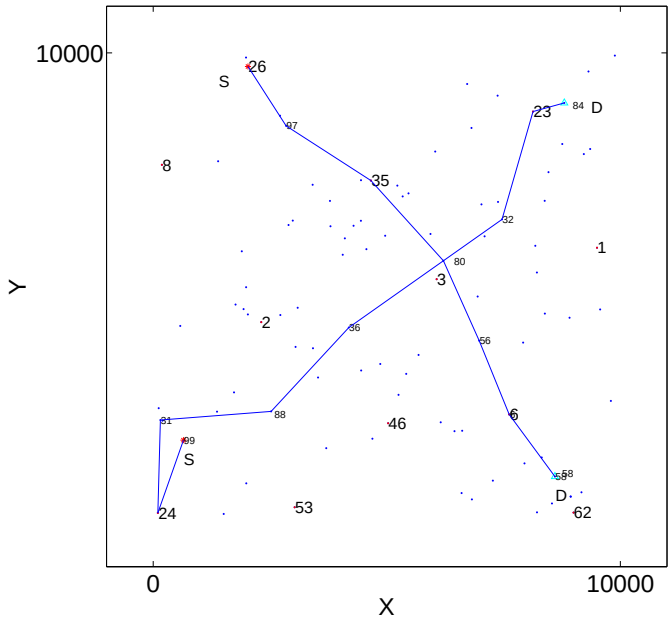

(a)

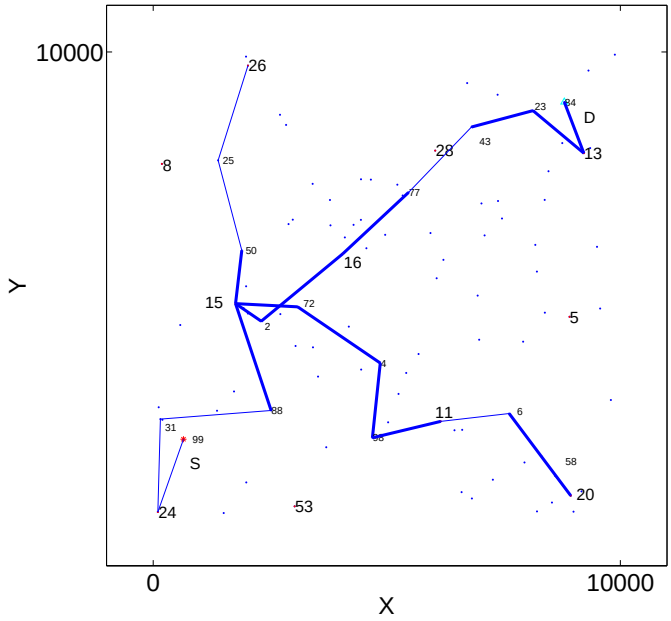

(b)

Figure 4.4: 100 node network routing example (a) without FSO links (b) with FSO links

4.4 Chapter Summary

In this chapter, we propose clustering and routing algorithms specially designed for hybrid FSO/RF networks. Detailed simulation results shown the advantages of having additional FSO links in WMNs. We show that our clustering algorithm is computationally efficient. Even for a large network, it takes a short time to reach convergence. The throughput improvement achieved by using our clustering algorithm is also illustrated.

As we mentioned above, this is a preliminary study on the topic of distributed routing for FSO/RF networks. In order to concentrate on the routing algorithm development, we have made simple assumptions on the channel state model. In future work, we can consider the physical layer limitations together with the network layer routing issue to form a cross-layer optimization problem. The study of this joint optimization problem can result in further network throughput and performance improvements.

Chapter 5

Conclusions

Hybrid FSO/RF communication is an emerging technology for increasing the wireless bandwidth availability to meet the growing need for data throughput. This dissertation focuses on developing theoretical analyses as well as implementation methods for hybrid FSO/RF technology. In order to form a complete hybrid FSO/RF broadband communication system, both physical layer point-to-point (P2P) hybrid systems and hybrid networks have been studied.

Point-to-Point Hybrid FSO/RF Systems

In our research on P2P hybrid FSO/RF communication systems presented in Chapter 2, we model the system as an independent parallel channel system and derive the theoretical throughput of this system. The major topics and conclusions in this part of the research are:

- The information-theoretic throughput for general independent parallel channel systems is derived in Section 2.2. This throughput is presented as a function of system parameters: the encoder rate, puncturing ratio, and symbol rates and modulations for each channel. We dynamically adjust these parameters to yield the maximum throughput.

- The throughput optimization problem assuming an encoder rate constraint is studied in Section 2.3. Both symbol rate and modulation adaptation algorithms are formulated in this section. For this case, we conclude that the system should operate as close to capacity as possible. We prove that the capacity is nearly-achievable by choosing optimal symbol rates with no code puncturing. The uniqueness of the optimal solution is also proved. We then provide a efficient search mechanism to find this solution.

- The throughput optimization problem with additional modem-rate constraints is developed in Section 2.4. The optimization problem needs to be separated into four cases based on the values of system parameters. We present a flow chart for determining which case applies and solving the optimization problem for each case. The major conclusion is that we should puncture a mother code to achieve a higher throughput when both channel conditions are good. Otherwise, the minimum encoder rate needs to be used while symbol rates and modulation formats need to be adjusted to obtain the optimal throughput.

- In Section 2.4.2, the optimization method is applied to FSO/RF hybrid systems. Numerical, simulation, and experimental results are present to show the throughput improvement of such a system comparing with nonadaptive systems.

The design of forward error control codes for nonuniform parallel channels to operate near capacity is an opportunity for future work. The code needs to be capable of handling channel diversity and of being punctured over a potentially large range of encoder rates. In addition, the practical issue of how to achieve reliable communication when exact channel state information is not available at the transmitter needs to be studied. A possible solution is to combine our method with the rateless code described in [36]. Once a single FSO/RF parallel system is fully understood, an ex-

tension of the link adaptation technique to a multiple-input multiple-output (MIMO) system is another fruitful area of future research.

Centralized Hybrid FSO/RF Networks

In our research on hybrid FSO/RF wireless mesh networks (WMNs), we first study centralized control algorithms in Chapter 3. In this approach, routing and scheduling functions are assumed to be regulated by one control unit with complete knowledge of the physical and network layers. We use mixed integer linear programming (MILP) to jointly solve the throughput optimization and routing problem. A summary of major topics addressed is as follows:

- We present our network model in Section 3.2. Unlike previous work on WMNs that only considers quasi-static network models, we formulate the link allocation, routing and scheduling problem based on either the protocol interference model or the physical interference model, addressing both nonfading and fading cases.

- In Section 3.3, optimization formulations for both quasi-static and fading network models are present. A MILP is used to optimally solve the throughput optimization problem. The FSO link allocation, throughput optimization, routing, and scheduling problems can be jointly solved by using the MILP. We present methods to find exact solutions and upper bounds to the optimal solution in Section 3.4. For large networks, two heuristic methods are also provided in this section.

- We can draw the following major conclusions based on numerical results for various network topologies illustrated in Section 3.5. First, the routing is more robust and results in higher network throughput if based on the physical model instead of the protocol model. This is because the physical model is more accu-

rate at modeling link interference behavior. Second, we show that our heuristic method is efficient in obtaining a near-optimal result for a mid-size network with many traffic demands. Lastly, numerical results for fading networks, where the influence of FSO and RF link outage probabilities are studied, are shown. An important conclusion is that, for the parameters and networks tested, a higher FSO link outage probability results in lower throughput while a higher RF link outage probability does not necessarily imply throughput degradation.

In our fading model, we assume a simple FSO model where links are either available or unavailable. A potential further throughput improvement can be achieved by using more sophisticated FSO link and subnetwork models, such as those given in [1, 2]. In addition, our goal in this research is to maximize the total throughput of the network without considering throughput fairness among different traffic demands, as shown in Section 3.5.2. Further research to address this problem is needed when fairness is required.

Distributed Hybrid FSO/RF Networks

Centralized control yields an optimal solution, yet it does not result in a scalable algorithm useful for larger networks due to its computational complexity. For large network applications, we propose a distributed routing algorithm in Chapter 4. In this framework, our algorithm first partitions the network into clusters. Then the cluster-head node in each cluster makes routing decisions based on local network link state information. The topics covered in this part of the dissertation are as follows:

- Section 4.2.1 lists the assumptions made and describes our distributed network model for hybrid FSO/RF WMNs. In particular, we assume that FSO links have been assigned to some network links *a priori*.

- A clustering algorithm based on exchanging RF and FSO 'hello' messages is presented in Section 4.2.2. Our algorithm assigns a higher priority to nodes with FSO links so that network clustering is tailored to the hybrid FSO/RF WMN. Our simulation results show that even with large networks, our algorithm usually requires no more than 10 'hello' message exchanges to obtain algorithm convergence.

- A shortest-distance based routing algorithm designed for FSO/RF networks is discussed in Section 4.2.3. We first compare the throughput of the network with and without FSO links to show that introducing high throughput FSO links can increase the network throughput dramatically. We then compare the throughput of the network based on our clustering algorithm with the performance using clustering algorithms that do not distinguish between FSO and RF links. The simulation results show that by using our clustering algorithm, which is designed especially for hybrid FSO/RF applications, the throughput of the network improves, depending on the number of FSO links.

As we discuss in Chapter 4, there are a few topics that can be studied in the future to further improve the network throughput. First, whether to enable some gateway and distributed-gateway nodes to calculate routes directly can be addressed. Second, how many distributed-gateways we should be allocated needs to be studied. In both cases, the tradeoff is between an increase in the number of network routing options and an increase in communications overhead. The right decisions on these questions could result in a higher throughput than our current design, but is likely to depend on the network topology. Third, a more complex model including cross-layer optimization can be studied to further increase the network throughput. Lastly, mobile networking using hybrid FSO/RF technology is also viable, but an exceptionally challenging problem.

This dissertation has provided a comprehensive study of hybrid FSO/RF systems including both the physical and network layers. The models and algorithms presented take into account the network diversity. The particular properties of FSO and RF subnetworks are highlighted in our study. The systems are designed to fully utilize the high bandwidth of FSO links while maintaining connectivity by relying on low rate but reliable RF links.

Bibliography

[1] X. Zhu and J. Kahn, "Free-space optical communication through atmospheric turbulence channels," *IEEE Transactions on Communications*, vol. 50, no. 8, pp. 1293–1300, Aug 2002.

[2] I. I. Kim and E. J. Korevaar, "Availability of free-space optics (FSO) and hybrid FSO/RF systems," in *Society of Photo-Optical Instrumentation Engineers (SPIE) Conference Series*, ser. Society of Photo-Optical Instrumentation Engineers (SPIE) Conference Series, E. J. Korevaar, Ed., vol. 4530, Nov. 2001, pp. 84–95.

[3] S. Wilson, M. Brandt-Pearce, Q. Cao, and J. Leveque, "Free-space optical MIMO transmission with Q-ary PPM," *IEEE Transactions on Communications*, vol. 53, no. 8, pp. 1402 – 1412, Aug. 2005.

[4] V. W. Chan, "Free-space optical communications," *Journal of Lightwave Technology*, vol. 24, no. 12, pp. 4750–4762, 2006.

[5] X. Wu, P. Liu, and M. Matsumoto, "A study on atmospheric turbulence effects in full-optical free-space communication systems," in *Wireless Communications Networking and Mobile Computing (WiCOM), 2010 6th International Conference on*, 2010, pp. 1–5.

[6] M. Rahman, S. Iqbal, and M. Islam, "Modeling and performance analysis of free space optical communication system," in *Informatics, Electronics Vision (ICIEV), 2012 International Conference on*, 2012, pp. 211–218.

[7] M. Al-Habash, L. C. Andrews, and R. L. Phillips, "Mathematical model for the irradiance probability density function of a laser beam propagating through turbulent media," *Optical Engineering*, vol. 40, no. 8, pp. 1554–1562, 2001.

[8] X. Liu, "Free-space optics optimization models for building sway and atmospheric interference using variable wavelength," *IEEE Transactions on Communications*, vol. 57, no. 2, pp. 492–498, 2009.

[9] [Online]. Available: http://esc.gsfc.nasa.gov/

[10] J. Barry, J. Kahn, W. Krause, E. Lee, and D. Messerschmitt, "Simulation of multipath impulse response for indoor wireless optical channels," *IEEE Journal on Selected Areas in Communications*, vol. 11, no. 3, pp. 367–379, 1993.

[11] O. Gonzalez, R. Perez-Jimenez, S. Rodriguez, J. Rabadan, and A. Ayala, "OFDM over indoor wireless optical channel," *IEE Proceedings - Optoelectronics*, vol. 152, no. 4, pp. 199–204, 2005.

[12] A. Azhar, T. Tran, and D. O'Brien, "A Gigabit/s indoor wireless transmission using MIMO-OFDM visible-light communications," *IEEE Photonics Technology Letters*, vol. 25, no. 2, pp. 171–174, 2013.

[13] M. Noshad and M. Brandt-Pearce, "Application of expurgated PPM to indoor visible light communications - part I: single-user systems," *to appear in IEEE/OSA Journal of Lightwave Technology*, 2013.

[14] ——, "Application of expurgated PPM to indoor visible light communications - part II: access networks," *to appear in IEEE/OSA Journal of Lightwave Technology*, 2013.

[15] W. O. Popoola and Z. Ghassemlooy, "BPSK subcarrier intensity modulated free-space optical communications in atmospheric turbulence," *Journal of Lightwave Technology*, vol. 27, no. 8, pp. 967–973, 2009.

[16] E. Bayaki, R. Schober, and R. K. Mallik, "Performance analysis of MIMO free-space optical systems in gamma-gamma fading," *IEEE Transactions on Communications*, vol. 57, no. 11, pp. 3415–3424, 2009.

[17] S. M. Navidpour, M. Uysal, and M. Kavehrad, "BER performance of free-space optical transmission with spatial diversity," *IEEE Transactions on Wireless Communications*, vol. 6, no. 8, pp. 2813–2819, 2007.

[18] M. Uysal, J. Li, and M. Yu, "Error rate performance analysis of coded free-space optical links over gamma-gamma atmospheric turbulence channels," *IEEE Transactions on Wireless Communications*, vol. 5, no. 6, pp. 1229–1233, 2006.

[19] K. Kiasaleh, "Performance of APD-based, PPM free-space optical communication systems in atmospheric turbulence," *IEEE Transactions on Communications*, vol. 53, no. 9, pp. 1455–1461, 2005.

[20] A. A. Farid and S. Hranilovic, "Outage capacity optimization for free-space optical links with pointing errors," *Journal of Lightwave technology*, vol. 25, no. 7, pp. 1702–1710, 2007.

[21] J. C. Juarez, A. Dwivedi, A. Mammons, S. D. Jones, V. Weerackody, and R. A. Nichols, "Free-space optical communications for next-generation military networks," *IEEE Communications Magazine*, vol. 44, no. 11, pp. 46–51, 2006.

[22] K. Kiasaleh, "Performance of coherent DPSK free-space optical communication systems in K-distributed turbulence," *IEEE Transactions on Communications*, vol. 54, no. 4, pp. 604–607, 2006.

[23] M. Safari and M. Uysal, "Relay-assisted free-space optical communication," *IEEE Transactions on Wireless Communications*, vol. 7, no. 12, pp. 5441–5449, 2008.

[24] S. Vangala and H. Pishro-Nik, "A highly reliable FSO/RF communication system using efficient codes," in *Global Telecommunications Conference, 2007. GLOBECOM '07. IEEE*, Nov. 2007, pp. 2232–2236.

[25] H. Tapse and D. Borah, "Hybrid optical/RF channels: characterization and performance study using low density parity check codes," *IEEE Transactions on Communications*, vol. 57, no. 11, pp. 3288 –3297, Nov. 2009.

[26] F. Nadeem, V. Kvicera, M. S. Awan, E. Leitgeb, S. Muhammad, and G. Kandus, "Weather effects on hybrid FSO/RF communication link," *IEEE Journal on Selected Areas in Communications*, vol. 27, no. 9, pp. 1687–1697, 2009.

[27] W. Zhang, S. Hranilovic, and C. Shi, "Soft-switching hybrid FSO/RF links using short-length raptor codes: design and implementation," *IEEE Journal on Selected Areas in Communications*, vol. 27, no. 9, pp. 1698–1708, 2009.

[28] A. Akbulut, H. G. Ilk, and F. Ari, "Design, availability and reliability analysis on an experimental outdoor FSO/RF communication system," in *Transparent Optical Networks, 2005, Proceedings of 2005 7th International Conference*, vol. 1. IEEE, 2005, pp. 403–406.

[29] F. Ahdi and S. Subramaniam, "Optimal placement of FSO links in hybrid wireless optical networks," in *IEEE Global Telecommunications Conference (GLOBECOM 2011)*, Dec. 2011.

[30] D. Wang and A. Abouzeid, "Throughput capacity of hybrid radio-frequency and free-space-optical (RF/FSO) multi-hop networks," in *Information Theory and Applications Workshop*, Feb. 2007.

[31] H. Moradi, M. Falahpour, H. Reafi, P. LoPresti, and M. Atiquzzaman, "Availability modeling of FSO/RF mesh networks through turbulence-Induced fading channels," in *INFOCOM IEEE Conference on Computer Communications Workshops*, March 2010.

[32] V. Rajakumar, M. Smadi, S. Ghosh, T. Todd, and S. Hranilovic, "Interference management in WLAN mesh networks using free-space optical links," *Journal of Lightwave Technology*, vol. 26, no. 13, pp. 1735–1743, July 2008.

[33] A. Kashyap and M. Shayman, "Routing and traffic engineering in hybrid RF/FSO networks," in *IEEE International Conference on Communications*, vol. 5, May 2005, pp. 3427– 3433.

[34] I. B. Djordjevic and G. T. Djordjevic, "On the communication over strong atmospheric turbulence channels by adaptive modulation and coding," *Optics Express*, vol. 17, no. 20, pp. 18 250–18 262, 2009.

[35] I. Sason and I. Goldenberg, "Coding for parallel channels: Gallager bounds and applications to turbo-like codes," *IEEE Transactions on Information Theory*, vol. 53, no. 7, pp. 2394–2428, July 2007.

[36] A. Abdulhussein, A. Oka, T. T. Nguyen, and L. Lampe, "Rateless coding for hybrid free-space optical and radio-frequency communication," *IEEE Transactions on Wireless Communications*, vol. 9, no. 3, pp. 907 –913, march 2010.

[37] I. Sason and G. Wiechman, "On achievable rates and complexity of LDPC codes over parallel channels: bounds and applications," *IEEE Transactions on Information Theory*, vol. 53, no. 2, pp. 580–598, Feb. 2007.

[38] R. Liu, P. Spasojevic, and E. Soljanin, "Reliable channel regions for good binary codes transmitted over parallel channels," *IEEE Transactions on Information Theory*, vol. 52, no. 4, pp. 1405–1424, April 2006.

[39] I. F. Akyildiz and X. Wang, *Wireless mesh networks*, 1st ed. John Wiley&Sons Ltd, 2009.

[40] I. K. Son and S. Mao, "Design and optimization of a tiered wireless access network," in *INFOCOM, 2010 Proceedings IEEE*. IEEE, 2010, pp. 1–9.

[41] O. Awwad, A. Al-Fuqaha, B. Khan, and G. Brahim, "Topology control schema for better QoS in hybrid RF/FSO mesh networks," *IEEE Transactions on Communications*, vol. 60, no. 5, pp. 1398–1406, 2012.

[42] M. Smadi, S. Ghosh, A. Farid, T. Todd, and S. Hranilovic, "Free-space optical gateway placement in hybrid wireless mesh networks," *Journal of Lightwave Technology*, vol. 27, no. 14, pp. 2688–2697, 2009.

[43] P. Harshavardhana, D. J. Tebben, A. Dwivedi, and A. R. Hammons, "DAPR (Distributed adaptive precomputed restoration): An Algorithm for Assured availability Directional RF and FSO MANET," in *Military Communications Conference, 2007. MILCOM 2007. IEEE*. IEEE, 2007, pp. 1–6.

[44] J. Derenick, C. Thorne, and J. Spletzer, "On the deployment of a hybrid free-space optic/radio frequency (FSO/RF) mobile ad-hoc network," in *Intelligent Robots and Systems, 2005. (IROS 2005). 2005 IEEE/RSJ International Conference on*, 2005, pp. 3990–3996.

[45] D. Kumar and Y. Murthy, "Hierarchical routing protocol for free-space optical mobile ad hoc networks (FSO/RF MANET)," *International Journal of Computer Applications*, vol. 60, no. 10, 2012.

[46] J. Sonnenberg, M. Oyler, R. Peach, and G. Burdge, "Routing impact in highly dynamic mesh networks of RF and FSO links," in *Military Communications Conference, 2009. MILCOM 2009. IEEE.* IEEE, 2009, pp. 1–7.

[47] O. Awwad, A. Al-Fuqaha, B. Khan, D. Benhaddou, M. Guizani, and A. Rayes, "Bayesian-based game theoretic model to guarantee cooperativeness in hybrid RF/FSO mesh networks," in *Global Telecommunications Conference, 2009. GLOBECOM 2009. IEEE*, 2009, pp. 1–7.

[48] R. S. Raghavan, A. Kam, and R. Y. Mannepalli, "Modeling & simulation to study the performance of hybrid free space optical/RF military communication networks," in *Military Communications Conference, 2008. MILCOM 2008. IEEE.* IEEE, 2008, pp. 1–7.

[49] J. Zhang, "Proposal of free space optical mesh network architecture for broadband access," in *IEEE International Conference on Communications, 2002. ICC 2002.*, vol. 4, 2002, pp. 2142–2145 vol.4.

[50] I. Ouveysi, F. Shu, W. Chen, G. Shen, and M. Zukerman, "Topology and routing optimization for congestion minimization in optical wireless networks," *Optical Switching and Networking*, vol. 7, no. 3, pp. 95–107, 2010.

[51] A. Desai and S. Milner, "Autonomous reconfiguration in free-space optical sensor networks," *IEEE Journal on Selected Areas in Communications*, vol. 23, no. 8, pp. 1556–1563, 2005.

[52] A. Desai, J. Llorca, and S. Milner, "Autonomous reconfiguration of backbones in free space optical networks," in *Military Communications Conference, 2004. MILCOM 2004. 2004 IEEE*, vol. 3. IEEE, 2004, pp. 1226–1232.

[53] J. Llorca, A. Desai, U. Vishkin, C. C. Davis, and S. D. Milner, "Reconfigurable optical wireless sensor networks," in *Remote Sensing*. International Society for Optics and Photonics, 2004, pp. 136–146.

[54] S. V. Kartalopoulos, "Protection strategies and fault avoidance in free space optical mesh networks," in *4th IEEE International Conference on Circuits and Systems for Communications, 2008. ICCSC 2008.* IEEE, 2008, pp. 797–801.

[55] Z. Hu, P. Verma, and J. Sluss, "Routing in degree-constrained FSO mesh networks," in *Future Generation Communication and Networking, 2008. FGCN '08. Second International Conference on*, vol. 1, 2008, pp. 208–215.

[56] Y. Shim, S. Gabriel, S. Milner, and C. Davis, "Topology control in a free space optical network," in *Telecommunications Modeling, Policy, and Technology*. Springer, 2008, pp. 291–310.

[57] D. N. Tse, "Optimal power allocation over parallel Gaussian broadcast channels," in *IEEE International Symposium on Information Theory*. Citeseer, 1997, pp. 27–27.

[58] X. Qin and R. A. Berry, "Distributed power allocation and scheduling for parallel channel wireless networks," *Wireless Networks*, vol. 14, no. 5, pp. 601–613, 2008.

[59] Y. Liu and E. Knightly, "Opportunistic fair scheduling over multiple wireless channels," in *INFOCOM 2003. Twenty-Second Annual Joint Conference of the IEEE Computer and Communications. IEEE Societies*, vol. 2. IEEE, 2003, pp. 1106–1115.

[60] G. Caire, G. Taricco, and E. Biglieri, "Optimum power control over fading channels," *IEEE Transactions on Information Theory*, vol. 45, no. 5, pp. 1468–1489, 1999.

[61] P. E. McIllree, "Channel capacity calculations for m-ary n-dimensional signal sets," Ph.D. dissertation, The University of South Australia, 1995.

[62] H. W. Kuhn and A. W. Tucker, "Nonlinear programming," in *Proceedings of the second Berkeley symposium on mathematical statistics and probability*, vol. 5. California, 1951.

[63] Y. Tang, M. Brandt-Pearce, and S. G. Wilson, "Adaptive coding and modulation for hybrid FSO/RF systems," *Asilomar Conference on Signals, Systems, and Computers*, Nov. 2009.

[64] Y. Tang and M. Brandt Pearce, "Link allocation, routing and scheduling of FSO augmented RF wireless mesh networks," in *IEEE International Conference on Communication (ICC 2012)*, June 2012.

[65] K. Jain, J. Padhye, V. N. Padmanabhan, and L. Qiu, "Impact of interference on multi-hop wireless network performance," *Wireless Networks*, vol. 11, pp. 471–487, 2005.

[66] J. Luo, C. Rosenberg, and A. Girard, "Engineering wireless mesh networks: Joint scheduling, routing, power control, and rate adaptation," *IEEE/ACM Transactions on Networking*, vol. 18, no. 5, pp. 1387–1400, Oct. 2010.

[67] M. Haenggi, "On routing in random Rayleigh fading networks," *IEEE Transactions on Wireless Communications*, vol. 4, no. 4, pp. 1553–1562, July 2005.

[68] G. L. Nemhauser and L. A. Wolsey, *Integer and Combinatorial Optimization*, 1st ed. John Wiley&Sons Ltd, 1999.

[69] A. Iwata, C.-C. Chiang, G. Pei, M. Gerla, and T.-W. Chen, "Scalable routing strategies for ad hoc wireless networks," *IEEE Journal on Selected Areas in Communications*, vol. 17, no. 8, pp. 1369–1379, 1999.

[70] X. Hong, K. Xu, and M. Gerla, "Scalable routing protocols for mobile ad hoc networks," *IEEE Network*, vol. 16, no. 4, pp. 11–21, 2002.

[71] M. Gerla and J. T.-C. Tsai, "Multicluster, mobile, multimedia radio network," *Wireless networks*, vol. 1, no. 3, pp. 255–265, 1995.

[72] C.-C. Chiang, H.-K. Wu, W. Liu, and M. Gerla, "Routing in clustered multihop, mobile wireless networks with fading channel," in *Proceedings of IEEE SICON*, vol. 97, no. 1997.4, 1997, pp. 197–211.

[73] C. E. Perkins and E. M. Royer, "Ad-hoc on-demand distance vector routing," in *Mobile Computing Systems and Applications, 1999. Proceedings. WMCSA'99. Second IEEE Workshop on.* IEEE, 1999, pp. 90–100.

[74] M. K. Marina and S. R. Das, "On-demand multipath distance vector routing in ad hoc networks," in *Ninth International Conference on Network Protocols, 2001.* IEEE, 2001, pp. 14–23.

[75] T. Clausen, P. Jacquet, C. Adjih, A. Laouiti, P. Minet, P. Muhlethaler, A. Qayyum, L. Viennot *et al.*, "Optimized link state routing protocol (OLSR)," *Network Working Group Network Working Group*, 2003.

[76] P. Jacquet, P. Muhlethaler, T. Clausen, A. Laouiti, A. Qayyum, and L. Viennot, "Optimized link state routing protocol for ad hoc networks," in *Multi Topic Conference, 2001. IEEE INMIC 2001. Technology for the 21st Century. Proceedings. IEEE International.* IEEE, 2001, pp. 62–68.

[77] G. S. Malkin, *RIP: an intra-domain routing protocol.* Addison-Wesley Longman Publishing Co., Inc., 2000.

[78] [Online]. Available: http://www.cisco.com/

[79] J. Moy, *OSPF version 2.* The Internet Society, 1997.

[80] H. Gredler and W. Goralski, *The complete IS-IS routing protocol*. Springer, 2005.

[81] [Online]. Available: http://wireless-matlab.sourceforge.net/